BIOPHYSICAL CHARACTERIZATION OF THE ASSEMBLY AND DISASSEMBLY OF THE ssDNA VIRUSES

By

ANTONETTE DENISE BENNETT

A DISSERTATION PRESENTED TO THE GRADUATE SCHOOL
OF THE UNIVERSITY OF FLORIDA IN PARTIAL FULFILLMENT
OF THE REQUIREMENTS FOR THE DEGREE OF
DOCTOR OF PHILOSOPHY

UNIVERSITY OF FLORIDA

2009

To my mother Iris Barrett-Browne, my brother Matthew Browne, my sister Shema Barrett, nephew Luke Walters and my son John-Claude Hutchinson

ACKNOWLEDGMENTS

I am indebted to Professor Mavis McKenna for her mentorship, her patience and for allowing me the opportunity to work with her, as well as, in her lab for the last 5 years. Her commitment to excellence in all aspects of science has inspired and motivated me. I would also like to thank Dr Nicholas Muzyczka for his Co-chairing of my committee as well as allowing me to work in his lab for part of this study and his co-mentorship is greatly appreciated. I would also like to thank the members of my supervisory committee, Dr. Michael Bubb, Dr. J. Bert Flannegan, and Dr Jane Polston. They have been helpful and supportive in the work that I am presenting.

I would like to thank the members of the McKenna lab and the Muuzyczka lab (past and present) for their assistance, friendship and their kindness. I would also like to show my appreciation of the Biochemistry staff and the IDP recruiting and clerical staff, without whom I could not have completed this work.

I want to thank my parents Iris and Eric Browne, my brother Mathew Browne, my sister Shema Barrett, cousins, my aunts, my uncles, and my son John-Claude Hutchinson. I want to thank them for supporting and believing in me. I want to especially thank my mother for loving, motivating, inspiring and supporting me, and without her none of this would have been possible.

TABLE OF CONTENTS

page

LIST OF TABLES

LIST OF FIGURES

LIST OF ABBREVIATIONS

AAV	Adeno-associated virus
BMSV-NCP	Baculovirus expressed maize streak virus
CP	Coat protein
CPV	Canine parvovirus
dsDNA	Double stranded DNA
DLS	Dynamic light scattering
DSC	Differential scanning calometry
EDTA	Ethylene diaminotetraacetic acid
EM	Electron microscopy
MALDI	Matrix-assisted laser desorption/ionization
MVM	Minute virus of mice
MSV	Maize Streak Virus
MSV-N	Maize Streak Virus (Nigerian Strain)
MT	Mutant
ssDNA	Single stranded DNA
SDS	Sodium dodecyl sulfate
STEM	Scanning transmission electron microscopy
TMV	Tobacco mosaic virus
TYLCV	Tomato yellow leaf curl virus
VP	Viral protein
WT	Wild type

Abstract of Dissertation Presented to the Graduate School
of the University of Florida in Partial Fulfillment of the
Requirements for the Degree of Doctor of Philosophy

BIOPHYSICAL CHARACTERIZATION OF THE ASSEMBLY AND DISASSEMBLY OF SSDNA VIRUSES

By

Antonette D Bennett

August 2009

Chair: Mavis-Agbanje McKenna
Co-chair: Nicholas Muzyczka
Major: Medical Sciences--Biochemistry and Molecular Biology

Viruses are the causative agents of many diseases that affect plants and animals and the mechanisms by which they assemble and disassemble represent critical steps in their replicative life cycle. The focus of this study was to elucidate the steps involved in the formation and disruption of the viral capsid of the *Geminiviridae* and *Pavoviridae* family of viruses.

Maize Streak Virus (MSV-N) belongs to the *Geminiviridae* family of virus. The *Geminiviridae* have caused significant economic loses and hardship due to their infection of a number of horticultural crops worldwide. MSV-N is a severe pathogen of maize and is used in this study as a model for understanding assembly and disassembly of this unique virus family. The goal of the study was to decipher the steps involved in the formation and disruption of the MSV capsid. This was accomplished by isolating and characterizing the capsid components and intermediates from maize agro-inoculated with MSV-N. These components and intermediates include the characteristic geminate capsid, a T=1 icosahedral (single) capsid, pentamers, and dimers of pentamers. This study also included a pH assembly/diasassembly assay that has been generated for MSV and could be developed as a method to test peptide inhibitors of these processes.

Adeno-Associated Virus serotype 2 (AAV2) belongs to the *Parvoviridae* family and it is an important therapeutic agent for clinical gene therapy. AAV2 has been extensively studied and it has been used in the treatment of several genetic diseases. However, there is still a large deficit in the amount of information available on the mechanism by which it assembles and disassembles. We have isolated and characterized subassemblies of recombinant AAV2. These include what appear to be pentamers, dimers of pentamers (DOPs) and pentamers of dimers (PODs). In the final aspect of this work, we used the crystal structure of AAV2, other AAV serotypes, other parvoviruses and site directed mutagenesis to identify residues and regions of the capsid that are important to the assembly and stability of the virus capsid.

CHAPTER 1
FUNDAMENTALS OF VIRUS ASSEMBLY AND DISASSEMBLY

Virus Capsid Function

Viruses are the causative pathogens of severe diseases and are ubiquitous in all organisms, infecting everything from bacteria to humans. To achieve such biodiversity they have evolved different strategies for host recognition, internalization, cellular trafficking, genome replication, capsid assembly and release of progeny to optimize their life cycle in their unique niche. This has resulted in viruses of different shapes and sizes, but invariably their viral coat proteins (CPs or VPs) form a protective shell (a viral capsid) around the infectious genomic nucleic acid, which can be ssDNA, ssRNA, dsDNA or dsRNA. The packaged viral genome encodes all the required structural CPs (or VPs) and auxiliary non-structural proteins that are required, in combination with host proteins, for host infection. Some viruses, termed enveloped viruses, also incorporate their host's lipids as either an internal and/or external envelope during assembly. For a number of viruses, CP recognition and encapsidation of the genomic nucleic acid is a prerequisite for infectious capsid formation, while for others the genome is packaged into preformed capsids via interactions with viral or host encoded proteins. In addition to genome encapsidation and protection during cellular entry and trafficking, the CP can also dictate many other viral functions, including host receptor/vector recognition, transmission and the genomic transduction efficiency during infection. The formation of the assembled mature viral capsid from CP (or VP) monomers is the focus of this study.

Virus Assembly

Virus assembly, utilizing a limited number of VP or CP building blocks, is an excellent example of a directed macromolecular interaction occurring in nature. Two basic principles govern the assembly of spherical (icosahedral) viruses: (i) Genetic Economy – the encapsidated

genome encodes a single or few CPs that assemble a protective shell (the viral capsid); and (ii) specificity – the CPs have to fold to recognize each other and form exact CP–CP interfacial interactions during the assembly pathway. For spherical virus assembly, the CP organization in the capsid architecture takes on the form of an icosahedron (a platonic solid with point group symmetry 5.3.2). This symmetric CP shell (44) is a consequence of it consisting of identical (or almost identical) gene products, consistent with the argument that there is insufficient volume inside a virus to accommodate a more complicated protein coding strategy. The exact 2-, 3- and 5-fold symmetry of the icosahedron permits the (quasi) equivalence symmetry (31) required to construct structures with 60 or multiples (denoted by a T number) of 60 subunits. Significant effort has been dedicated toward understanding the driving forces behind icosahedral viral capsid assembly. Structural biology tools, such as X-ray crystallography and cryo-electron microscopy (cryo-EM) combined with 3D homology model building, enable the atomic visualization of interface interactions between protein–protein subunits and protein nucleic acids in virus capsids (12, 71). Combined with biochemical and molecular biology analysis, these studies indicate a high degree of fidelity in the steps that result in the assembly of mature infectious virus capsids. They also show that the fundamental principles governing successful viral capsid assembly, efficient polymerization of CP subunits utilizing specific interface interactions that spontaneously terminate, often employ structural polymorphisms to facilitate the required interactions (e.g. (71, 72)). However, there are still many unanswered questions regarding the numerous steps that ensure the polymerization of protein subunits, with precise accuracy, in the successful assembly of infectious virions. This study will limit itself to only include the simplest single stranded (ss) DNA families, which assemble a T=1 or twinned pseudo T = 1 icosahedral capsid.

Experimental Techniques Used to Study Virus Assembly

There are several methods available to study the forces involved in orchestrating the CP:CP or VP:VP interactions that occurs in virus assembly and disassembly. X-ray crystallography provides the high resolution molecular information of purified viral CP and capsid in the crystalline state (71). Cryo-electron microscopy provides low resolution structural information of virus capsids in the aqueous state (90). Negative stain electron microscopy provides information about the overall shape of the virus capsid and possibly the shape of any intermediates (33, 176). Scanning transmission electron microscopy can be used to determine the molecular mass, as well as, visualize the virus capsid and any stable intermediates (109). Cryo-electron tomography has been used to show viruses in different cellular organelles as well different stages of assembly (60). Analytical gel filtration chromatography, analytical ultra-centrifugation and dynamic light scattering have been used to determine the molecular mass, sedimentation coefficient, and the diameter of the viral capsid components, respectively (33, 176). The isolation of stable capsid intermediates has been shown to present numerous challenges based on the fact these intermediates are extremely transient (30). The use of CP mutants however, has been successfully used to generate capsid intermediates that were stable enough to be characterized (30, 32).

The CP from many viruses can reversible assemble and disassemble in response to solution conditions (174), for example, changes in pH (13, 14), CP concentration (65), ionic strength (146), temperature or the presence of a chaperone or scaffold (4, 100, 110, 124, 138). The determination of the specific chemical environment that facilitate assembly and disassembly of ssDNA viruses being studied in this study is addressed. Similarly, certain small molecules have been shown to inhibit or misdirect assembly or disassembly. This is illustrated in the use of WIN

compounds that stabilize viral capsid of rhinovirus (7, 10, 11, 99), which inhibit uncoating and infection (177).

The detailed structures of viral capsids can illustrate how the CPs interact with each other and how they interact with their packaged genome (155). The determination of the CP interaction with each other and its interaction with the viral genome is critical to the understanding of the assembly and disassembly processes. The polyoma VP1 protein for example contains a jelly roll β- barrel core and long flexible N and C- terminal arms, the C terminus being extremely positive and may be important in binding the viral DNA (137). Both arms are dispensable for pentamer formation but indispensable for inter-pentameric interaction. In CCMV on the other hand, 25 of the N- terminal residues of the CP contain a high proportion of basic amino acids which have been modeled to interact with the viral RNA; deletion of these residues eliminates the ability of this virus to assemble RNA containing particles in vivo(158). To date significant progress has been made in the deciphering of the mechanism of assembly and disassembly of several ssRNA, dsRNA and dsDNA virus families (39, 118, 137). However, with the exception of the *Microviridae* very little is known about these mechanisms for the ssDNA virus families.

The ssDNA Virus Families

There are six ssDNA virus families: *Microviridae, Inoviridae, Nanoviridae, Geminiviridae, Circoviridae and Parvoviridae* (132). The first two families infect bacteria, the next two infect plants, and the last two infect mammals, with the *Parvoviridae* also infecting invertebrates. Despite this diverse host range and no genetic homology between them, the CPs/VPs for four of the six viruses (*Microviridae, Nanoviridae, Circoviridae* and *Parvoviridae*) assemble a T = 1 icosahedral capsid, the *Geminiviridae* assembles a unique twinned pseudo T = 1 icosahedral capsid, and the *Inoviridae* are filamentous. This study discusses what is known

about the structural architecture of the CPs/VPs and assembled capsids of two ssDNA virus families, the *Geminiviridae* and *Parvoviridae*. These families provide two disparate examples of capsid assembly that result in a T = 1 capsid or twinned pseudo T = 1 capsids: the Geminiviridae involving the assembly of two incomplete shells from a single CP to accommodate its genome; and the Parvoviridae which orchestrate interactions between the common region of two to four overlapping VPs.

Geminiviridae

The *Geminiviridae* are a family of highly pathogenic viruses that cause significant crop losses due to their infection of horticultural plants such as maize, tomatoes, beans, squash, cassava and cotton (Table 1-1, (156)). They are normally transmitted from host to host via a whitefly or leafhopper vector. Efforts aimed at geminivirus control are mainly focused on identifying resistance/silencing genes that can be engineered into plant crops. The *Geminiviridae* package either one circular ssDNA genome (monopartite), of 2.5–2.8 kb, or two ssDNA molecules (bipartite, with component A and B) totaling 5.2 kb, into one or two different twined pseudo-icosahedral capsids, respectively. The capsid is ~ 200Å x 400Å in diameter. The *Geminiviridae* are divided into four genera: *Mastrevirus, Curtovirus, Begomovirus* and *Topocuvirus*, based on the genome organization, host range and the insect vector used (126). Members of the *Mastrevirus* have a monopartite genome and are transmitted by specific species of leafhoppers (*Cicadellidae* sp.). Members of this genus infect monocotyledonous plants; *Bean yellow dwarf virus* and *Tobacco yellow dwarf virus* infect dicotyledons. *Maize streak virus* (MSV-N) is the prototype member of this genus. The *Curtoviruses* have monopartite genomes and are transmitted by leafhoppers to dicotyledonous *Bemisia tabaci* plants. *Beet curly top virus* is the prototype member of the genus. The *Begomoviruses* can have a single (e.g. *Tomato yellow leaf curl virus* (TYLCV) and *Bean yellow vein mosaic virus* or bipartite genome (e.g. *Bean*

golden yellow mosaic virus), and are transmitted by whiteflies, and infect dicots. *Bean golden mosaic virus* is the prototype species. The genus *Topocuvirus* has only one member, *Tomato pseudo-curly top virus*. This virus has a monopartite genome and is transmitted by treehoppers.

In this study, the Nigerian strain of MSV (MSV-N) will serve as the viral model for the *Geminiviridae* (23). MSV-N is one of the best characterized members of its family. The virus is transmitted specifically by the leafhopper *Cicadulina mbila* (Figure 1-1A). The symptoms of MSV-N infection include deformed cob and chlorotic streaks on the maize leaves (Figure 1-1B). The 2.7 kb genome encodes four gene products, CP, replication proteins Rep and RepA, and the movement protein, MP. The MSV-N virion is assembled from 110 copies of a single CP (244 amino acids, 27 kDa). The CP is required for a variety of viral life cycle functions that include; insect transmission, systemic infection and encapsidation of ssDNA (6, 21, 37, 94, 101-103, 131). The expressed CP accumulates in the nucleus and facilitates nuclear and cell to-cell transport of the genomic ssDNA via an interaction with the MP. In addition, the Rep and RepA proteins have multifunctional roles that include genome replication (reviewed in (108)).

MSV-N Assembled Capsid Architecture

The twinned quasi-isometric incomplete T = 1 icosahedral capsid (geminate) architecture for the geminiviruses was predicted from negative stain images and verified by the cryo-EM image reconstruction of the MSV-N capsid at 25Å resolution (173). This geminate architecture is unique among all known virus families. The MSV-N capsid dimensions are, 220Å x 380Å (Figure 1-2B). The 2.7 kb genome is packaged into an internal capsid volume of $1.2 \times 10^6 Å^3$. The capsid consists of 22 pentameric capsomers and they are arranged with a 5.2 point group symmetry. Each incomplete icosahedral 'head' (55 CPs) is missing 5 CPs (a pentamer) compared to a regular T=1 capsid assembled with 60 CPs (singles). The structure is built from distinct pentamers that protrude radially outwards from the capsid surface (Figure 1-2A). Three 'classes'

of pentameric building blocks are observed. They are the two apical – that are located at each end of the capsid; the 10 peripentonal – that are adjacent to the apical pentamers; and the 10 equatorial – that line the waist of the capsid at the interface between the two fused incomplete icosahedra (Figure 1-2A). A gap of 25Å containing fifteen regions of tubular density, which connects the two heads. A small protrusion is observed at the icosahedral 3-fold axis and there is a small depression at the 2-fold interfaces between non-equatorial pentamers. Recently, a cryo-EM image reconstruction of 'single' head capsids of MSV-N with T = 1 icosahedral symmetry which package sub genomic ssDNA has been determined to 10.2 Å resolution (not shown; Reutzel et al. unpublished data). This structure shows a capsid constructed exclusively from pentameric building blocks that resemble the apical capsomers of the geminate.

The Structure of MSV-N CP Monomer and its Symmetry Related Interactions

A pseudo-atomic model of the MSV-N CP, residues 19–244, has been built into the cryo-EM envelope of MSV-N based on an amino acid sequence alignment with the CP of satellite tobacco necrosis virus (Figure 1-2B, (173)). The first 18 amino acids were not built because their location could not be unambiguously assigned. The MSV-N CP model contains an eight stranded anti-parallel β-barrel motif that forms the core contiguous capsid, the BIDG sheet is closest to the interior of the capsid. This core motif represents 60% of the CP amino acids. The MSV-N CP model also contains two α-helical regions, residues 19–34 and 138–144, α1 and α2, respectively (Figure 1-2B). The N-terminal helix (α1) extends from the β-barrel motif and α2 is located in the EF loop (Figure 1-2B). The 2-fold axis is formed by α1 and the interaction at the c-termini of one CP (Figure 1-3A). In each of the 10 equatorial pentamers, the α1 helix of the CP that forms the 2-fold head connection is rotated, around the Cα of residue 35 (compared to the other CPs) to satisfy ten inter equatorial connections (not shown). The α1 helix and the βCD and βGH loops form the 3-fold axis (Figure 1-3C). The main 5-fold interface interaction includes the interaction

between the α1 helix and the EF loop. The 5-fold axis is formed by the GH loop, and it creates a channel that runs from the inside to the outside of the capsid (Figure 1-3E).

Geminivirus Assembly/Disassembly Studies

The Geminivirus capsid is the most unique of all virus families. It has been illustrated that the assembled capsid is required for insect transmission and systemic host infection (94). However, while there is considerable data available about the infection (94), replication (24), transcription (24, 115), translocation, and systemic infection (115) of the geminivirus within the host as well as it's mode of circulation in the vector, further work is required for the detailed dissection of the mechanism of assembly or disassembly.

In geminiviruses, the CP can perform diverse roles. It is the only protein component of the virion and is required for vector transmission (9) and it determines insect specificity (26).The CP is also important for the transport of the viral DNA in and out of the nucleus (89, 105, 153, 154). Deletion mutagenesis have been used to identify regions of the CP that are important for DNA binding and multimerization (153). The mechanism by which geminiviruses disassemble is not yet known except for the disassembly of *African Cassava Mosaic Virus* (ACMV). pH, heat treatment, EM and chemical cross-linking experiments of ACMV was used to illustrate the expulsion of the viral genome while still attached to the viral capsid (70). In order to decipher regions of the geminivirus CP that are important for maintaining the capsid structure the mastrevirus CP sequence were aligned and residue K182 was identified as one of the most conserved residue. Mutations at this position, for example, K182V, have been shown experimentally to disrupt capsid assembly, proposed to be due to capsid instability (104), however, intermediates formed have not been characterized. In addition to this residue the N-terminal region also been shown to be important for MSV-N assembly and DNA binding (101). Our study of the assembly and disassembly of MSV-N will focus on isolating, purifying and

characterizing assembly/disassembly components formed during a wild type infection. In addition, none of the antiviral therapies being explored is utilizing the disruption of geminivirus capsid assembly or the prevention of disassembly. The second part of the MSV-N studies will focus on the environmental factors affecting these processes and the development of an assay that can be used to test geminivirus assembly or disassembly disrupters. The third part of this work will focus on the baculovirus expression of the MSV-N mutant K182V, N-terminal truncation and wt CP.

Significance of Plant Virus Assembly/Disassembly Studies

For several vector-borne plant virus families, successful virus resistance has been reported by utilizing a process referred to as pathogen derived resistance. Pathogen derived resistance is defined as the use of resistant genes obtained from the viruses own genome. Two main examples, in which this method was successfully utilized by transforming the plant with viral CP gene, include tobacco resistance to Tobacco mosaic virus (TMV) (120) and papaya resistance to Papaya ringspot virus (152). Resistance for TMV is caused by interference with viral uncoating. In the case of geminiviruses, resistance has not been achieved using this approach because the mechanism of assembly and disassembly is not known and so it has been difficult to develop resistance strategies utilizing the CP (156). In the past, the pathogen derived resistance method utilized for geminiviruses include the expression of the mutant or truncated viral proteins that interferes with virus infection. The other method utilized to confer resistnce to geminiviruses is, the transcription of viral RNA sequences that silences the expression of virus genes. Recent methods include the use of Geminivirus –inducible toxic proteins to kill the infected plant cell, or the expression of DNA binding proteins, peptide aptamers or GroEL homologues that either lessen their harmful effects or disrupt geminivirus infection. These methods have provided some success in several lab strains, they have not provided durable resistance to geminivirus infections

(reviewed in (144)).The aim of our study is to decipher the mechanism of viral capsid assembly and disassembly , and we believe that information on these mechanisms will provide a platform for the design of improved control strategies.

Parvoviridae

The *Parvoviridae* also exhibit diverse host range and tissue tropism, with an infection outcome spectrum of non-pathogenicity to lethality. The *Parvoviridae* package linear (-) or (- and +) sense ssDNA that is ~5 kb into capsids that are ~260Å in diameter. The family is divided into two subfamilies: *Parvovirinae*, which infect vertebrates, and the *Densovirinae*, which infects insects (150). This study will focus specifically on the *Parvovirinae*, which infect a wide distribution of hosts including mice, cats, dogs, pigs, cows, monkeys and humans. This subfamily is subdivided into five genera: *Parvovirus, Erythrovirus, Dependovirus, Amdovirus* and *Bocavirus*. The prototype member for the Parvovirus genera is *Minute virus of mice* (MVM) which infects mice, with other members infecting rats, cats, dogs and pigs. This genus contains both pathogenic and non-pathogenic strains. The genus *Erythrovirus* contains *human parvovirus B19* as the prototype member and includes viruses that infect non-human primates such as rhesus monkeys and pigtailed macaques. The genus *Dependovirus* comprises the *Adeno-associated viruses* (AAVs), which require helper functions from viruses such as Adenovirus and Herpes virus for replication, hence the name of the genus. These viruses, for which there has been no disease association, have been isolated from a wide range of hosts, including mice, rat, cows, snakes, non-human primates and humans. The prototype member for this genus is AAV serotype 2 (AAV2). The *Amdovirus* genus currently contains one member, Aleutian mink disease parvovirus infecting minks. Members of the *Bocavirus* genus are *bovine parvovirus*, which infect cows and *human bocavirus*, recently discovered in children and associated with respiratory disease and gastroenteritis. For this study, AAV2 will serve as the parvovirus model. This virus

is also the best characterized member of the *Dependovirus* genus, mostly because of interest in its development and use for gene delivery applications. The AAV2 genome of 4.7 kb contains a replication (rep) and a capsid (cap) ORF. The rep ORF encodes four non-structural overlapping proteins Rep78, Rep68, Rep52 and Rep40 that are involved in viral DNA replication (116). The cap ORF encodes three overlapping structural proteins, VP1 (735 amino acids, 87 kDa), VP2 (598 amino acids, 72 kDa) and VP3 (533 amino acids, 62 kDa), that are alternatively spliced. These proteins have a common C-terminal region (the VP3 sequence) with VP2 and VP1 having N-terminal extensions compared to VP3 of 65 and 202 amino acids, respectively. The AAV2 capsid is ~260Å in diameter, is assembled from 60 copies (in total) of VP1:VP2:VP3 in a ratio of 1:1:8. The VP3 common region is known to be important for cell binding, antigenic recognition and genomic DNA packaging (20). VP1 and VP2 contain nuclear localization sequences and are suggested to play a role in transporting VP3 to the nucleus. VP1 has a unique N-terminal region (of 136 amino acids) which displays a phospholipase A2 activity required for endosomal escape during cellular trafficking (55).

AAV2 Assembled Capsid Architecture

The AAV2 capsid structure has been determined by cryo-EM and X-ray crystallography to 10Å and 3.2Å resolution, respectively (90, 168). The characteristic surface features of the capsid include depressions at the icosahedral 2-fold axes, three spike-like protrusions around the icosahedral 3-fold axes, and a cylindrical channel at the icosahedral 5-fold axes surrounded by a moat (Figure 1-2C). This surface topology forms a caspid that is, 220Å, 230Å and 240Å in diameter at the icosahedral 2-, 3- and 5-fold axes, respectively, with a diameter of 290Å at the maximal extremity of the protrusions surrounding the 3-fold axes (Figure 1-2D). The internal volume of the capsid that packages the 4.7 kb genome is ~3.5 x 10^6 $Å^3$.

The Structure of AAV2 CP Monomer and its Symmetry Related Interactions

The crystal structure of the AAV2 capsid has provided information on the common VP3 amino acids 217–735 only, despite the fact that VP1, VP2 and VP3 were present in the samples studied(168). The lack of ordering of the N-terminal regions of VP1–VP3 is consistent for all parvovirus structures determined to date (reviewed in ref. (3)). The low copy numbers of VP1 and VP2 and possible multiple conformations of the N-termini of all three capsid VPs, which is incompatible with the icosahedral symmetry imposed during the structure determination, are likely responsible for this apparent disorder. The main structural motif of the AAV2 common VP3 region is an eight-stranded anti-parallel β-barrel motif which forms the core contiguous capsid with large inter-strand loops (Figure 1-2D). The AAV2 β-barrel is oriented tangential to the capsid surface. The BIDG sheet also forms the interior surface of the AAV2 capsid. The inter-strand loop insertions constitute 70% of the VP3 fold and contain small stretches of β-strand and α-helical structure (Figure 1-2D). A conserved loop region at the C-termini of the VP3 (residues 696–704), located after βI, invade neighboring icosahedral 2-fold related VP3 monomers to form the floor of the depression at the 2-fold axis (Figures 1-2D and 1-3B). The 2-fold interface interactions also involve a conserved helix, αA, which forms the wall of the surface depression at this axis (Figures 1-2C and 1-3B). The 2-fold is the thinnest region of the capsid shell, being only one polypeptide chain thick, as is also the case in the MSV-N capsids. The interactions between the icosahedral symmetry 3-fold related monomers are the most extensive in AAV2 and involve residues within the βBC, βEF and βGH loops. The βGH loop has the most amino acid sequence variability among the parvoviruses and interdigitate to form the surface spike-like protrusions around the icosahedral 3-fold axes characteristic of members of the dependovirus genera of the *Parvoviridae* (Figure 1-3D). The spike-like protrusions surround a depression at the icosahedral 3-fold axis (Figure 1-2C). The loop extensions from the narrow end

of the β-barrel wedge form the icosahedral 5-fold VP3 symmetry related interactions with elements of the BIDG sheet and the N-terminal residues in the adjacent monomer. In addition, the βHI loop (structurally conserved in all parvoviruses) is positioned above the β-strands of adjacent VP3 monomers forming the floor of the conserved depression that surrounds the icosahedral 5-fold axis (Figures 1-2D and 3F). As observed for MSV-N, AAV2 also has a channel that connects the inside and outside of the capsid at the 5-fold axis formed by the βDE ribbon which assembles a surface turret at this axis.

Parvovirus assembly/disassembly Studies

The assembly/disassembly of several parvoviruses have been studied by: determining the functions of the VPs in their life cycle (27, 123), the characterization of any intermediates formed (107, 172), analyzing mutagenesis data, and by understanding the effects of other virally associated proteins(42, 66, 128). Genetic analysis of the expression of the major VPs of the parvoviruses proves that they are sufficient for capsid assembly, e.g. MVM (123), CPV (27, 136), ADV (38), B19 (27, 75) and AAV2 (57, 135, 165). The mutagenesis of several of the AAV2 VPs amino acids have shown that there are several conserved residues that are important for capsid assembly and disassembly (58, 145, 159, 165, 175). The first part of the AAV2 section of this study will focus on mutating residues involved in symmetry related interactions of VP3 and combining the information with existing data to determine if there are regions of the capsid that are important for capsid assembly.

The examination of several parvovirus assembly systems have illustrated that there is an apparent connection between virus assembly and nuclear localization. For example, co-expression of AAV2 VP3 with either VP1 or VP2 which both contain a NLS, is important for the transport of VP3 to the nucleus, and VP2 is important for capsid assembly (66, 159, 160). N-terminal VP2 deletion mutants that were unable to accumulate in the nucleus of COS cells were

also not able to assemble into capsid; the N-terminal addition of a NLS conferred assembly competence to VP3 (66). Similarly MVM VP2 mutants which affected nuclear transport also affected assembly (107) and a panel of CPV mutants which are located within possible NLS also appeared to affect assembly (151).

The identification of VP multimers or subassemblies represents potential steps in the assembly of the parvovirus capsid. Sedimentation analysis of soluble cytoplasmic pools of newly synthesized AAV2 VP1-3 showed capsid protein oligomerization and no capsid. This oligomerization is consistent with VP monomers and pentamers (160, 161) which were present in the cytoplasm of the cell. The next observation which represents a step in virus assembly is the formation or accumulation of empty AAV2 capsids in the nucleus. Trimeric subassemblies were identified for MVM and CPV (107, 133, 172). The final section of this study will focus on the purification and the biophysical characterization characterization of assembly/disassembly intermediates of baculovirus expressed AAV2.

There are several proteins that are believed to be associated with the assembly and packaging of the parvovirus capsid. For example when CPV VPs were expressed alone in mammalian cells, they assemble utilizing more VP1, compared to capsids formed in infected cells; this suggests an influence of other viral gene products in the assembly process (172). Nucleolin is a nonviral protein that has been identified to be associated with assembled AAV2 capsid (73, 128). The nonstructural proteins (NS1) expressed by the parvovirus genus and the Rep proteins from the dependoviruses have been shown to be important for the packaging of the viral genome (41-43, 47, 91, 125).

Significance of AAV2 Assembly Studies

AAV has several key features which makes it an ideal vector for gene therapy applications. AAV is stable and exhibits no pathogenicity, it can be manufactured and purified in a high titer

and it can also be utilized in a form that does not express any viral gene product. Consequently, there are several clinical trials that are presently complete that utilized AAV vectors to treat diseases like hemophilia (76-78), cystic fibrosis (48-50, 52-54), retinal diseases (1, 2, 5, 62), neurodegenerative diseases (Parkinson and Alzheimer) (79-84) and lysozomal storage diseases (45, 63, 134, 139, 140, 157, 170). These factors have generated significant interest in all aspects of the basic biology of AAV. To date there is a limited amount of data available on the mechanism assembly of AAV viral particles. Furthermore, it has been shown that tissue specificity, immune evasion and vector retargeting can be enhanced by using different serotypes and chimeric vectors (36, 46, 59, 61, 97, 98, 122, 143, 149, 166). Our study of the assembly and disassembly of AAV2 will focus on isolating, purifying and characterizing assembly/disassembly components formed during a baculovirus expression; as well as, the mutational analysis of symmetry related interactions of VP3. The information obtained from the proposed assembly and disassembly studies will expand our basic knowledge of the interactions/conditions controlling theses processes, a requirement for vector development. Understanding the basic mechanism of assembly of AAV2 will provide the ground work for understanding this mechanism in other AAV vectors (different serotypes and chimeras), as well as, determine residues or regions of the capsid that can or cannot tolerate change.

Overall Goals

The overall goal of this project is to biophysically study the steps involved in the assembly and disassembly of two families of ssDNA viruses, the *Geminiviridae* and *Parvoviridae*. The study is divided into three specific aims. The first aim is focused on utilizing biophysical techniques to characterize assembly/disassembly intermediates. The second aim will expose the virus capsids to different host environmental conditions to dissect their role in the

assembly/disassembly process. The third aim is to utilize the available 3 dimensional structures to generate assembly/disassembly mutants and to characterize the mutants generated.

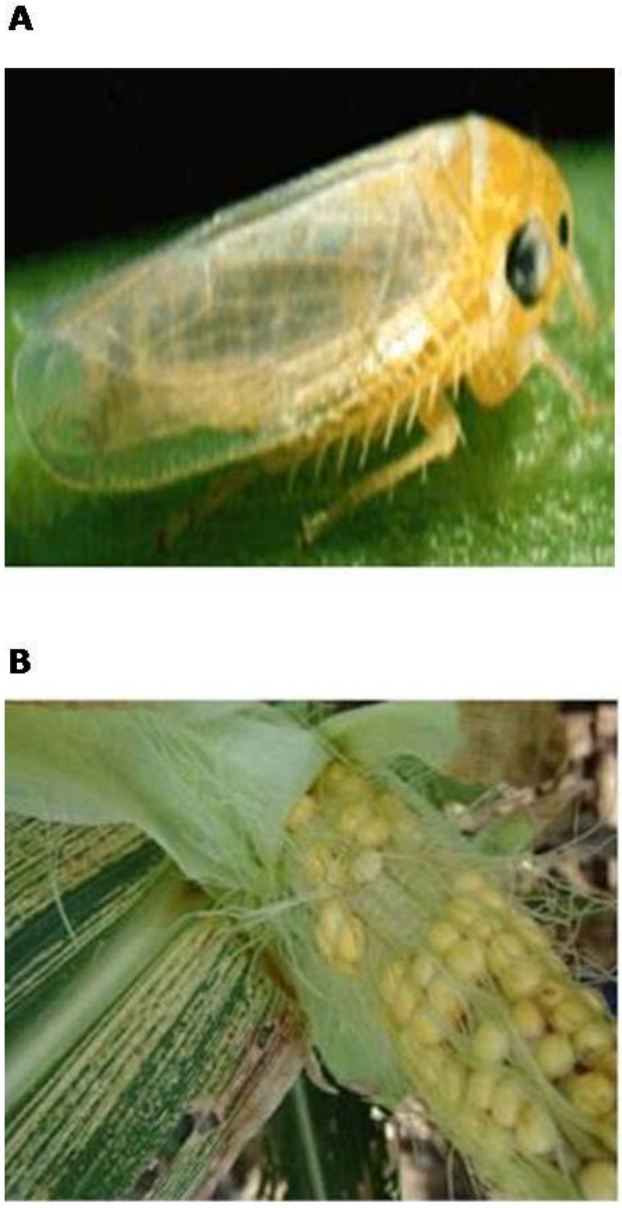

Figure 1-1. MSV-N Infection. A) Symptoms caused by MSV-N, which includes deformed cob and chlorotic streaks on leaves. B) Cicadellidae mbilla the leafhopper that transmits MSV-N.

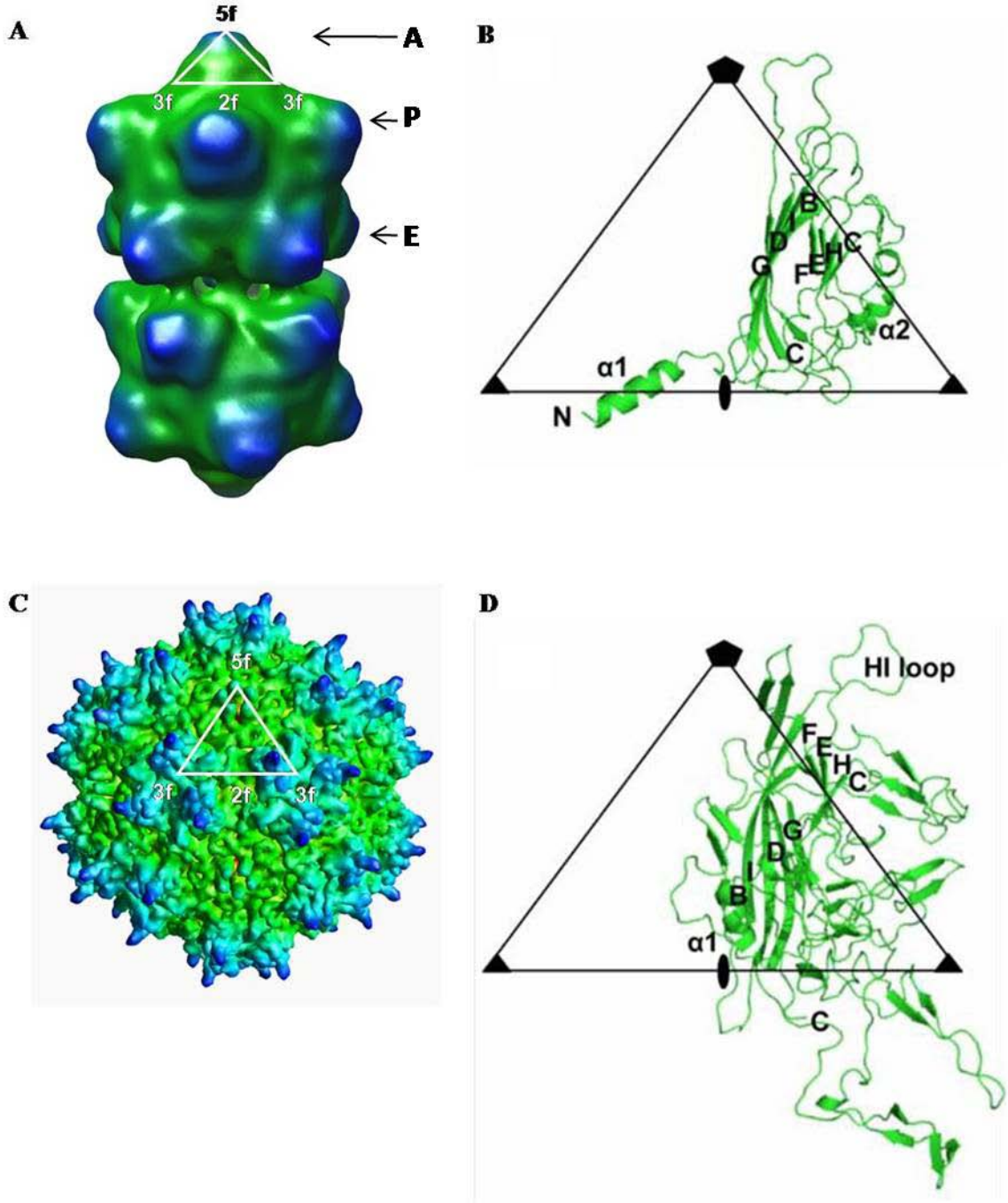

Figure 1-2. MSV-N and AAV2 virus capsid and CP/VP structures. Surface representation of the virus capsid (A) MSV-N with A=apical, P=peripentonal and E=equatorial pentamer locations, and (C)AAV2. Ribbon diagram of (B) MSV-N CP and (D) AAV2 VP3.

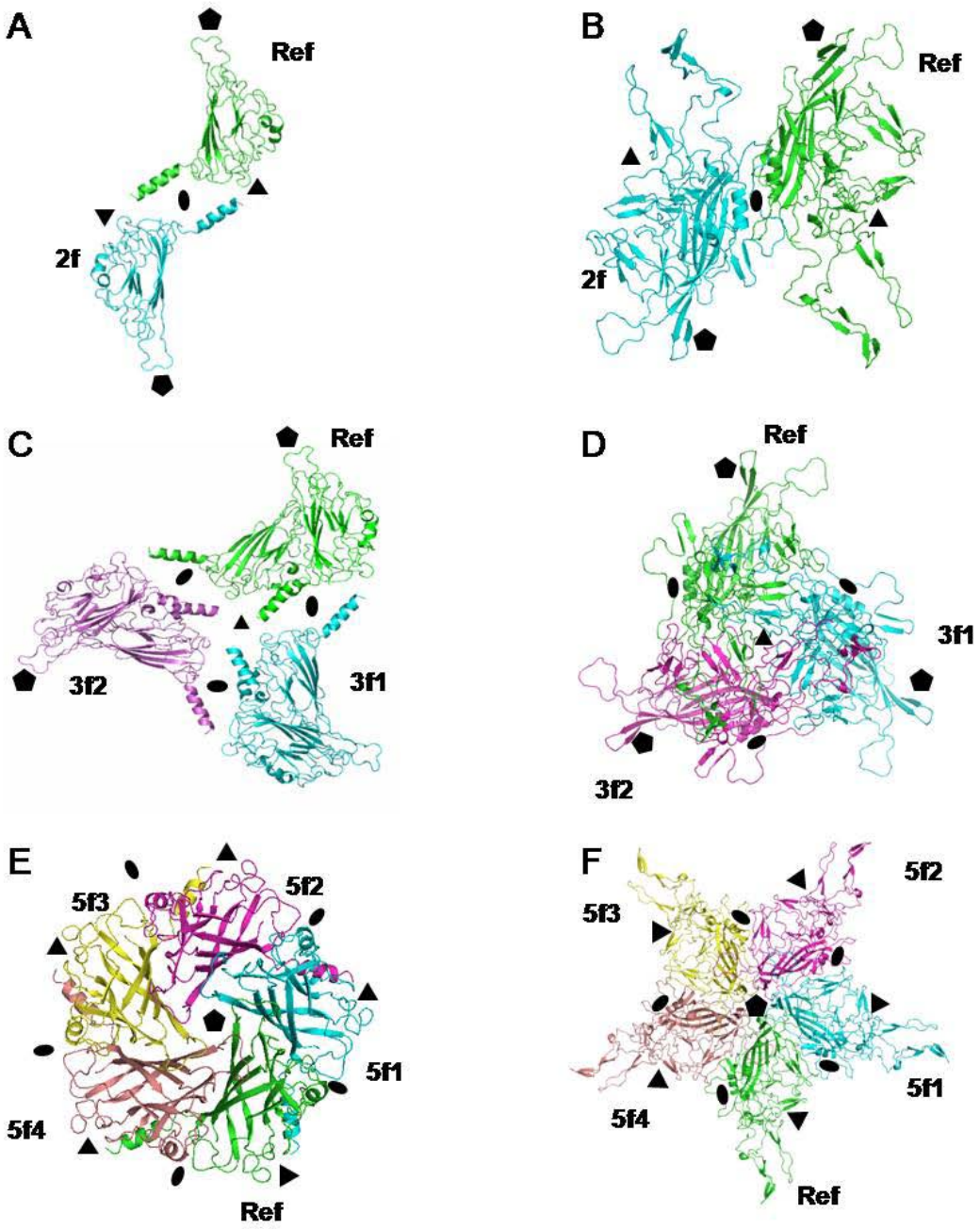

Figure 1-3. Capsid protein interfaces. Ribbon drawings of the icosahedral 2-, 3- and 5-fold symmetry related interfaces for MSV-N CP [(A), (C), and (E)] and AAV2 VP [(B), (D), and (F)]

Table 1-1. List of the economically important viral diseases caused by geminiviruses

Disease name	Virus genus	Virion structure	Host crop	Epidemic region	Yield loss
Maize streak disease	Mastrevirus	Monopartite	Maize	Sub-Saharan Africa	Average 20%, up to 100%
Cassava mosaic disease	Begomovirus	Bipartite	Cassava	Africa, India	Overall 15 – 24%, up to 90%
Cotton leaf curl disease	*Begomovirus*	Monopartite (associated β-component)	Cotton	Pakistan	Average 30%, up to 80%
Bean golden mosaic disease/bean golden yellow mosaic disease	*Begomovirus*	Bipartite	Bean	Florida, Central and South America	10% - 100%
Yellow mosaic disease	Begomovirus	Bipartite	Grain legumes	India	10% − 90%
Tomato leaf curl disease/tomato yellow leaf curl disease	Begomovirus	Monopartite	Tomato Europe, Asia,	Americas, Australia	20% − 80%, up to 100%

CHAPTER 2
MATERIALS AND METHODS

Introduction

This chapter describes common experimental methods and reagents utilized throughout this thesis. This study is divided into four main sections: two sections are based on the purification and biophysical characterization of MSV-N and AAV2 CP/VP intermediates; the other two sections are based on the generation and biophysical characterization of the CP/VP mutants that were predicted to be important for the assembly and disassembly of both viruses.

Purification of MSV-N CP

Maize streak virus (MSV-N) capsids and intermediates were purified from maize plant leaves agro-inoculated with MSV-N (25). The symptomatic leaves were harvested t ~ 25 days post agro-innoculation. Infected maize plant tissue were cut into small pieces (~3 cm in lengths), rapidly frozen and stored at -20^0 C (173). The infected plants were kept brittle with the use of liquid nitrogen, crushed with a mortar for approximately 30min or until the leaves were powder-like in appearance. The crushed leaves were transferred to a blender along with 500ml of Buffer A (0.1 M NaAc pH 5.2, 1mM Ascorbic acid, and 1mM EDTA), 5mg of cellulose, and 7.5mg of hemicellulase. The mixture was burst blended (1min every 10min) for a total of 1hr using a blender. Plant material was separated from the soluble virus containing fraction by adding 250ml of chloroform and the mixture was stirred at 4º for 30min.The mixture was centrifuged for 30min at 9961xg. The clarified aqueous upper layer was transferred to another flask with 10% (PEG 8000) and 125mM NaCl added. The mixture was allowed to stir overnight at 4^0C and the virus was pelleted at 10400xg for 90min. The pellet was resuspended in 50ml Buffer B (0.1M NaAc pH4.8). The mixture was further purified and concentrated on a 5ml 15% sucrose cushion and centrifuged at 210 000xg for 3hr. The pellet was resuspended in 1ml Buffer B and loaded unto a

5-40% step sucrose gradient. The blue bands were dialyzed against Buffer B and the virus concentration determined at 260nm wavelength and extinction coefficient of 7.5. The supernatant from the 15% sucrose cushion was diluted 2 times and loaded unto a 5% sucrose cushion. The pellet formed was loaded onto a new sucrose gradient (1ml 10% sucrose, 5ml 15% sucrose, and 5ml 20% sucrose).The virus sedimenting into tight blue bands which appears blue under white light were extracted with a needle and syringe and dialyzed against Buffer B The virus bands were dialyzed into final Buffer (0.1M NaAc pH 4.8). The MSV-N purification scheme is illustrated in Figure 2-1A.

Biophysical Characterization of MSV-N CP Components

The MSV-N containing sucrose gradient fractions were characterized by a series of biophysical techniques. These techniques include negative stain EM, 12% sodium dodecyl sulphate (SDS) polyacrylamide gel electrophoresis (PAGE), western blot, analytical gel filtration chromatography, STEM and DLS.

Negative Stain EM

5µL of sample was loaded unto carbon coated copper grids and negatively stained with 5µL 2% uranyl acetate. The grids were air dried then examined in a JOEL 1200 EX transmission electron microscope. The instrument was set to collect images at 50,000x magnification and on film.

12 % SDS PAGE and Western Blot

10µg of each sample was denatured and loaded unto two different 12% SDS gel. One gel was coomassie stained and the other gel was transferred to a Immobilon-P transfer membrane (Millipore, cat#IPVH20200) for western blot analysis using polyclonal antibody raised against purified MSV-N CP as the primary antibody and goat anti-rabbit antibody (Biorad, cat #170-

6515) was used as the secondary antibody (1:10,000 dilution). The MSV-N–antibody complex was detected with the ECL substrate (Amersham, cat#RPN2109).

Genome extraction and agarose gel electrophoresis

The genomic material of each sample was isolated by phenol chloroform extraction and ethanol precipitation.10µg of each sample was digested with 4µl proteinase K (Roche, cat#1373196), 20µL of 10x proteinase K Buffer (10mM Tris HCl pH 8.0, 10mM EDTA, 10% SDS) and the solution diluted with sterile distilled water to a total volume of 200µl. The mixture was incubated for 1hr in a water bath at 37^0 C, treated twice with an equal volume of phenol chloroform (Roche, cat#1373196), and the upper aqueous layer transferred to a clean eppendorf after each extraction. The aqueous fraction was then treated with chloroform (Fisher, cat#C298-500) and the aqueous layer transferred to a clean eppendorf. The DNA was precipitated overnight at -20^0C, after adding 10% NaAc pH 5.2, 1µl glycogen, and 3x volume of 95% ethanol. The sample was then pelleted for 20 min at 13050xg. The pellet was air dried and resuspended with 20µL water. The sample was loaded unto a 0.8% agarose gel with ethidium bromide (Bio-rad, cat#161-0433) and the DNA bands detected with the program Gel Doc.

Native Gel Analysis

Native gel analysis was performed by loading three known protein standards, bovine serum albumin (BSA), alcohol dehydrogenase (ADH) and β amylase (BA) with molecular masss 66kDa, 150kDa, and 200kDa respectively and 5µg of MSV-N fraction purified from the 10% sucrose gradient unto a native phast gel (GE Healthcare cat#17-0517-01)((4-15%). The gel was then silver stained in order to detect all the proteins.

Analytical Gel Filtration Chromatography

Analytical gel filtration chromatography was performed with a superpose 6 analytical column (Amersham Pharmacia) calibrated with the same proteins used in the native gel as well

as carbonic anhydrase (30kDa) and apoferritin (400kDa) and Blue Dextran. The elution volumes of the standards were plotted against the log of their molecular mass; this is defined as the calibration curve for the column. 250µL of purified MSV-N containing fractions were loaded unto the pre-calibrated and pre-equilibrated analytical superpose 6 gel filtration column using the AKTA FPLC system. The system pump was set at 0.5ml/min and the elution volume fraction at 1ml. The elution volumes for MSV-N fractions were determined and the molecular mass calculated from the calibration curve.

Scanning Transmission Electron Microscopy (STEM)

Scanning Transmission Electron Microscopy (STEM) was performed at Brookhaven National Laboratory (BNL). The technique has the advantage of accurately measuring molecular mass of relatively small amounts of heterogeneous, macromolecular assemblies. The technique utilizes 2µL of unstained sample at a concentration between 50-300 µg/µL. The sample are loaded onto 2.3mm carbon coated titanium grids and freeze-dried in liquid nitrogen at ultra high vacuum. The grids are then transferred to the microscope, which is operated at 40 keV and utilizes a 0.25nm focused probe for scanning. An array of detectors collects scattered electrons, with the intensity signal detected being proportional to specific features of the specimen and can be used to calculate the mass of the sample in the path of the beam. The software packaged PCMASS 27 (developed at BNL and available at stem/bnl.gov) was used for viewing, manual mass measurement and statistical summaries. The program calculates net signal (intensity minus background) for each pixel and multiplies it by a calibration constant. The calibration constant was determined from TMV for which the expected mass/length ratio is 133kDa/nm. The absolute accuracy of the system ranges from 10% for a 100kDa molecule to 4% for a 1MD molecule. The MSV-N samples masses were determined by PC MASS 27 and the statistical analysis was performed using the program “Graph Pad Prim” (114).

Dynamic Light Scattering (DLS)

The Precision Detectors Model PDDLS/Batch and Cool/Batch is the instrument that was used to collect and process DLS data for the different MSV-N components. The instrument was first equilibrated with 500µL of Buffer B. 500µL of MSV-N containing fractions at a concentration of 0.5 mg/ml in a cuvette and they were placed in the instrument. The fluctuations in scattered light intensity were monitored; their correlation function calculated and deconvoluted into a distribution of diffusion coefficients and a radii calculated for the scattering particles. Data acquisition, recording and analyses were performed by the program "Precision Deconvolution".

Development of MSV-N Capsid Disassembly and Reassembly Assay

The final or stabilizing Buffer for MSV-N geminate capsids is 0.1M NaAc pH4.8. To test the effect of pH on capsid stability, 200µL of sample in the final Buffer was dialyzed into Buffers with pH changes of ±0.2 pH units in the range 4.8 to 7.2, for a period of ~24 hr at 4ºC. 20µl of the sample was removed at the end of each dialysis run for analysis by negative stain EM and gel electrophoresis. For each sequential change in pH, all other chemical environmental factors, such as ionic strength, the presence or absence of divalent ions, temperature, and initial capsid concentration, were all kept constant. The same procedure was used for screening the effect of ionic strength, utilizing changes in NaCl concentration. Ethylene diaminotetraacetic acid (EDTA) is a divalent cation chelator, thus in addition to evaluating the effects of ions on the capsid structure; this chelator was added to remove divalent cations that might already be present in the viral capsids.

MSV-N CP Post Translation Modification Determination

All purified MSV-N components with the exception of Gemini capsids, resolve as two CP bands when analyzed by SDS PAGE and western blot analysis. To decipher this differential

electrophoretic mobility of the CP, the samples were checked to see if they were post-translationally modified. MSV-N geminate capsid at pH 7.2 was exposed to a sequential increase in concentration of DNase (Promega, cat # M10A) and calf intestinal alkaline phosphatase (CIAP) (Invitrogen, cat #18009-019). CIAP was used to digest any available phosphate in both the geminate capsid and disassembled geminate capsid at pH 7.2 and the DNase was used to degrade any unprotected DNA. The recommended starting concentration of CIAP is 10units for 10μM of protein and for DNase it is 1unit to 10μg of DNA. The samples were allowed to incubate at 37ºC for 1hr before loading unto a 12 % SDS gel. To check if the CP is phosphorylated as well as if it binds DNA, the samples were treated with both CIAP and DNase. The MSV-N sample was then treated with 20units DNase for 1 hr at 3º C, followed by 80 units of CIAP and the mixture was allowed to incubate at 37ºC for 1hr before it was loaded on a 12% SDS gel.

Baculovirus MSV-N (Wildtype (wt) and Mutant (mt)) CP Production and Purification

To clone MSV-N CP (wt and mt) into the Spodoptera frugiperda (sf9) insect cells, the genome sequence of MSV-N CP wt (MSV-NCP), MSV-N CP mutants K182V (MSV-NCP182), and N-terminal truncation (MSV-NCP201) were digested from *Eschericha* Coli (E. coli) pET vector (101) and ligated into a pFAST baculovirus transfer vector. The recombinant transfer vector is then homologously recombined in a specialized E.coli vectors (DH10 Bac) which contains the bacmid genome. The expression protocol was used according to the manufacturer's protocol (Invitrogen, cat#10359-016).

The recombinant baculovirus MSV-NCP (BMCP), MSV-NCP182 (BMCP182) and MSV-NCP201 (BMCP201) were transfected into sf9 insect cells. The innoculum was then amplified and used for subsequent sf9 infection.

Cloning of MSV-N Recombinant Donor Plasmid (pFastBac)

The components of the transfer vector pFastBac are illustrated in figure 4-1. The vector is controlled by the Autographa Californica Multiple Nuclear Polyhedrosis Virus (AcMNPV) polyhedron promoter. The expression cassette is flanked by the left and right arms of Tn7, it also contains a gentamicin resistance gene and a SV40 polyadenylation signal. The restriction enzymes EcoRI and XbaI were used to extract the region of the pFast Bac ORF that will accommodate the MSV-NCP, MSV-NCP182and MSV-NCP201 genes. 5 µg of pFastBac was digested with EcoRI and XbaI in a 50µL total volume. The MSV-NCP and MSV-NCP182 were released from the pET vector using the restriction enzymes BamH1 and XBa1 while the MSV-NCP201 was digested with BamH1 and Nde1. The newly generated protruding ends were blunted using Klenow fragment and incubated for 15 min at room temperatue. The blunt ended pFast Bac was further dephosphorylated with CIAP and purified by phenol chloroform extraction and ethanol precipitation. The pFastBac and the MSV-NCP, MSV-NCP182and MSV-NCP201 genes were ligated with DNA ligase (NEB, cat#M0202S). 1µL of ligation mixture was used to transform electrocompetent JM109 cells. The recombinant donor bacmid PMSV-NCP, PMSV-NCP182and PMSV-NCP201 genes were screened on gentamicin agar plates and their proper orientation determined by BamHI, FspI and NcoI restriction enzyme analysis.

Transformation of DH10 Bac *E.Coli* Cells

DH10 Bac *E. coli* cells were purchased with the Bac-to-Bac Expression Systems (Invitrogen cat#10359-016). The DH10Bac *E.coli* contains a baculovirus shuttle vector (bacmid) and a helper plasmid. The Bacmid is specialized as it contains a mini-attTn7 target site adjacent a lacZ αpeptide encoding a gene. The helper plasmid encodes a transposase as well as tetracycline resistance. The key feature of this DH10Bac Ecoli is that it facilitates the transposition of the PMSV-NCP, PMSV-NCP182 and PMSV-NCP201 into the recombinant Bacmid by homologous

recombination between the pFastBac (Tn7) and the mini-attTn7 Bacmid. The main advantage of this cell is the ability to generate blue and white colonies depending on whether the MSV-N gene is inserted into the bacmid gene segment that encodes Lac Zα peptide. This is the basis of the blue and white screen. Lac Z is the enzyme that interacts with galactosidase which is a component of bluo gal (Invitrogen cat#15519-028). This reaction causes the substrate and consequently the colony to look blue. If the PMSV-NCP gene is inserted in the Bacmid then the colony generated will be white, but if it is not properly inserted into the Bacmid then, Lac Z will be expressed and the colony will be blue.

5ng of recombinant PMSV-NCP, PMSV-NCP182 or PMSV-NCP 201was added to 100µL of DH10Bac cells in a pre-chilled 15ml round-bottom polypropylene tube, the cells were gently mixed then incubated on ice for 30min. The cell and DNA mixture were then heat shocked for 45sec at 45ºC then immediately transferred to ice and chilled for 2min. 900µL of S.O.C medium (Invitrogen cat.#15544-034) was added to the newly transformed cells. The tube containing the transformants was shaken for 4hr at 225rpm. The transformation mix was then serially diluted and 100µL of each dilution plated on Luria broth (LB) agar plates containing 50µg/ml kanamycin, 7µg/ml gentamicin, 100µg/ml bluo-gal, and 40 µg/ml IPTG (bluo-gal plates). The plates were incubated for 48 hr at 37ºC and white colonies were picked and restreaked on fresh bluo-gal plates and incubated overnight at 37ºC. Once the phenotype was confirmed, the clone was used to inoculate LB medium containing 50µg/ml kanamycin, 7µg/ml gentamicin with a shaking speed of 250 rpm for 24 hr at 37º C. 1ml of the cells were harvested in a 1.5 ml microcentrifuge tube by centrifugation. The supernatant were then removed by aspiration and the cells gently resuspended in 0.3 ml of solution I (15mM Tris pH 8.0; 10Mm EDTA, 100-g/ml RNase A), mixed gently with 0.3 ml of solution II (0.2M NaOH, 1%SDS), then incubated for

5min at room temperature. 0.3ml potassium acetate (3M, pH 5.5) was slowly added and the contents of the tube was gently mixed and incubated for 10 min. After centrifugation at 14000xg for 10min, 1:1 ratio of the supernatant will be mixed with isopropanol and kept on ice for 10 min. The DNA was precipitated after centrifugation with 0.5 ml ethanol and the sample air dried. The bacmid was resuspended in 40µl of Tris-EDTA, pH 8.0 and analyzed by agarose gel electrophoresis. The purified BMSV-NCP, BMSV-NCP182 or BMSV-NCP201 was used to transfect sf9 cells to generate P1 stocks.

Transfection of sf9 Cells

1µg of purified bacmid DNA was added to100µL unsupplemented Grace's medium was added to a mixture of cellfectin (6µL) and unsupplemented media (100µL). The mixture was then incubated for 45 min at rt, it was then added to the 6 well tissue culture plate containing 0.5 x 10^{6} sf9 cells and 0.8 ml of Grace's medium. The cells were allowed to incubate for 5 hr and then the DNA:Cellfectin mix removed. 2ml sf9 medium was then added to the cells and it was allowed to incubate for 72 hr. The 2ml of media contained the recombinant bacmids and the sample represents the P1 viral stock. The schematic for the Baculovirus cloning and expression of BMSV-NCP, BMSV-NCP and BMSV-NCP is illustrated in Figure 2-2.

Baculovirus MSV-N CP Expression

The P1 viral stock was amplified to P2 then P3 using a moi of 0.1. The P3 viral stock was then used to infect 300µl of sf9 suspension cells at a moi of 5 for 72 hr in a 24 well dish. 300µL of cells were collected 0hr, 24hr, 48hr, and 72hr. The cells were harvested and resuspended in lysis Buffer (50 mM Tris, pH8.5, 20mM EDTA, 0.15 M NaCl, and 1%w/v Triton X-100), 50mM Tris pH 8.5) and recombinant BMSV-NCP, BMSV-NCP182 or BMSV-NCP 201 proteins released from the cells by 3 freeze thaws. The cell lysate was then clarified by centrifugation at

10,000 rpm for 15 min. The expressed proteins in the cell lysate were analyzed by SDS-PAGE with coomassie blue staining and western blot analysis.

Baculovirus MSV-N CP Purification

Two methods were utilized to purify MSV-N from the clarified cell lysate. The first method attempted was the use of a 5ml HiTrap SP column (GE Healthcare, cat#17-5158-01). This method was selected based on the reported pI of MSV-N which is 10.8 and higher than what is reported for most known proteins and so would selectively bind the SP column at a pH below its pI. The cell lysate was diluted 2x with Buffer C (20mM Tris pH=8.5 and 15mM NaCl), loaded onto a SP column that was previously equilibrated with 25ml of Buffer C, and at a flow rate of 2.5ml/min. The column was washed with 50ml of Buffer C then eluted with 50 ml Buffer D (20mM Tris pH=8.5 and 1M M NaCl) at 2.5ml/min. All the samples were checked for the presence of MSV-N by western blot analysis. The second method attempted was the use of ammonium sulphate precipitation. The proteins were salted out of the cell lysate by sequentially adding 10% $(NH_4)_2SO_4$, stirred at 4^0C for 30min, and centrifuged at 5,000xg for 30min. The expressed proteins in the cell lysate were analyzed by SDS-PAGE with coomassie blue staining and western blot analysis.

Purification of Baculovirus AAV2 VP1-3

Cell Culture and Virus Infection

The recombinant baculovirus vector containing AAV2 VP1-3 was donated by Sergei Zolotukin (Gene therapy Center, University of Florida). An appropriate volume of the recombinant bAAV2 was used to infect sf9 cells maintained at 2.0 x10^6 cells/ml of suspension at 27^0 C. The cells were harvested 72hr post infection by centrifugation at x1100g for 15min and the pellet collected.

Virus Purification

The recombinant AAV2 was purified according to the published protocol (101). The pellet was resuspended in lysis Buffer (150 mM NaCl, 50mM Tris, pH8.5) and freeze thawed 3x in a dry ice-ethanol slurry and 37^0C water baths. 1µl Benzonase (Sigma, cat#E1014) was added to the cell lysate (50 U/ml final concentration) and incubated for 30min at 37^0C. The crude cell lysate is clarified by centrifugation at 4000xg for 20min and the clarified supernatant was then loaded onto a discontinuous 15-60% iodixanol step gradient prepared from Optiprep (Nycomed, cat#1114542). The iodixanol gradient was then centrifuged at 350,000xg for 1hr at 18^0C. The gradient was fractionated and the fractions containing VP1-VP3 determined by Western blots probed with B1 as primary antibody(178). The fractions from the higher percentage iodixanol gradient (40/60%, 40%, 40/25 and 25%) were further purified on an anion exchange 5ml HiTrap Q column (GE Healthcare, cat#17-5159-01). The clarified cell lysate was diluted with 2xBuffer E (20Mm Tris, 15mM NaCl, pH8.5) loaded onto the column at 2.5ml/min, washed with 50 ml Buffer E, and the sample was eluted with 25 ml Buffer F (20Mm Tris, 15mM NaCl, pH8.5). The fractions were collected and biophysically characterized. The schematic for the purification of Baculovirus AAV2 VP1-3 is illustrated in Figure 2-3.

Biophysical Characterization of AAV2 VP1-3 Components

These techniques are the same as those used for the characterization of MSV-N and so the main focus of this section will be on the use of the reagents relevant to AAV2.

SDS Gel Electrophoresis and Immunoblots

The primary antibody used for the detection of VP1-3 is B1 diluted 1:3,000and it recognizes an epitope in the C-terminus of VP3. A20 and C37 were used to detect the conformational epitope present on assembled capsid. The secondary antibody used to detect B1, C37 and A20 is the anti-mouse antibody diluted 1:5,000. The AAV2–antibody complex was

detected with the ECL substrate (Amersham, cat#RPN2109). The immunoblots were treated as both denatured and native dot blots as the names suggest the native samples were unboiled and the denatured samples were boiled for 5min at100^0C.

The Production and Characterization of AAV2 VP1-3 Mutants

The production and biophysical characterization of AAV2 assembly mutants is divided into 4 parts. The first part is the visualization and structural comparison of the dimer, trimer and pentamer of AAV2 and MVM by using their crystal structures. The second part is the site directed muatagenesis of the VP. The third part is the transfection of the Human Embryonic Kidney 293 cell line (HEK 293 cells) to express the mutant proteins. The fourth part is the biophysical characterization of the expressed mutant VP.

Selection of residues for mutagenesis

Symmetry operators were used to generate the dimers, trimers and pentamers of AAV2, MVM and MSV-N in the program O. The co-ordinates for the monomers of AAV2 and MVM were accessed from the protein database (PDB, accession #s 1LP3, 1Z14, respectively). The coordinates for the dimer, trimer, and pentamer interface were then written in the PDB format and saved. Input files for CNS were then generated and SEGID ID created for each interface. The data was then merged using the CNS subroutine called ‘merge’. A table of the interface residue distances was then generated in the CNS subroutine called ‘contact’, the maximum cut off distance used was 3.2 Å. Pymol was used to generate the images of the monomers, dimers, trimes and pentamers. A list of 19 mutants was generated based on residues that were structurally conserved between AAV2 and MVM. Another 4 residues were selected based on residues that were identified in previous mutagenesis studies that were believed to be important for AAV2 assembly (20, 57, 58, 165).

Site Directed Mutagenesis of AAV2 VP3

The AAV2 plasmid pIM45 was used as a template for site directed mutagenesis. Site directed mutagenesis was performed according to the Stratagene site directed mutagenesis kit (Strategene, cat#200524). The primers were generated with silent mutation including a specific restriction enzyme site to facilitate the screening of the PCR clones generated. The PCR product was then digested with DpnI to remove the parental DNA. The clones were selected based on ampicillin resistance and the restriction enzyme screen. Positive clones were sequenced and the mutated gene sub-cloned into the pIM45 backbone to eliminate any background mutations.

Cell Culture

HEK 293 cells were maintained in Dubelcco's modified Eagle 's medium supplemented with penincillin and streptomycin at 100U/ml and 10% FBS and they were maintained in $15cm^3$petri dish at 37^0C and 5% CO_2.

Transfection and Recombinant AAV2 Production

The mutants for AAV2 were generated by site-directed mutagenesis in the non-infectious AAV plasmid pIM45 template (Figure 2-6) which contains all the AAV2 DNA sequence except the two terminal repeats required for DNA packaging(112). To produce rAAV with mutant capsid protein, 293 cells were triple transfected with mutant pIM45 (18µg), pXX6 (54µg) which contains the adenovirus helper genes (167), and pTRUF11 (18µg) which contains the green fluorescent protein (gfp) driven by the CMV promoter and the AAV terminal repeats required for packaging (85). Transfection will utilize 293 cells at 75% confluency mixed at 3:1:1 ratio of the three plasmids (pXX6:pIM45: pTRUF11) respectively. The plasmids were Cesium Chloride (CsCl) purified and used to transfect the cells by calcium phosphate precipitation, and incubated for 48hr at 37^0C. The cells were then harvested by centrifugation at 1,140xg for 20min and the pellet resuspended in 10 m lysis Buffer (0.15 M NaCl, 50mM Tris-HCl pH 8.5).The virus was

then released by three freeze/thaws and treatment with benzonase to remove nucleic acid. The lysate was clarified by centrifugation at 3,700xg for 20min and was further purified by a step iodixanol gradient and ion exchange chromatography. The purification is described in the Baculovirus expressed AAV2 purification section.

Biophysical Characterization of AAV2 VP1-3 Mutants

The characterizations of the AAV2 mutants generated were divided into two main sections. The first section includes immunoblots, A20 Elisas, RT-PCRs, and GFP assays of the cell lysate. The second section includes the purification by iodixanol gradient and visualization by EM of mutant capsids and subassemblies.

Gel Electrophoresis and Immunoblots

The crude cell lysate was analyzed similar to the purification of AAV2 baculovirus expressed VP. The only additional detail was the use of the 1F antibody to determine the expression of the replication protein.

Total Virus Capsid, Genome and Infectivity Quantification

Total capsid titer was determined by A20 enzyme-linked immunosuorbent assay (ELISA) according to the manufacturer's instruction (American Research Product, cat#PRATV). The clarified cell lysate were serially diluted and 100µl added to the kit well. The readings that were within the detection limit of the kit were used to calculate the both empty and full particles.

Total packaged genome or copy number was determined by real time PCR (RT-PCR). 20 µL of crude lysate was treated with DNAse1 for 1hr at 37^0C to degrade any DNA that is not encapsidated and each sample was digested with 4µl proteinase K (Roche, cat#1373196), 20µL of 10 x proteinase K Buffer (10mM Tris HCl pH 8.0, 10mM EDTA, 10% SDS) and the solution diluted with sterile distilled water to a total volume of 200µl. The mixture was incubated for 1hr in a water bath at 37^0 C, treated twice with an equal volume of phenol chloroform (Roche,

cat#1373196), and the upper aqeous layer transferred to a clean eppendorf after each extraction. The aqueous fraction was then treated with chloroform (Fisher cat#C298-500) and the aqueous layer transferred to a clean eppendorf. The DNA was precipitated overnight at -20^{0}C, after adding 10% NaAc pH5.2, 1µl glycogen, and 3xvolume of 95% ethanol. The sample was then pelleted for 20min at 13050xg. The pellet was air dried and resuspended with 20 µl water. 1µl of the viral DNA, 1µl of primers (forward and reverse) to GFP, 12.5µl of iQ SYBR Green Supermix which contains Taq DNA polymerase.(Biorad, cat#170-8882) was combined to a total volume of 25µL with sterile water. The sample was run on the Biorad my IQ system.

The infectvity or infectious units/ml of mutants was determined by GFP Assay (165). The crude cell lysate was serially diluted with DMEM containing Ad5 at a moi of 10, and a 100 µL of each dilution was added to the 80% confluent HEK 293 cells, that were grown in a 96 well plate. The cells were then incubated for 24hr at 37^{0}C and the number of green cells for each dilution counted using the fluorescent microscope.

AAV2 Capsid Wildtype and Mutant Purification

The wt and mt cell lysates were loaded onto a discontinuous 15-60% iodixanol step gradient prepared from Optiprep (Nycomed, cat#1114542). The iodixanol gradient was then centrifuged at 350,000xg for 1hr at 18^{0}C. The gradient was fractionated and the fractions containing VP1-VP3 determined by denatured dot blots probed with B1 as primary antibody (162). The fractions from the higher percentage iodixanol gradient (40/60%, 40%, 40/25 and 25%) were further purified on an anion exchange 5ml HiTrap Q column (GE Healthcare, cat#17-5159-01). The clarified cell lysate was diluted with 2xBuffer E (20Mm Tris, 15mM NaCl, pH8.5) loaded onto the column at 2.5ml/min, washed with 50 ml Buffer E, and the sample was eluted with 25 ml Buffer F (20Mm Tris, 15mM NaCl, pH8.5). The fractions were collected and

biophysically characterized. The schematic for the production, purification, and characterization AAV2 mt and wt is illustrated in Figure 2-4.

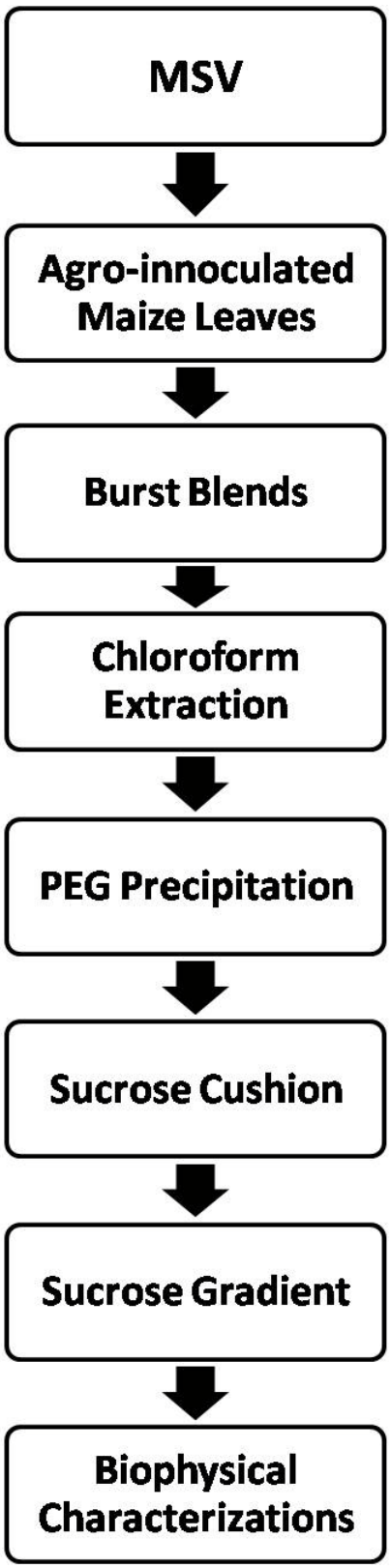

Figure 2-1. Schematic of MSV-N CP components purification and characterization.

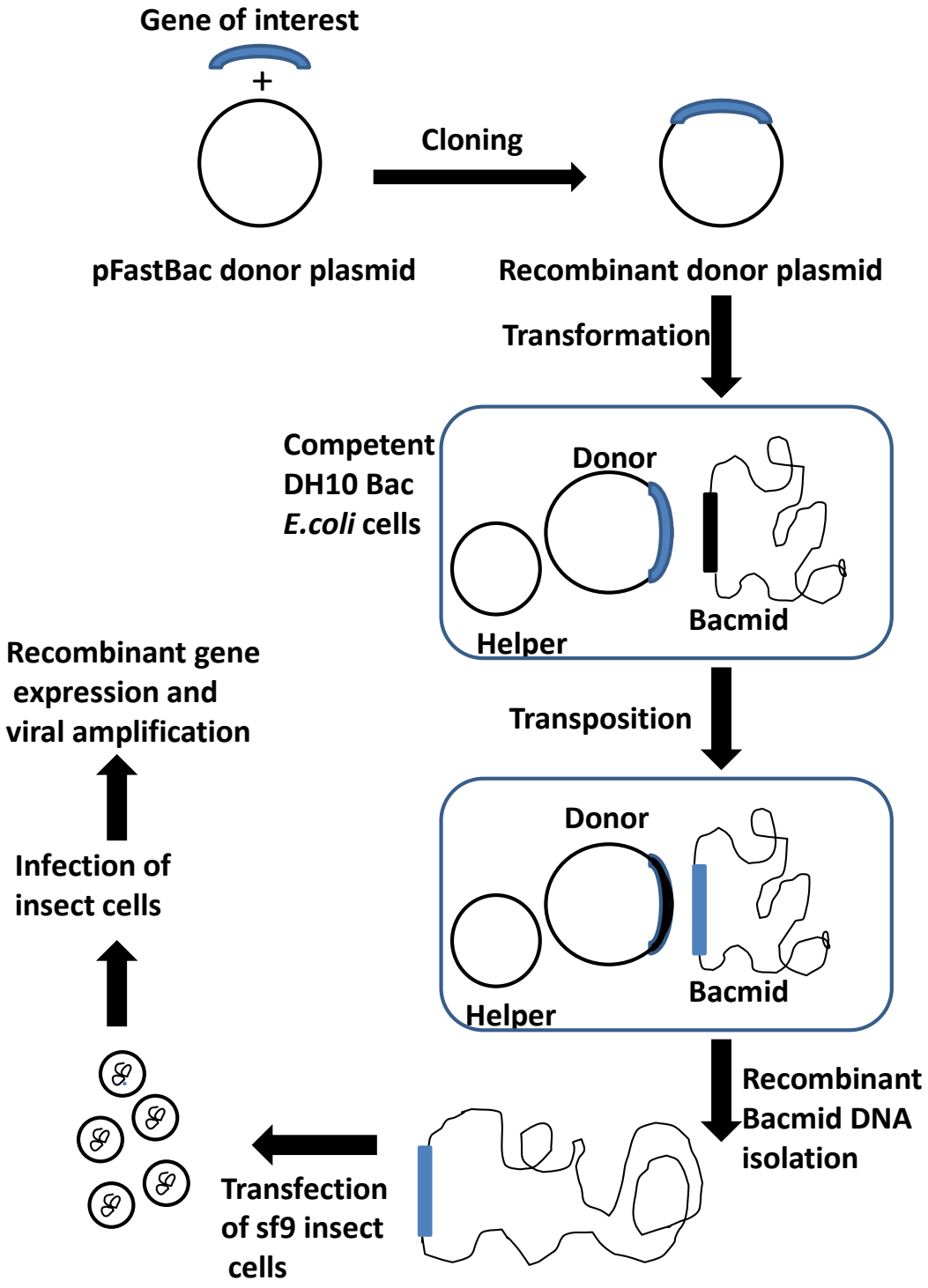

Figure 2-2. Diagram of the production of recombinant MSV-N CP (wt and mutants).

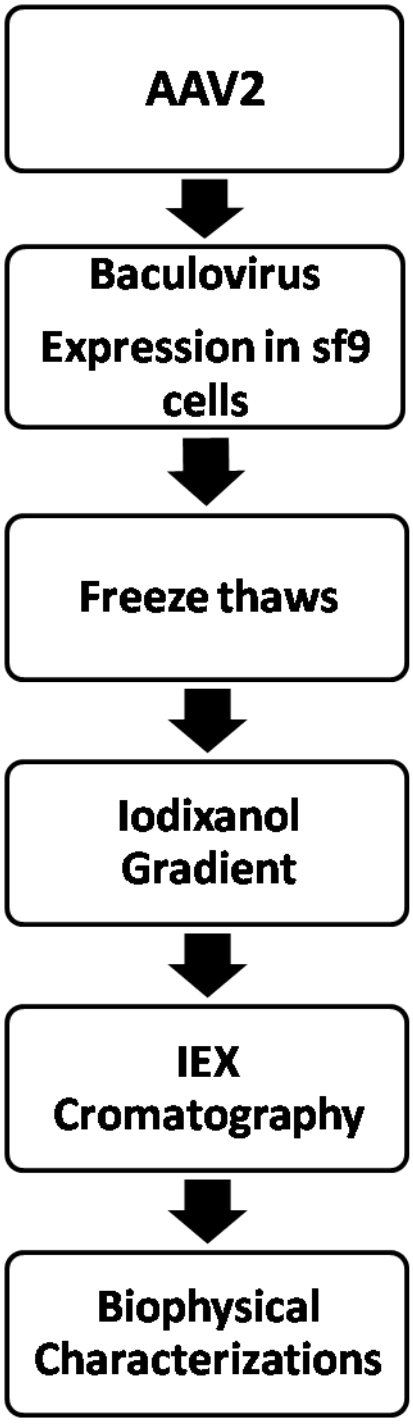

Figure 2-3. Schematic AAV2 VP components purification and characterization.

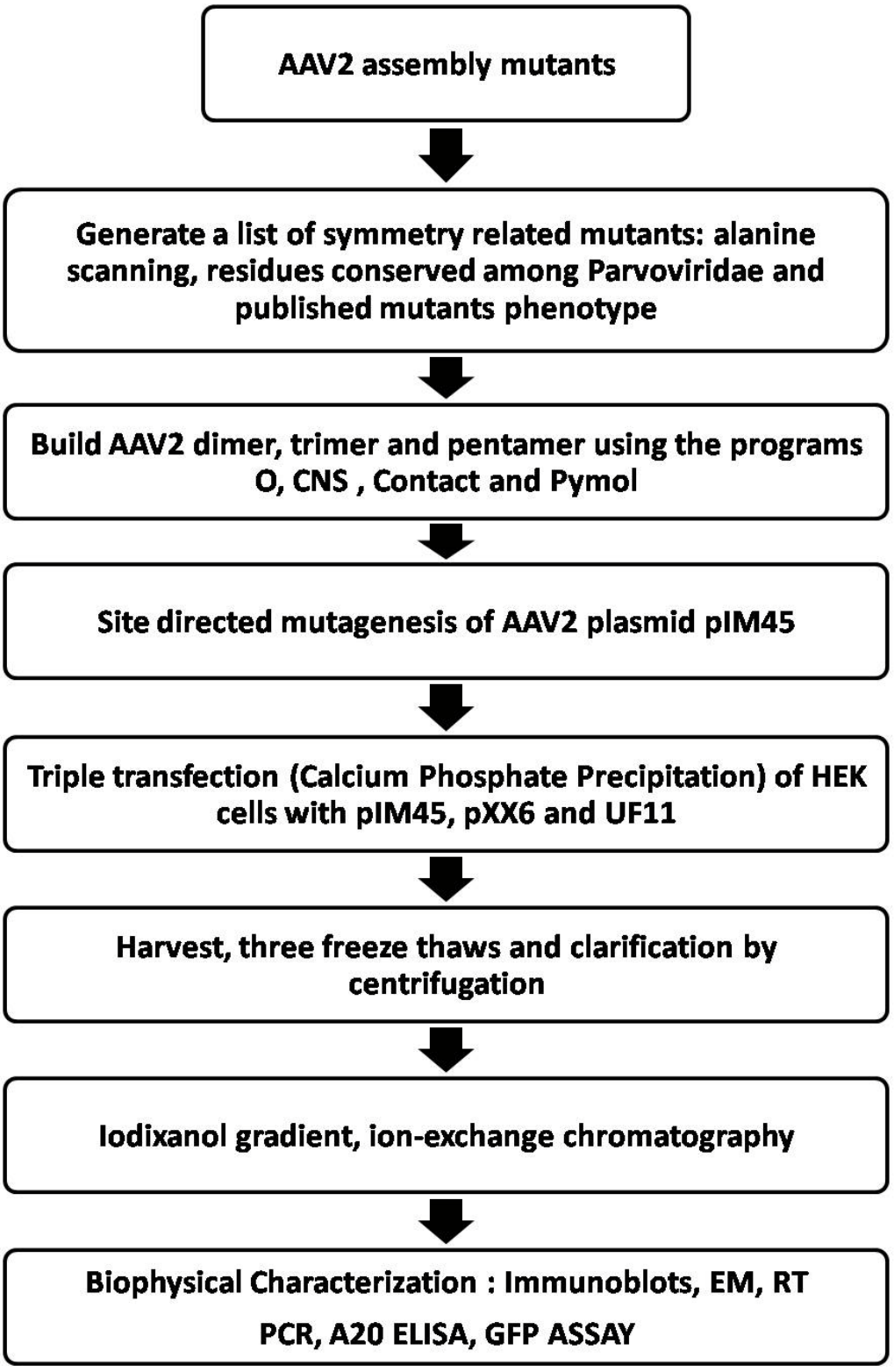

Figure 2-4. Schematic of the production, purification and characterization of AAV2 symmetry related mutants.

CHAPTER 3
MSV-N ASSEMBLY/DISASSEMBLY COMPONENTS

Introduction

MSV-N is a prototypic *Mastrevirus* and it causes the devastation of maize crops in sub-Saharan Africa. The architecture of MSV-N is a quasi-isometric (geminate), pseudo T=1 icosahedral shell which is formed by 110 copies of the CP. The MSV-N capsid encapsulates a circular ss DNA genome which is 2687 nucleotides in length (67, 93, 115). The MSV-N genome encodes four proteins and they are all required for viral infection. Rep and RepA are the early gene products and they are responsible for the viral DNA replication (94). The other two proteins are the CP (27kDa) and the MP (10.9kDa), which are expressed later in infection. The MP is important for the long distance transport of the virus and the CP is necessary for the accumulation and encapsulation of the viral ssDNA (22, 25, 94). To date MSV-N is one of the most extensively studied Geminivirus. This study is focused on understanding the mechanism by which the MSV-N capsid assembles and disassembles during its replicative life cycle.

The life cycle of MSV-N is illustrated schematically in Figure 3-1. MSV-N is transmitted to *Cicadellidae mbila,* during an acquisition probe into the maize plant mesophyll during feeding. The ultimate goal of the *Cicadellidae mbila* is that its stylet reaches the phloem where it acquires a liquid meal. The virus containing meal is then transported to the bucal cavity where powerful muscles in the pharynx transport the liquid meal to the esophagus. It has been proposed based on viral vector specificity that MSV-N is then internalized by cells of the vector's filter chamber by receptor mediated endocytosis. The aggregated virus is then enveloped in the endoplasmic reticulum. It has also been proposed that MSV-N is then transcytosed into cells of the ventriculus (foregut) with inclusions breaking off into the hemolymph. MSV-N is then transported across the insect's gut lining into the hemocoel and eventually the salivary glands via

specialized secreatory cells. MSV-N is introduced into the cytoplasm of the phloem cell of an uninfected plant host, from the infected vector, during feeding (111). The geminate capsid has been shown to travel within the plant host in what is described as a phloem limited pathway (28). It is not known whether disassembly occurs in the maize cell cytoplasm or the nucleus. It is believed that the viral genome, once it is released from the capsid is replicated via a dsDNA intermediate. The mechanism by which the virus genome is uncoated and delivered to the nucleus is not known. Replication has been shown to occur in the nucleus by a rolling circle mechanism and utilizes a ds DNA replicative as well as host enzymes. The dsDNA is bidirectionally transcribed to produce both viral and complimentary strand transcripts (113, 115). The complimentary strand transcripts are translated to form replication proteins Rep and RepA, and the viral strand transcripts from both the CP and the MP (101, 103). The translated viral proteins are transported to the nucleus where it is believed the unique geminate capsid is assembled. The mechanism by which the geminate capsid assembles is not known. This data begs the question "what are the steps involved the assembly of the geminivirus capsid?" The first part of this chapter will report results from efforts to characrterize the components assembled from the MSV-N CP and its genome. This includes the isolation and purification of pentameric intermediates as well as single and geminate capsid.

It has been previously reported that certain viruses assemble and disassemble with a change in their environmental pH, CP concentration and ionic strength (177) (147). Based on this information and what is known about the environmental conditions encountered by MSV-N geminates within its host and vector; purified MSV-N geminates were exposed to varying concentrations of Ca^{2+}, Na^{+} and pH. In this chapter we will show that intact geminate virus disassembles and reassembles reversibly in the presence of increasing and decreasing pH,

respectively. The information obtained forms the basis for a model developed to explain the assembly and disassembly of MSV-N geminate capsid with changes in environmental pH. This assay may be used to test MSV-N assembly inhibitors or capsid stabilizers.

Results

MSV-N Wt Components Purification and Characterization

MSV-N Wt Components Isolated

To identify MSV-N CP and CP-DNA components isolated in agro-inoculated maize plants, infected leaves were purified according to the protocol described in the materials and methods section in Chapter 2. There were three gradient fractions that contained MSV-N CP components in the sucrose gradient. These were at the 8-10% interface, between the 14 and 16%, and 25% to 30% sucrose gradient fractions and these bands were enriched with MSV-N intermediates characterized as capsomers singles, and geminates, respectively. They were visualized by negative stain EM (Figure 3-2A). Western blot analysis and coomassie stained SDS-PAGE confirmed that the three different size components isolated were composed purely of MSV-N CP (Figure 3-2B).The capsomers, singles and geminates had CP species with different electrophoretic mobility. Two MSV-N CP bands were observed at approximately 27 and 29kDa for the capsomer while only one main band at 29kDa was observed for the singles and geminates. In some preparations (not shown) the single capsid samples also contains a small portion of the faster migrating CP.

MSV-N Wt Components Genome Extraction

To determine if the geminates, singles and capsomers are associated with DNA, they were protease treated and DNA extracted by phenol chloroform. The DNA was precipitated using ethanol and the genomic material visualized on an agarose gel. The results show that the

capsomers are not associated with any detectable genome, compared to the assembled singles and geminate which encapsulate sub genomic and genomic material, respectively (Figure 3-2C).

Native Polyacrylamide Gel

To determine the approximate molecular mass of the purified capsomer, a native polyacrylamide gel calibrated with three known protein standards whose molecular masss are 66kDa, 150kDa, and 200kDa was used. The protein bands obtained would indicate that there are two capsomeric components with different molecular masses. The most abundant capsomer has an approximate molecular mass of 150kDa and the less abundant capsomer has a molecular mass greater than 200kDa (Figure 3-2D).

Size Exclusion Chromatography

Size exclusion gel filtration chromatography was used to more accurately determine the molecular mass of the purified capsomer. A superose 6 analytical column was calibrated with the same proteins used in the native gel, as well as, carbonic anhydrase (30kDa), apoferritin (400 kDa) and Blue Dextran (2000kDa). Using the calibration equation in (Figure 3-3A), the elution volume of each MSV-N intermediate was then used to calculate its approximate molecular mass. The calculated molecular mass of the capsomer is 157.7kDa. As described above, there are two MSV-N CP species observed in a SDS-PAGE for the capsomeric sample, one migrating at approximately 29kDa and the other at approximately 27kDa (Figure 3-2A). The calculated molecular mass of a pentamer (5CP) containing the 27kDa or 29kDa CP is approximately 135kDa or 145kDa. This suggests that the approximately 157.7 kDa specie observed by the size exclusion chromatography analysis is likely to be a pentamer.

Dynamic Light Scattering (DLS)

DLS was used to experimentally determine the diameter of the MSV-N geminate, singles and capsomers. The diameter of the capsomer was shown to be approximately 8nm, the singles

were approximately 20nm and the geminate capsid approximately 20-40nm (Figure 3-3B). This data is consistent with the sizes measured from the cryo-EM reconstructions of the single and geminate capsid structures and the models built into the reconstructed densities ((173) Reutzel unpublished data).

STEM Analysis

To further visualize the structures and confirm the molecular mass of the different MSV-N components, they were sent to the Brookhaven National Laboratory for STEM analysis. The statistical results are presented as histograms (Figures 3-5 to 3-8) and numerical data (Table 3-1). The shape of each component was visualized on STEM micrographs (Figure 3-4). For the capsomeric components two different samples were sent for analysis: a “fresh” sample (C1) which was sent two to three days post purification and an “old” sample (C2) which was at least one month old (Figure 3-4). The C1 sample contains predominantly capsomers and the C2 samples contain predominantly interacting capsomers. The singles and geminates structures are consistent with what was already observed by negative stain em. The molecular mass distribution for the samples are presented as histograms (Figure 3-5 to 3-8) and in Table 3-1. The molecular mass of the C1 sample sample ranged from 54-512kDa, with a mean at approximately 193kDa and a standard deviation of approximately 64kDa (Table 3-1). This molecular mass is consistent with the size of seven CP. In consideration of the standard deviation which is approximately equivalent to two MSV-NCP and our previous molecular mass measurement by native PAGE and size exclusion chromatography, the mean could be interpreted as a pentamer plus a dimer. In the C2 sample the the molecular mass ranged from 27-898 kDa with a mean of 332 kDa and a standard deviation of approximately 165kDa (Table 3-1). This mean value is consistent with the size of 12 MSV CPs. Interestingly rather than a Gaussian distribution this sample clearly separated into three distinct peaks P1, P2, and P3 (Figure 3-6) at 162kDa, 297kDa and 513kDa,

respectively. This would correspond to building blocks or subunits that are pentameric. The mean molecular mass of the single sample is approximately 2210kDa (Table 3-1 and Figure 3-7). The molecular mass of the geminate capsid is 4,198kDa (Table 3-1 and Figure 3-8). These two masses with calculations based on the predicted number of CPs that assemble these capsids and their packaged genome. The calculated standard error for each data set was lower than 10% which is reported to be within the acceptable range (Table 3-1).

Discussion for MSV-N CP Purification and Characterization

Three stable components have been isolated from a wt infection. The data confirms what was already known about the molecular mass, particle dimensions, and genomic content of geminate single capsids (29).The capsomeric components appear to be assembled from from pentameric components with the three specie identified in the old sample characterized by STEM representing 5CPs, 10CPS, and approximately 20CPs. This interpretation was also supported by native gel electrophoresis and gel filtration. The DLS data provided structural measurement also consistent with a pentameric building block. These pentameric intermediates are not associated with any detectable genomic material. Interestingly, the capsomeric components contain two CP specie, one consistent with the calculated molecular mass at 27kDa and the other at approximately 29kDa (Figure 3-2B). The observation that the assembled geminate and single capsids contain predominantly the larger molecular mass CP, suggests the requirement for a CP modification for assembly (29).

MSV-N Assembly/Disassembly Assay

MSV-N pH Components Isolated

To determine the effect of different environmental conditions on the stability of the MSV-N geminate capsid, it was exposed to increasing pH, and different concentrations of Ca^{2+}, Na^{+} and EDTA. The viral capsid disassembled in increasing concentration of pH, Ca^{2+}, Na^{+}, but was

unaffected by EDTA (data not shown). The data for change in pH which recapitulates conditions encountered in the insect vector (pH4.5-5.8) and plant host cell (pH7.4) are discussed (Figure 3-1). The pH assay shows that the geminate virus appears intact from pH 4.8- pH 6.0. The virus then starts to disassemble at pH 6.4 and completely falls apart by pH 7.2 (Figure 3-9A). If the disassembled virus is returned sequentially to its original pH of 4.8, there appears to be the formation of reassembled geminate capsids (RG) singles (RS) and capsomers (RC) (Figure 3-9B). These three components appear to be similar to those isolated in the wt infection. It should be noted that negative control geminates were transferred every 24 hr to a freshly made final Buffer (0.1M NaAc pH4.8) and at the end of the assembly /disassembly assay the sample that was kept in Buffer at 4.8 was viewed by EM and the geminate capsids were still intact. The MSV-N CP species observed on a SDS-PAGE for the virus at pH6.4 and pH7.2 was consistent with the differential electrophoresis mobility observed with capsomers isolated from the wt infection (Figure 3-10A). A SDS-PAGE of the purified reassembled geminate and single capsid contained predominantly the higher molecular mass CP specie (Figure 3-10A).

MSV-N pH Components Genome Extraction

The genome extracted from the sample at pH6.4 and 7.2 was a mixture of the complete genome (2.7 kb) and a smear (Figure 3-10B). Thus would imply that the increasing pH results in the release of the of the encapsulated genome aaand the also results in the sharing following deprotection. The RS and RG sample contained some full length genome and a smaller proportion of sheared DNA (Figure 3-10), while the RC sample was devoid of any DNA. Thus while the RC and RG recapitulates the the geminate and capsomers isolated in the wild type infection, the RS is able to associate with full length genome. This observation may be due to the fact that DNase was not used to remove unencapsulated genomic material prior to purification.

MSV-N pH Components STEM Analysis

STEM micrographs of the different components observed at pH6.4 and 7.2 and the different reassembled components are shown in Figure 3-11. The predominant size of the disassembled MSV-N CP specie at ph 6.4 had a median and modal molecular mass ~ 291 kDa and 270kDa respectively (Figure 3-12 and Table 3_2), consistent with that of 10 MSV-N CP at 27 kDa each.. The molecular mass of the geminate at pH 6.4 is consistent with that of 10 CP at 29 kDa for each CP. The sample at pH 7.2 was too aggregated, even when diluted, to be adequately analyzed. The distribution of molecular masses for the RS and RG samples are illustrated in Figure 3-13 and Figure 3-14, respectively and detailed in Table3-2. The mean, median and modal molecular mass values for the RS were ~ 1643, ~ 1616, and ~ 1620, respectively. These values are consistent with a capsid assembled from 60CPs of 27kDa without genomic material. This suggests that the DNA isolated form this sample reported above, is likely just a co-purification artifact. The mean, median and modal molecular mass values for the RG were ~ 3168, ~ 3185, and ~ 3240, respectively. These sizes are all smaller than that observed for the wt geminate capsids. Assuming that genomic interaction is required for geminate capsid assembly, as has been reported, the smaller molecular mass suggests that this capsid assembly contains lessthan 110 copies of the CP, and is missing approximately 7 pentameric capsomers.

MSV-N pH Assembly/Disassembly Assay in the Presence of Protease Inhibitor

To determine if (i) the smaller size of the RS and RG and (ii) the two CP species observed for the RC and due to protein cleavage, the pH assembly/disassembly assay was repeated in the presence of protease inhibitors. Following disassembly with increasing pH, which mimicked the process in the absence of protease inhibitors, the reassembly conditions produced a much smaller number of RS (Figure 3-15A last panel). Western blot analysis showed the presence of a double CP banding pattern for the pH 6.4 and 7.2 samples while the purified reassembled sample

(pRSG) which contains both single and geminate capsids, showed only the larger molecular mass CP (Figure 3-15B).

The STEM micrographs (Figure 3-15C), as well as the resulting histograms (Figure 3-16 and 3-17), also showed that the reassembled sample contains fewer singles compared to the samples reassembled without protease inhibitor. The mean molecular mass of the pRS is 2204 kDa which is very similar to the wild type singles (Table 3-3). The molecular mass of the reassembled geminates with and without protease inhibitor and the wt geminates is given in Table 3-3. The molecular mass of the reassembled geminates in the absence of protease inhibitor is the smallest of all three samples analyzed. The reassembled geminates in the presence of protease inhibitors have a higher molecular mass than the reassembled geminates formed in the absence of protease and contain nine more CPs. Thus, despite the increase in molecular mass, these geminate capsids are still significantly smaller than wt capsids. These observations suggest that a host component may be required to play a role in the successful wt capsid assembly.

Discussion of MSV-N pH Disassembly/Reassembly Assay

MSV-N geminates disassemble when there is an increase in environmental pH and reassemble when the pH is decreased. These observations are likely to be relevant to events that occur in a wt infection. The introduction of the geminate capsid into the maize leaf cytoplasm (pH7.4) likely facilitates the disassembly and the release of the viral genome for replication.The translated viral protein likely assembles into geminate capsids provided they are exposed to pH4.8 and they interact with ssDNA. Geminate capsid assembly in the presence of protease inhibitor is still missing several CPs, this would imply that either host factors may be required or the effective CP concentration in the assay is less than optimal to replicapitulate the *in vivo* assembly conditions.

Post translational Modification

The question of the differential electrophoretic mobility of the intermediate MSV-N CP species isolated components was first addressed by Casado 2004 (29). Mass Spec Analysis (MS-MALDI-TOF) was used to identify the two species observed as MSV-N CPs. The C and N-terminal 5 amino acids were blocked and could not be resolved. However based on peptide mass measurements it was predicted that that the CP may be post translationally modified by either myristoylation, phosphorylation or glycosylation were unresolved, but based on the mass measurements it was predicted that MSV-N-A may be myristoylated, phosphorylated or glycosylated (29).

Post- Translational Modification Determination

To address the question of the potential post translational modification of the MSV-N CP we hypothesize that if geminate capsid assembly requires CP post translational modification then either the capsid contains an auto-regulatory region/domain, or it packages an enzyme, or the sample preparation is "contaminated" with a modifying enzyme. This enzyme function would thus explain the conversion of the lower molecular mass CP species observed in the pH6.4 and 7.2 samples to the larger migrating protein on pH decrease. A second hypothesis is that if this modification is reversed then the higher molecular mass CP species will be chased into the lower one. The two modifications tested were phosphorylation and the interaction with DNA. The two enzymes used to treat the pH7.2 sample (generated in the presence of pI) were CIAP and DNase 1 which facilitates dephosphorylation and DNA removal, respectively.In the presence of increasing concentration of CIAP very little change was observed in the intensity of the two CP species migration at ~.27kDa AND 29kDa, respectively (Figure 13-18). However at the CP band that migrates between 45 and 66kDa which is interpreted as being a CP dimer, a shift to a lower

molecular mass is observed, with the most dramatic shift observed at a CIAP concentration of 70U/µl (Figure 13-18)

Post-Translational Modification Prediction

The program Net Phos K was used to predict whether the CP was phosphorylated and more specifically what residues. The program is based on the assumption that if there are enough homologous proteins both in terms of sequence and structure, then it, predicts a consensus phosphorylation site. The access site is http://www.cbs.dtu.dk/services/NetPhosK/. The results indicate that there were not enough homologous proteins to MSV-N CP to predict a consensus phosphorylation sequence, but there was enough data about well known kinases to predict which residues may be phosphorylated. There are several substrate sites predicted for MSV-N CP, the highest score was Threonine 19 which had a score of 0.94 out of a maximum of 1(Table 3-3 and Figure 3-19). Several MSV-N CP samples were selected and submitted to MS to positively identify potential phosphorylation residues of MSV-N CP. The results obtained for MS were inconclusive, therefore using a phosphostain or specific antibody for phosphorylation is a part of the future directions.

Discussion

In this study we isolated and characterized several intermediates from maize plants agro-inoculated with MSV-N. These include the characteristic geminate capsid, a complete T=1 icosahedral (single) capsid, pentameric intermediates (capsomers) and possible dimers of pentamers (DOP) or pentamers of dimers (POD) and higher species. These data provide the information about the biophysical characterization of possible intermediates involved in geminivirus assembly/disassembly that can be correlated to the pH conditions encountered by the virus during it's life cycle that includes trafficking through their insect vector and the host plant.

This study also describes the development of an assay that can be used to test potential inhibitors of geminivirus assembly/disassembly.

The disassembly/assembly assay was discovered while trying to decipher the effects of different environmental conditions on the stability of the geminate capsid. The function of the vector is to transport the virus from one host to the next. There is no report of viral amplification in the vector. This information is consistent with our experimental observation which shows the geminate capsid is intact between pH 4.8-6.0. Thus given that observation the internal passage of the vector utilized by the virus is between (pH 4.5-5.8) the capsid is likely to remain intact during transmission and assembly. If the geminate is exposed to a pH greater than or equal to 6.4 it disassemble to form a pentameric intermediate (pentamer, DOP or a POD) that is still associated with the viral genome. If the pH is increased to a neutral pH (7.2) which is similar to the internal environment of the maize plant cell cytoplasm, the pentameric intermediate would continue to disassemble into a CP structure that is still associated with the viral genome. This data was confirmed by DNA gel electrophoresis analysis. The generation of this pH assay ideally serves three main functions; (i) it has illustrated a possible mechanism for the disassembly of the geminate capsid; (ii) it can be utilized to test assembly/disassembly inhibitors and (iii) it has provided some insights into the intermediates associated with the assembly/disassembly of the geminate and single capsids.

In conclusion, though we have not totally deciphered the mechanism by which MSV-N assembly and disassembly occurs we have illustrated some features of these mechanisms. The first step in the assembly of the geminate capsid appears to be the formation of a pentameric intermediate, followed by the addition of further pentamer The CP interactions during this assembly still needs to be tested by mutagenesis. DNA extracted from the wt geminate and single

capsids indicates that the geminates packages full length genomic material while the singles package subgenomic material confirming previous observation (29). Our data would suggest that there is some phosphorylation of the CP dimer, however this needs to be further investigated. The development of an assembly system utilizing baculovirus expressed CPs (wt and mutant) could allow us to systematically decipher the possible components required to assemble the unique geminate capsid.

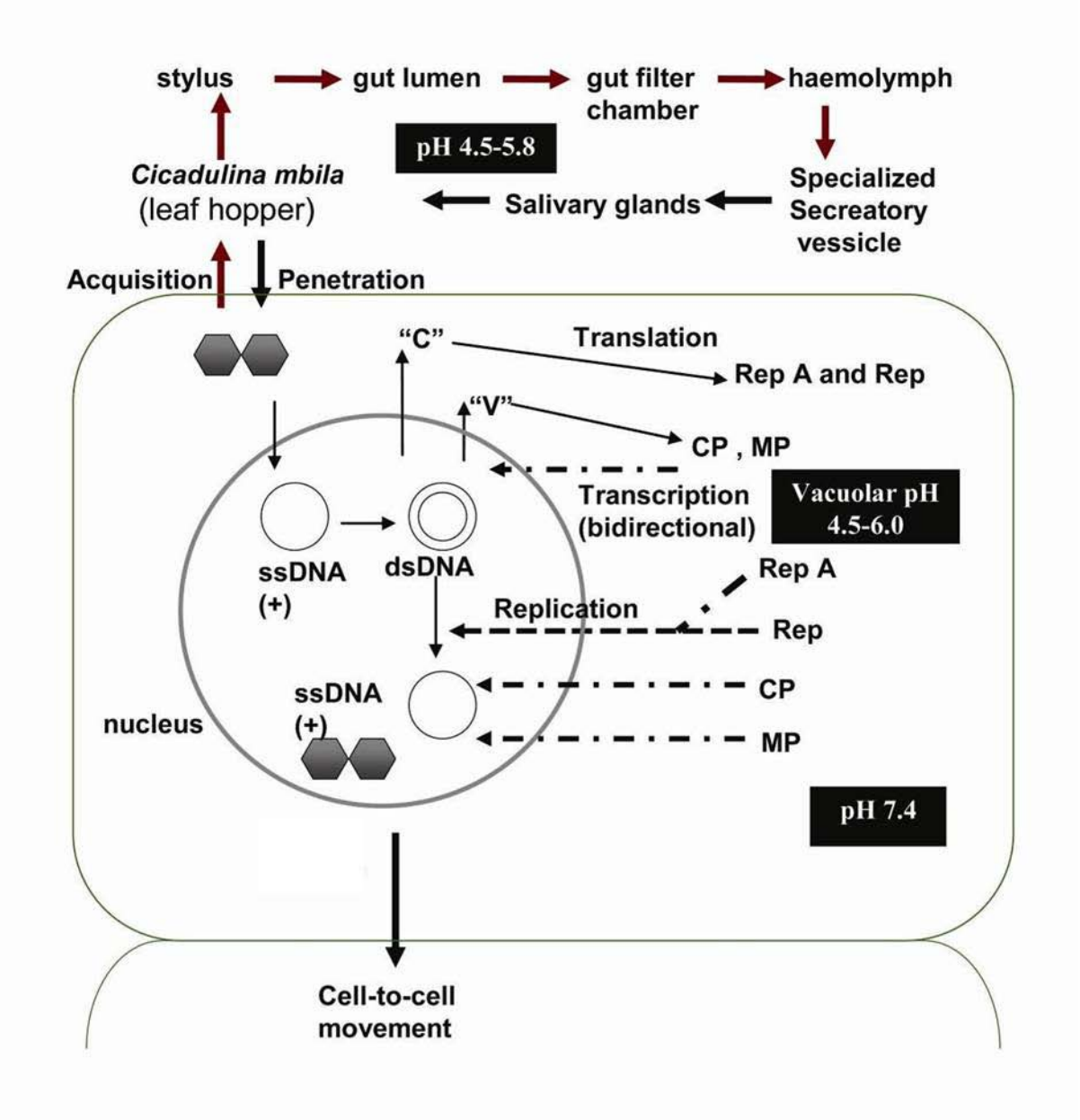

Figure 3-1. Schematic of the life cycle of MSV-N within its' plant host and insect vector. The virus once introduced within the cytoplasm of the maize plant the virus is exposed to a pH of 7.4 . The assembled virus when transmitted via the insect vector the new external environment of the virus ranges from pH 4.5-5.8

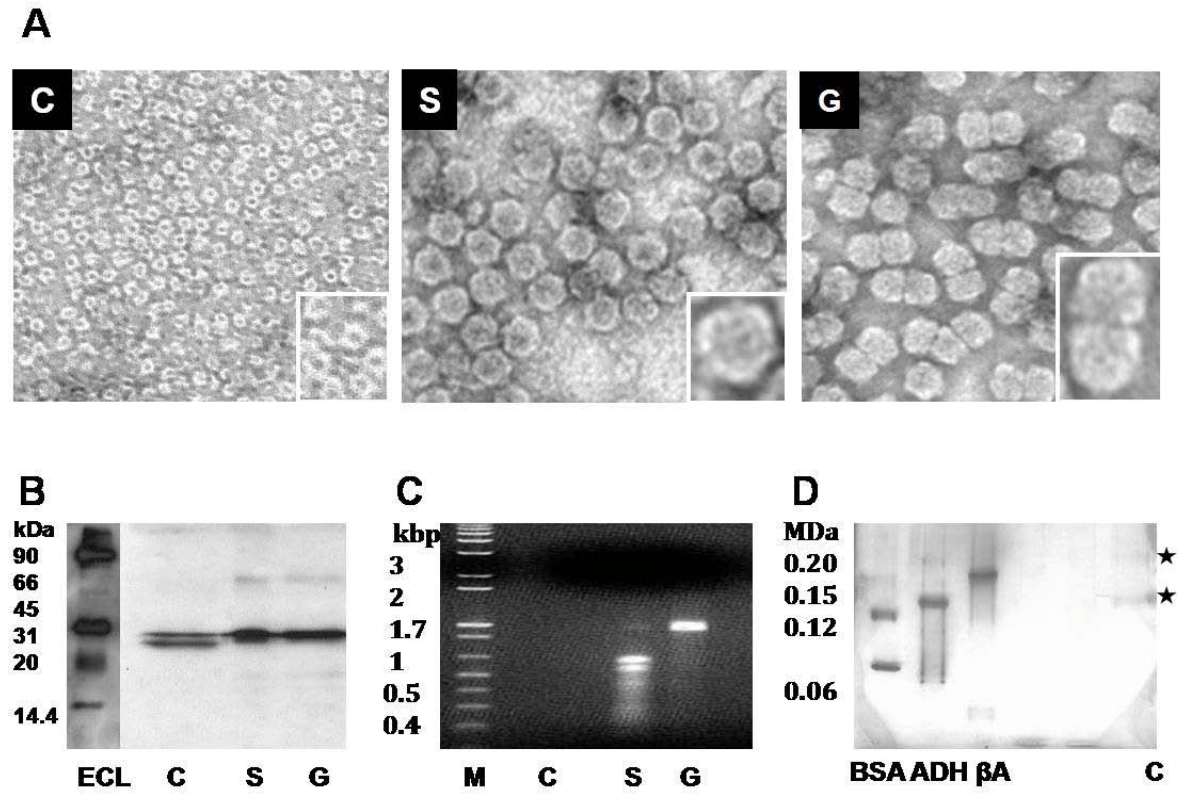

Figure 3-2. Characterization of purified MSV-N components. A) Electron micrographs of purified MSV-N capsomers (C), single capsids (S) and geminate capsids (G). B) Immunoblot analysis of MSV-N components with MSV-N primary antibodies. C) Agarose gel of MSV-N components. D) Native gel of the MSV-N capsomeric components . The asterisks indicate the position of the capsomeric bands.

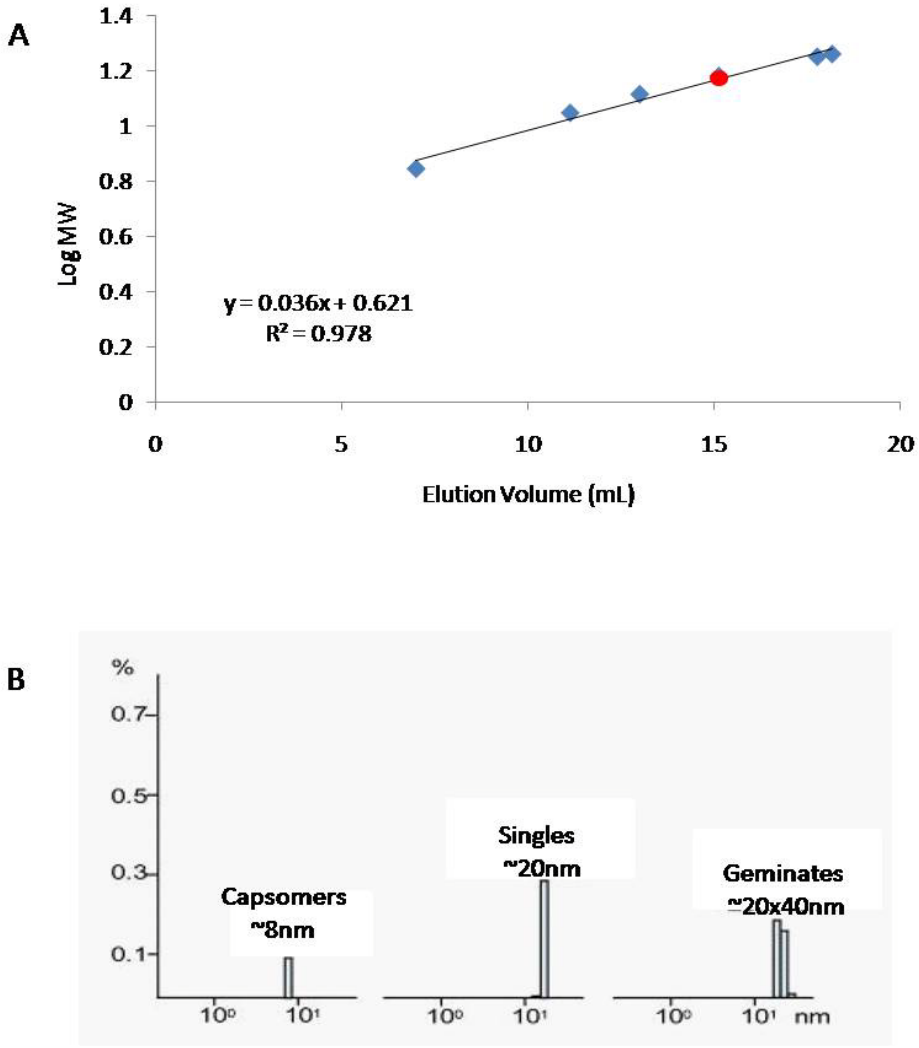

Figure 3-3. Determination of the molecular mass and diameter of purified MSV-N components. A) Calibration curve used to determine the molecular mass of MSV-N capsomeric component separated and characterized on a superose 6 analytical column. The red circle indicates the position of the MSV-N capsomer and the blue diamonds are the calibration standards. (B) Dynamic Light Scattering histograms of MSV-N capsomers, single capsids and geminate capsids.

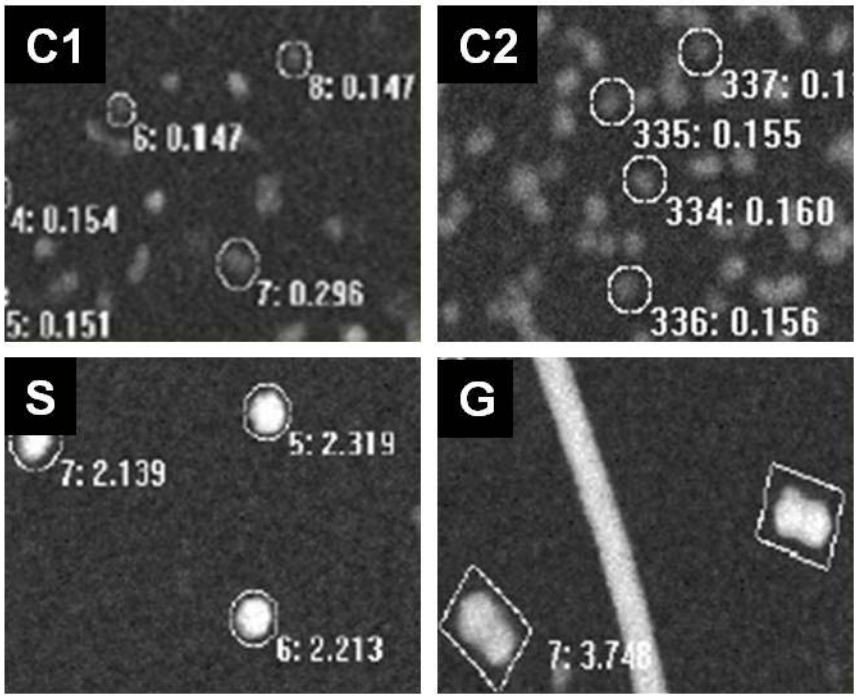

Figure 3-4. STEM micrograph of purified MSV-N components: C1 = fresh capsomers, C2 = capsomers 1 month post purification, S = singles and G = geminate capsids. There are two numbers beside each sample that has been selected, the number on the left represents the component number and the number at the right represents the molecular mass in MDa.

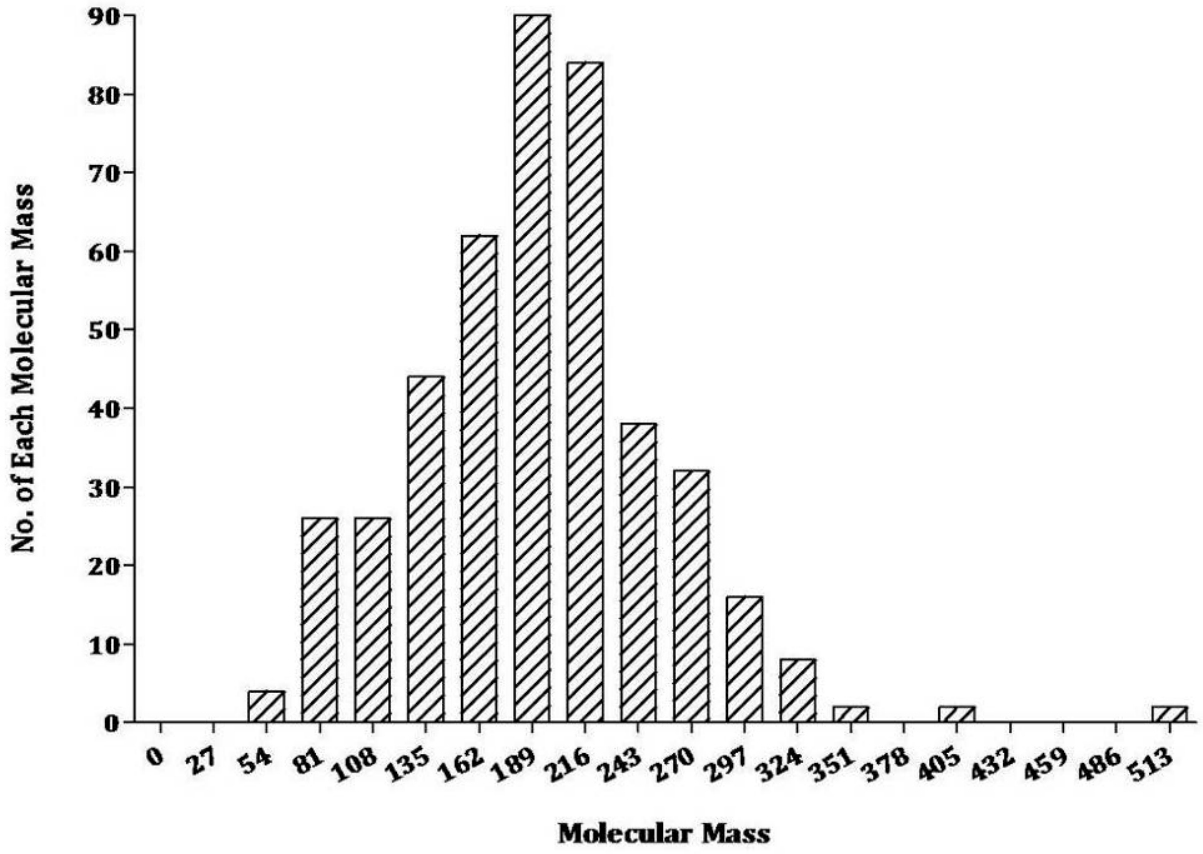

Figure 3-5. STEM histogram of MSV-N a fresh capsomeric sample which appear to fit a Gaussian distribution.

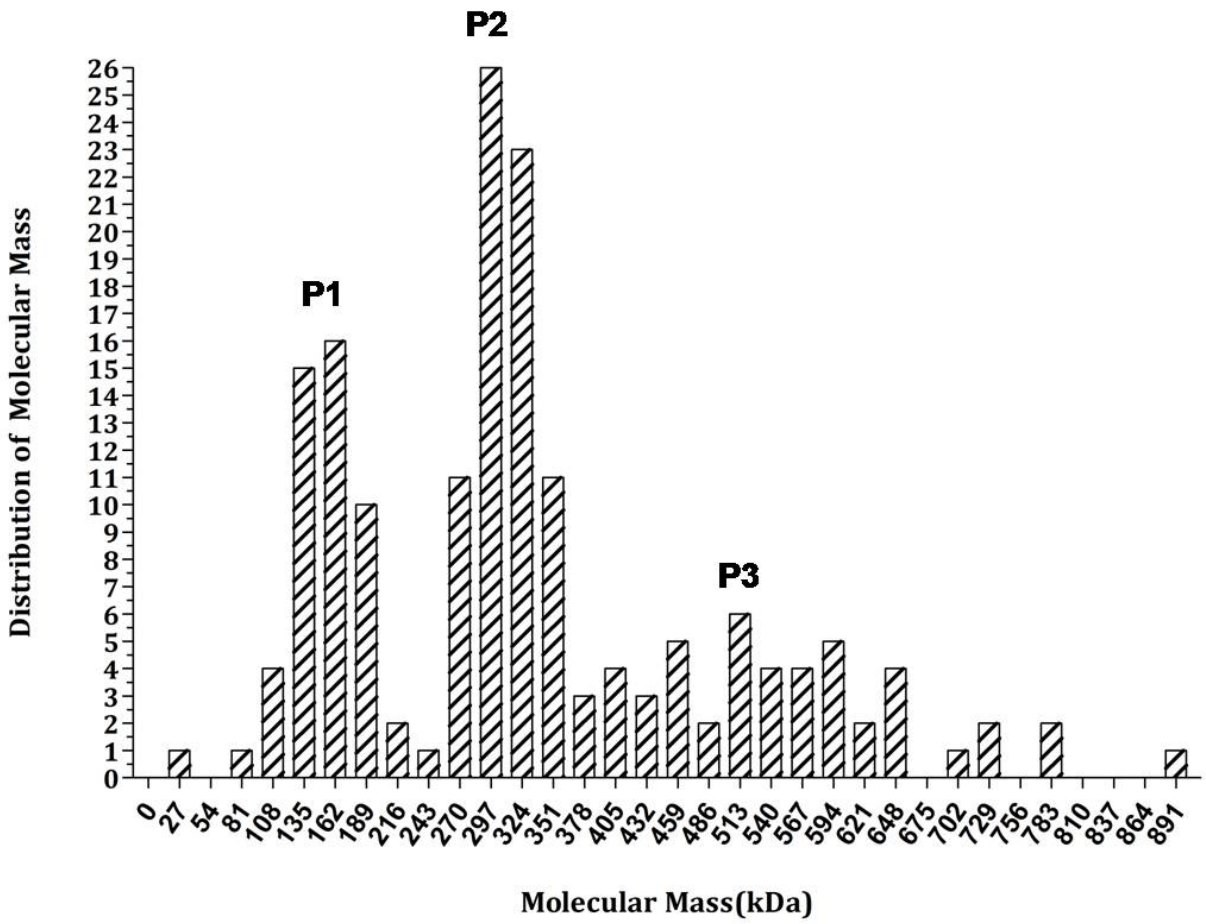

Figure 3-6. STEM histogram of an old capsomeric sample. P1, P2 and P3 represent the three different populations of capsomers and it does not appear to fit a Gaussian distribution.

A

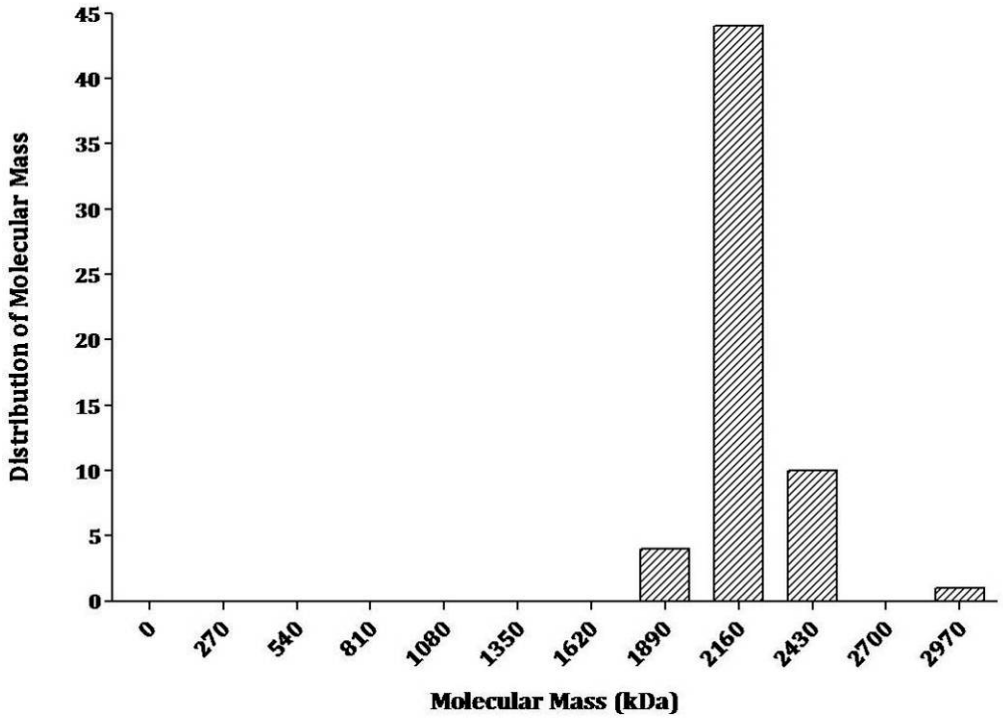

Figure 3-7. STEM histogram of purified MSV-N single capsids.

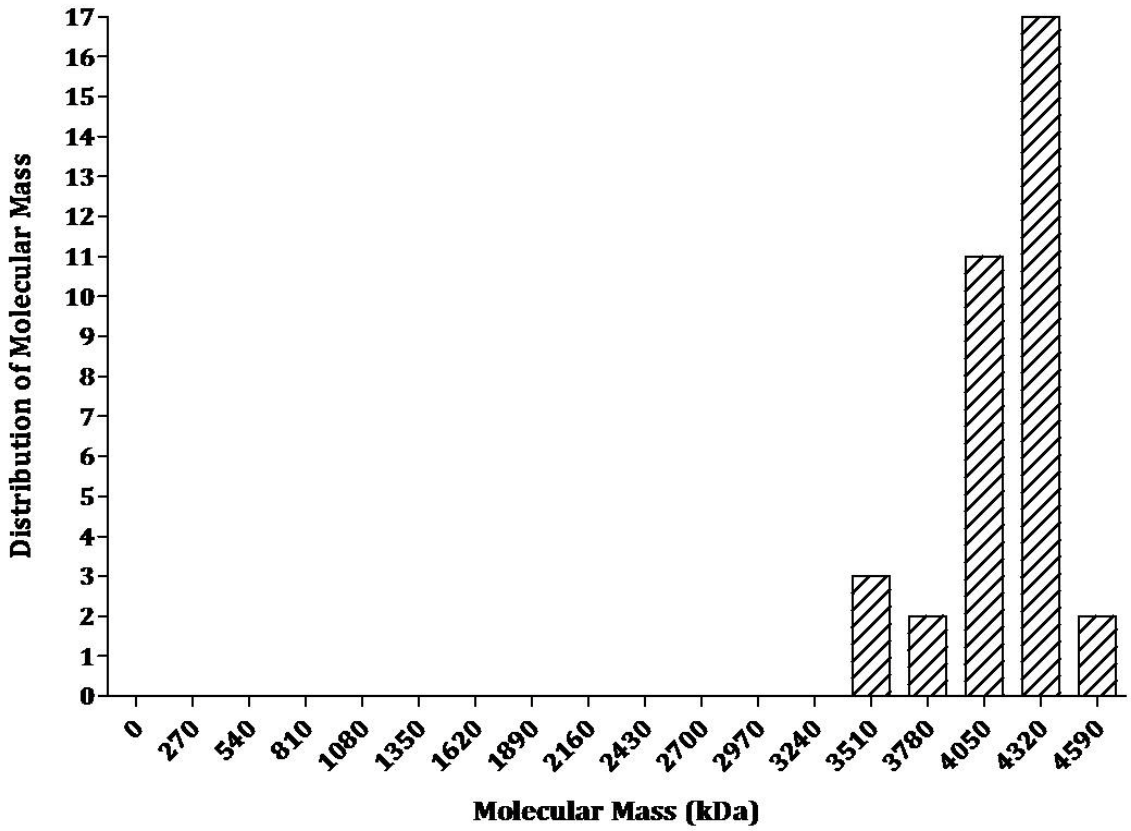

Figure 3-8. STEM histogram of purified MSV-N geminate.

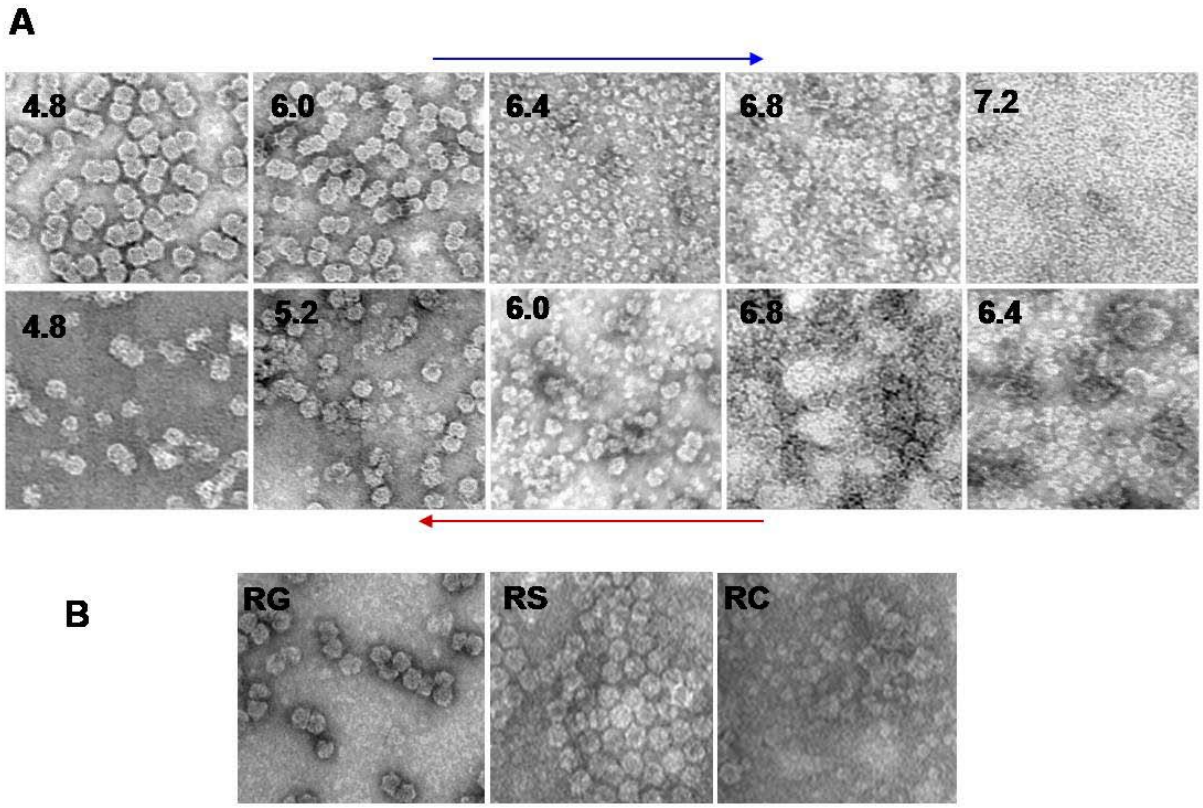

Figure 3-9. MSV-N pH assembly/disassembly assay. A) Illustrates the disassembly of geminate capsid with increasing pH from 4.8-7.2 (blue arrow) and reassembly of intermediates to form both geminate and single capsids in pH 7.2- 4.8 (red arrow). B) Purified reassembled MSV-N components at pH 4.8.

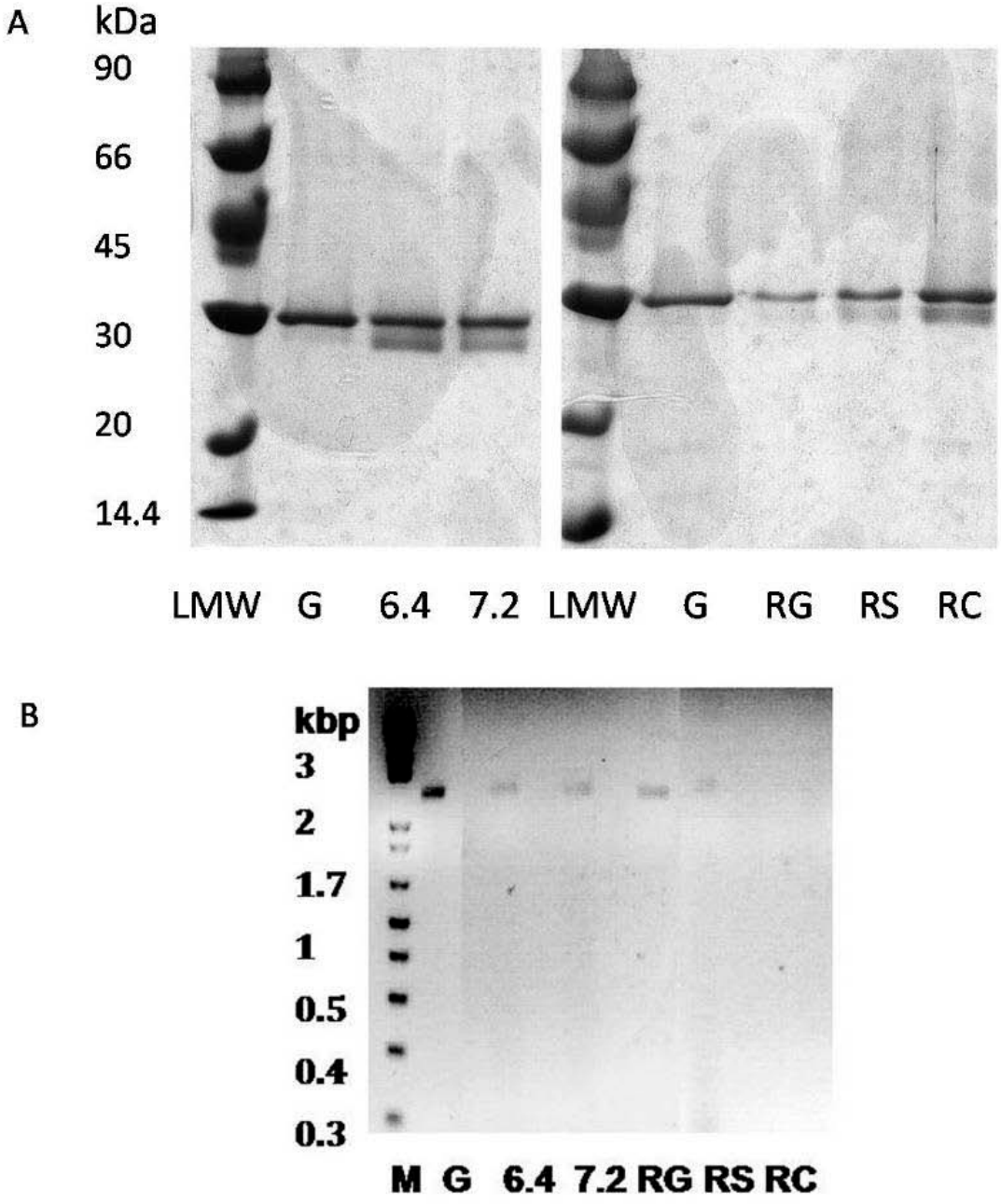

Figure 3-10. MSV-N pH Assay. A) Coomassie stained gel of disassembled/reassembled geminate (G) capsid at pH 6.4, 7.2 and 4.8. B) DNA extraction of geminate treated at pH 6.4, pH 7.2, reassembled geminate capsids (RG), reassembled single capsids (RS) and reassembled capsomers (RC).

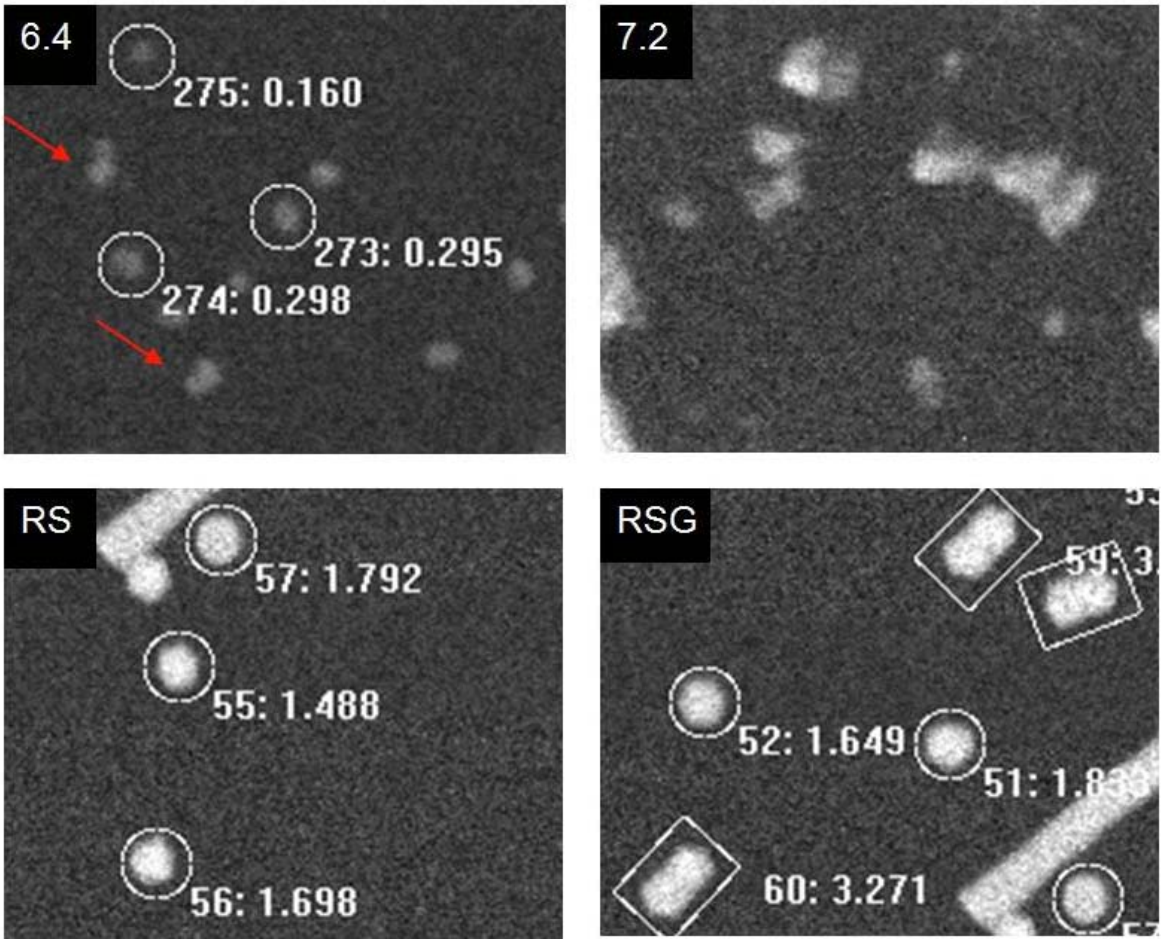

Figure 3-11. STEM micrographs of MSV-N pH components. The samples are disassembled geminates at pH6.4, geminates at pH7.2, red arrows show two interacring capsomer, reassembled singles (RS), and reassembled geminates and singles (RS and RG) at pH 4.8.

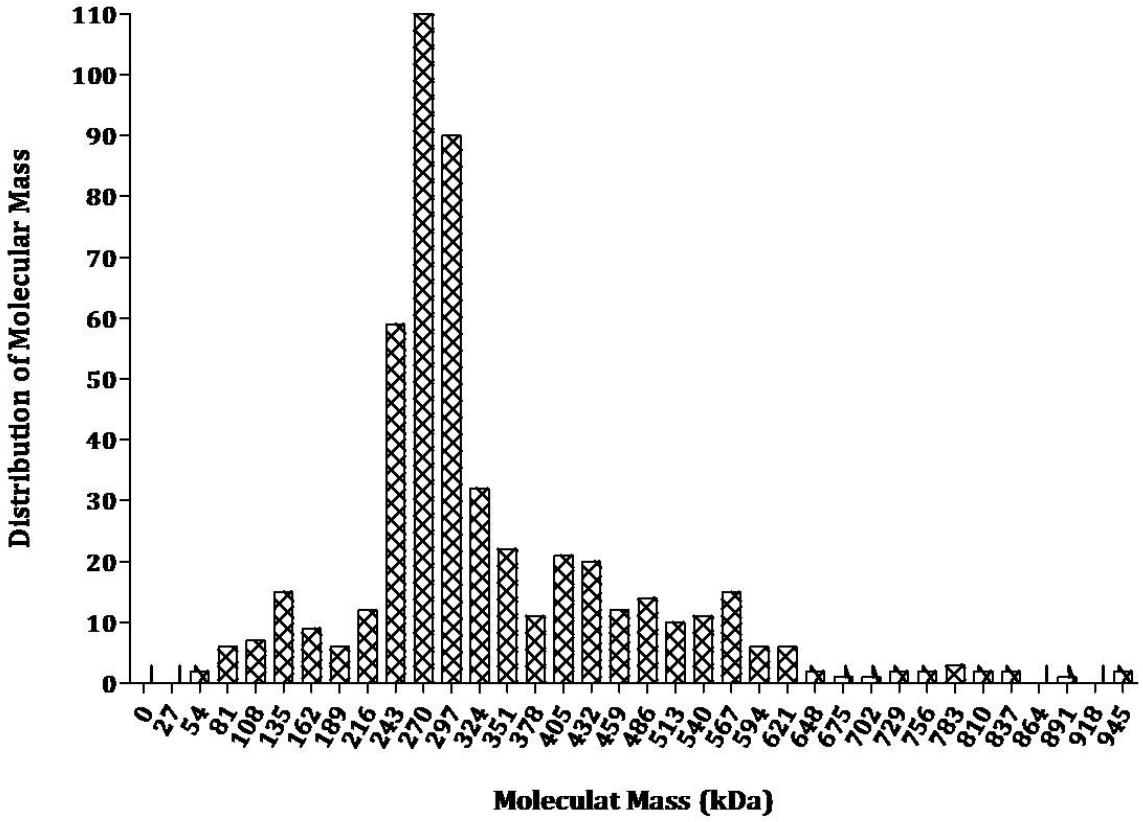

Figure 3-12. STEM histogram of MSV-N geminate capsids at pH 6.4.

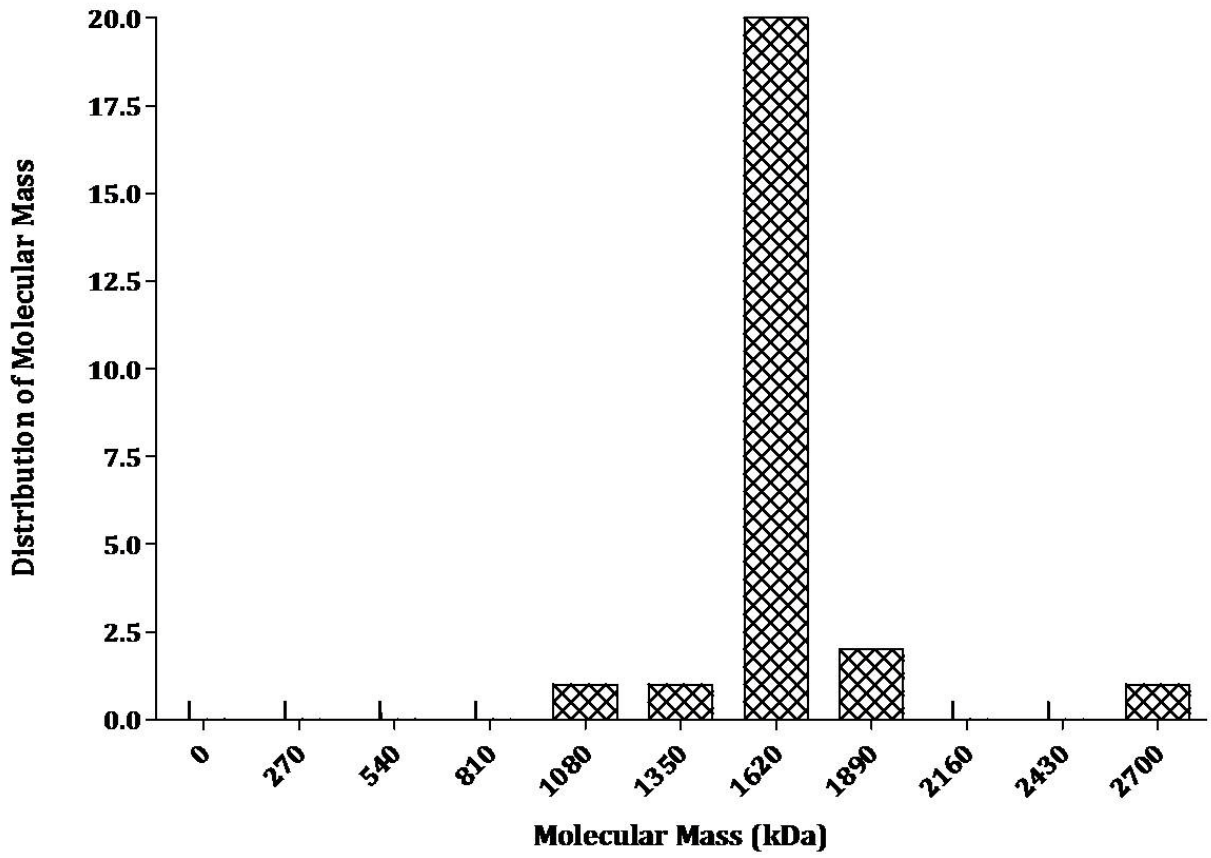

Figure 3-13. STEM histogram of MSV-N pH assay reassembled singles (RS) at pH 4.8.

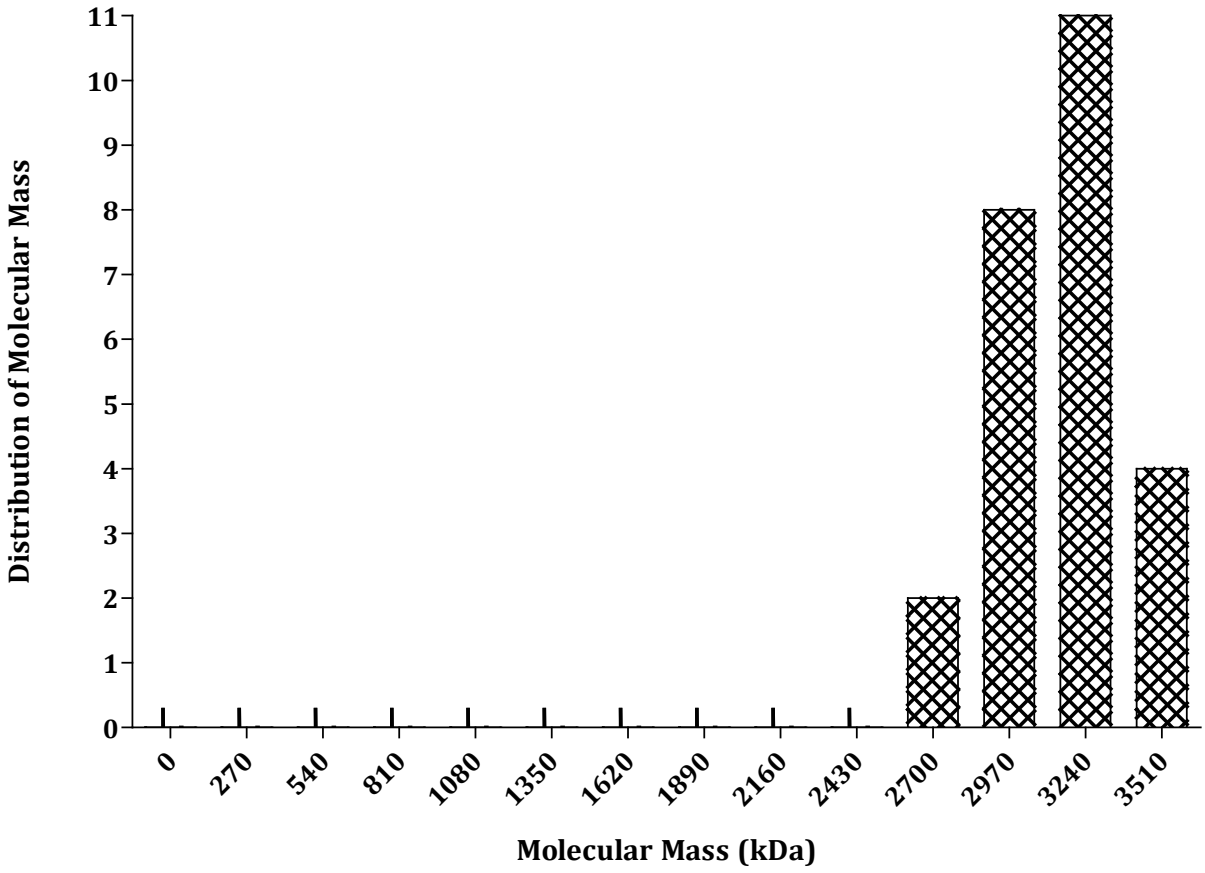

Figure 3-14. Stem histogram of MSV pH assay reassembled geminates (RG) at pH 4.8.

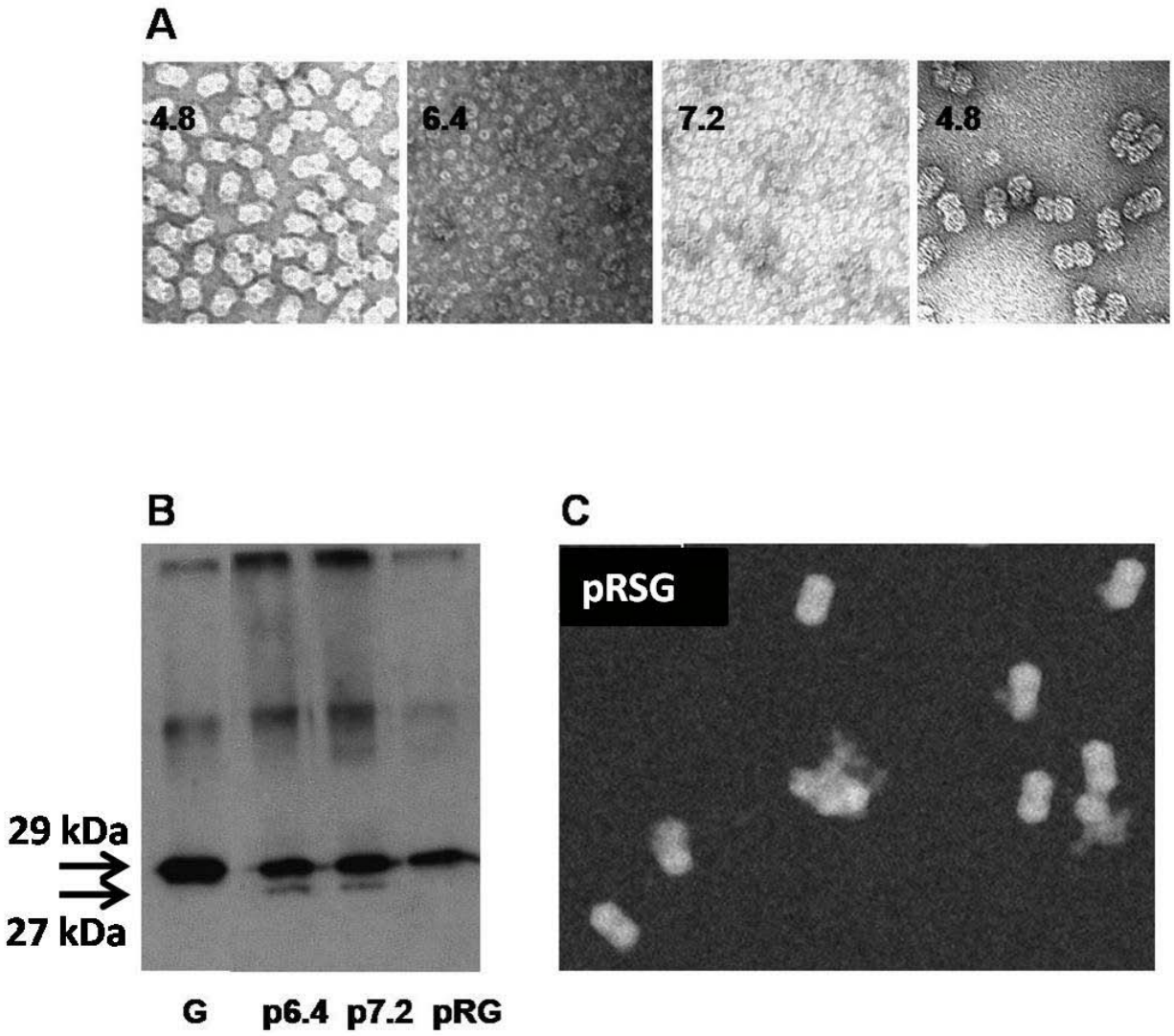

Figure 3-15. MSV-N pH assay in the presence of protease inhibitor. A) Electron micrographs of left to right wt geminate capsids; disassembled sample at pH6.4, and pH7.2, and purified reassembled sample at pH4.8. B) Immunoblot analysis of MSV-N sample as listed in (A). C) STEM micrograph of purified reassembled sample.

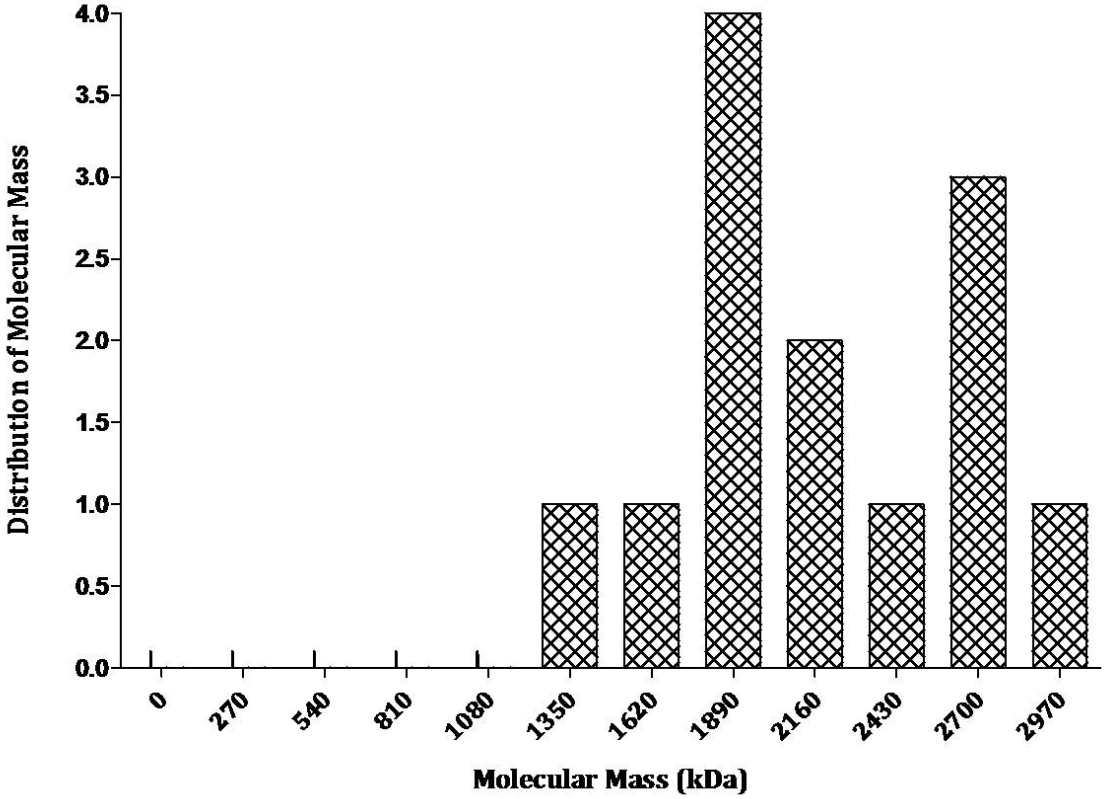

Figure 3-16. STEM histogram of reassembled MSV-N singles (pRS) at pH4.8 assayed in the presence of protease inhibitor.

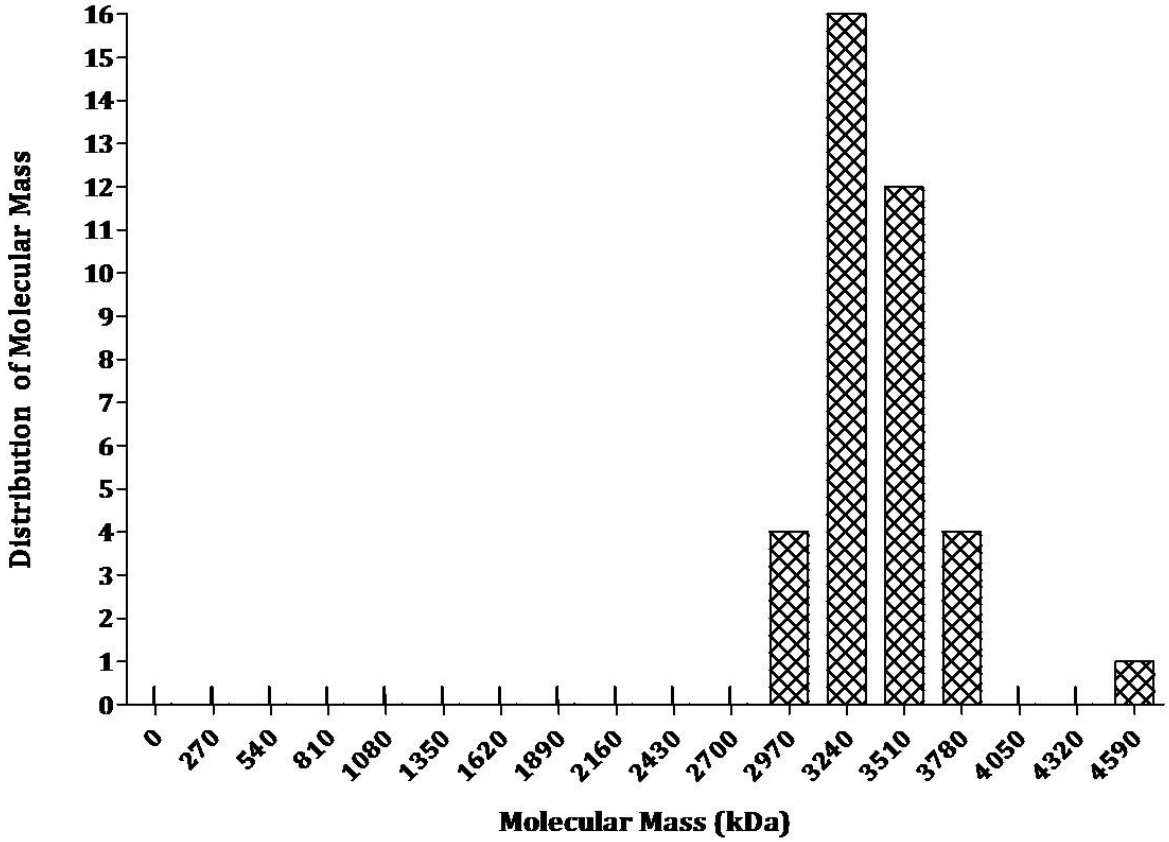

Figure 3-17. STEM histogram of reassembled MSV-N geminates (pRG) at pH 4.8.assayed in the presence of protease inhibitor.

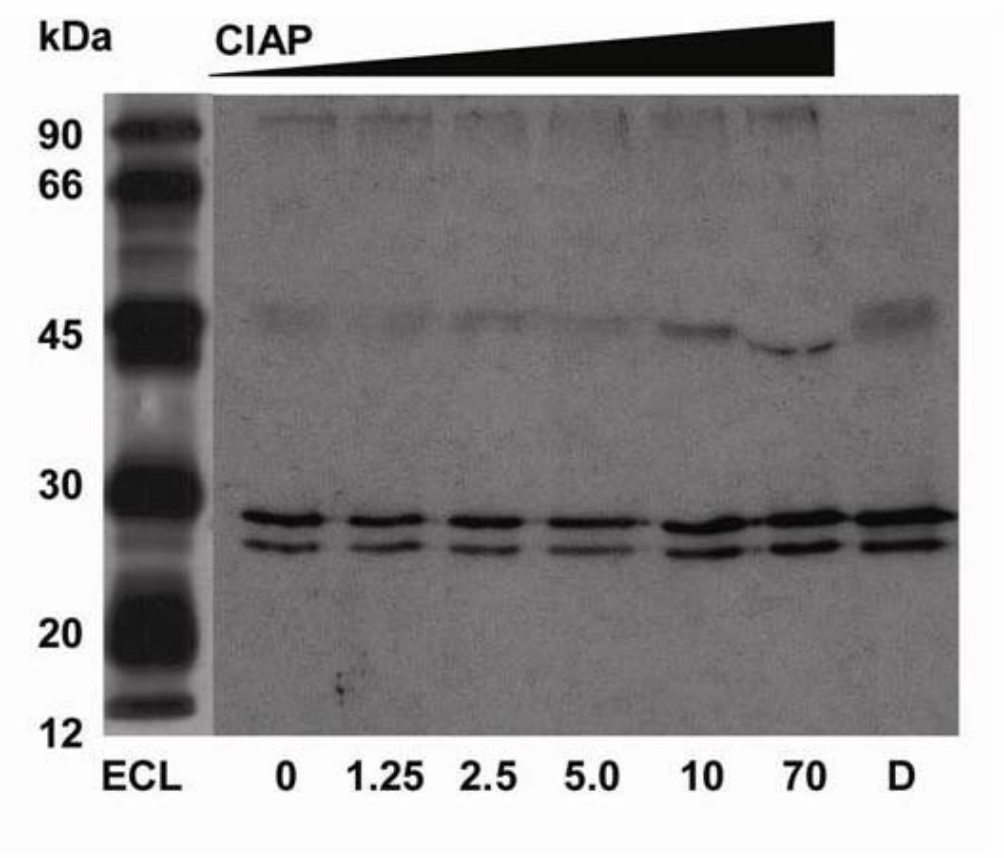

Figure 3-18. Protease inhibited (PI) MSV-N pH assay assembly/disassembly. A) Immunoblot analysis of the MSV-N components treated with DNase and CIAP separately and together. B) Immunoblot analysis of the MSV-N subassembly formed at pH 7.2 treated with increasing concentrations of CIAP (U/µL) and the final lane is treatment with DNase I only.

Table 3-1. STEM statistical analysis of purified MSV-N capsomers, single and geminate capsids.

	Capsomers (fresh)	Capsomers (old)	Singles	Geminates
Total number of measurements	436	170	59	35
Minimum	45.9	27.1	1776.9	3620
25% Percentile	153.3	187.1	2126.7	4081.3
Median	193.4	306.7	2210.4	4198.6
75% Percentile	225.6	415.3	2273.1	4263.9
Maximum	512.6	898.0	3077.8	4461.5
Mean	192.7	332.1	2210.8	4132.4
Std. Deviation	63.8	164.5	175.5	221.3
Std. Error	3.1	12.6	22.85	37.4
Lower 95% CI of mean	186.7	307.2	2165.0	4056.3
Upper 95% CI of mean	198.7	356.9	2256.5	4208.4

Table 3-2. STEM statistical analysis of MSV-N assembly/disassembly components from the pH assay

	pH 6.4	RS	RG	pRS	pRG
Total number of measurements	514	25	25	13	37
Minimum	64.5	1144.2	2806.4	1447.4	3019.3
25% Percentile	258.3	1529.7	3033.9	1839.45	3280.7
Median	291.2	1616.3	3185.7	2192.9	3358.9
75% Percentile	400.5	1678.3	3288.7	2756.8	3532.5
Maximum	949.9	2608.3	3626.1	2917	4510.1
Mean	333.9	1643.1	3168.3	2204.4	3404.2
Std. Deviation	140.9	244.7	206.4	489.4	263.6
Std. Error	6.2	48.9	41.3	135.7	43.3
Lower 95% CI of mean	321.7	1542.1	3083.1	1908.6	3316.3
Upper 95% CI of mean	346.2	1744.1	3253.5	2500.1	3492.1

Table 3-3 Comparison of the Molecular Mass (kDa) of the pH reassembled geminates and singless compared to wt.

	Singles	Geminates
wt samples	2210	4132
Reassembled samples	1643	3168
Reassembled samples (protease inhibitor)	2204	3404

Table 3-3. MSV-N CP phosphorylation prediction table

Sequence site	Kinase	Score
S-2	PKC	0.8
T-3	PKC	0.91
S-4	PKC	0.91
S-15	PKC	0.85*
T-19	PKC	0.94 **
S-24	PKA	0.63
S-33	RSK	0.51
S-33	PKC	0.71
S-33	PKA	0.67
S-39	PKA	0.83*
T-50	cdc2	0.51
T-51	PKC	0.58
T-66	DNAPK	0.52
S-79	PKA	0.64
T-81	PKC	0.7
T-83	PKC	0.8*
Y-101	INSR	0.53
S-102	PKA	0.65
T-115	cdc2	0.54
T-116	p38MAPK	0.54
T-123	p38MAPK	0.5
T-123	cdk5	0.52
T-126	PKC	0.72
T-133	PKC	0.73
T-140	PKC	0.75
S-177	PKC	0.8*
T-198	DNAPK	0.51
Y-217	INSR	0.53
T-227	PKC	0.55

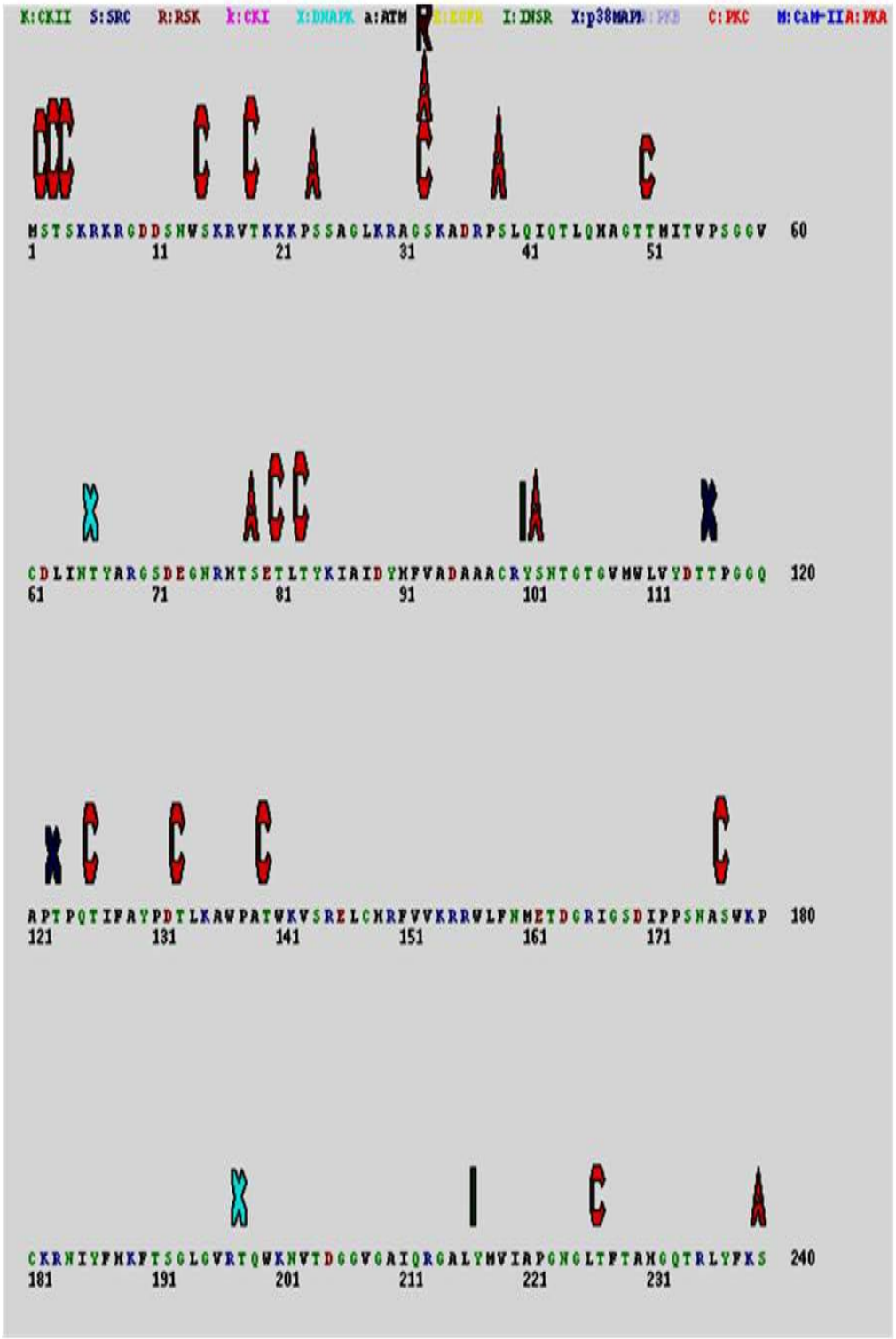

Figure 3-19. Kinase landscape of MSV-N CP sequence kinase prediction with scores above 0.5 shown by uppercase letters and with size proportional to the scores. Color codes and kinase symbols are listed at the top of the figure.

CHAPTER 4
WILDTYPE AND MUTANT MSV-N CP BACULOVITUS CLONING AND EXPRESSION

Introduction

The assembly and disassembly of the viral capsid represents key steps in the replicative life cycle of the virus. The CP-CP and the CP-DNA interactions are important to the formation or assembly of the viral capsid.The detailed structures of viral capsids can illustrate how the CPs interact with each other and how they interact with their packaged genome. The determination of the CP interaction with each other and its'interaction with the viral genome are critical to the understanding of the assembly and disassembly processes. The polyoma VP1 protein for example contains a jelly roll β- barrel core and long flexible N and C- terminal arms, the C terminus being extremely positive and may be important in binding the viral DNA. Both arms are dispensable for pentamer formation but indispensable for inter-pentameric interaction (137). CCMV on the other hand 25 of the N terminal residues of the coat protein contains a high proportion of basic amino acids which have been modeled to interact with the viral RNA, deletion of these residues eliminates the ability of this virus to assemble RNA containing particles *in vivo* (158). The previous chapter was focused on the purification of assembly/disassembly components of MSV-N to decipher the possible steps involved in these processes. This chapter is focused on the cloning and expression of baculovirus MSV–N CP wt and mt, the aim is to determine their structure and to correlate it, to their role in the assembly of the virus.

MSV-N is a pathogenic plant virus that encapsidates the covalently closed 2.687 kb genome in a unique twinned pseudo T=1 icosahedral capsid. The capsid is composed of 110 copies of the CP. The CP of MSV-N is translated from the viral transcript V1 (25), it is 244aa in length and 27kDa in molecular mass. The MSV-N CP is required for a variety of functions

which includes insect transmission (94), systemic infections of maize plants (93), binding of single and double stranded DNA (101), and for the specific accumulation and encapsulation of single stranded DNA in infected tissue (25). The CP accumulates in the nucleus and facilitates nuclear transport (103) and cell to cell transport of MSV-N DNA via an interaction with the movement protein (MP) (102). The N- terminal residues 5-22 contain 9 basic amino acid domains that are important for binding both ss and dsDNA (101). These domains have also been predicted to contain the NLS important for the transport of the viral genome to the nucleus (101).

There are certain CP residues along with N and C-termini residues that have been reported to be essential for geminate capsid assembly. CD studies of MSV-N and structure prediction (74) of the prototype members of the four geminivirus genera (MSV-N, BCTV, TPCTV, BGMV) have been used to validate the secondary structural element composition of our MSV-N CP model. The CP structure was then used to guide a multi-sequence alignment generated by Clustal W (171) of 46 different viruses sampled from the four genera. The alignment results were mapped onto the MSV-N CP model, and only five residues were identical for all 46 sequences compared. These identical residues are located in the β strand regions, consistent with a requirement for forming the core CP structure. The alignment of geminivirus sequences also showed that residue K182 (104), conserved among the mastreviruses, is located at the base of a channel formed by pentameric CP interactions (Figure 4-1). Mutations at this position, for example, K182V, have been shown experimentally to disrupt capsid assembly; however, intermediates formed have not been characterized. The biophysical characterization of capsid or intermediates resulting from this mutant protein would elucidate the contribution K182 to the stability and assembly of the MSV-N viral capsid. In addition to this residue, the N-terminal region has also been shown to be important for MSV-N assembly, and DNA binding (25, 101).

This chapter will focus on the use of a recombinant baculovirus expression system to express the wt MSV-NCP as BMSV-NCP, K182V mutant as BMSV-N182, and the N-terminal truncation as BMSV-NCP201.

Results

To generate the BMSV-NCP, BMSV-NCP201 and BMSV-NCP182, the Bac-to-Bac (Invitrogen) expression system was used and the details are listed in Chapter 2.

Cloning of MSV-N CP (wt and mutant) into pFastBac

The pFastBac donor vector was used to transpose the MSV-N CP wt and mt into the baculovirus genome. The pFastBac plasmid and the recombinant wt and mt MSV-N CP are shown in Figure 4-2A-D. The MSV-N CP gene fragments are ligated into the digested pFastBac. pFastBac contains a gentamicin resistant gene which allows for screening of recombinant pFastBac and MSV-N CP wt and mt colonies.

pFast Bac (wt and mutant) Clone Selection

To determine which clones contain the recombinant pFBMSV-NCP, pFBMSV-NCP182 and pFBMSV-NCP201, the clones were examined on a DNA gel before and after restriction digest analysis and the results are shown in Figure 4-3A-B. All the clones are circularized except pFBMSV-NCP201-4. pFastBac contains a BamHI restriction site in the promoter and MSV-NCP gene contains an Nco1 restriction site. Fsp1 is an additional site present in pFBMSV-NCP182 and is used for screening bacterial colonies. Double digestion of the ligated pFastBac vector containing MSV-NCP wt and mt insert generated two DNA fragments. Clones 1 and 2 of pFBMSV-NCP201, CP and 182, all contain the expected fragments (Figure 4-3B). The other clones 3 and 4 did not appear to contain the MSV-NCP insert and CP201 appears to have two pFastBac ligated to itself (Figure 4-3). The positive clones were then transformed into DH10Bac *E. coli* cells.

BMSV-NCP, BMSV-NCP182 or BMSV-NCP201 recombinant identification

To determine the MSV-N CP that clone that was transposed into the the baculovirus vector each white clone generated was analyzed by restriction digestion. Recombinant MSV-NCP wt and mt clones were first selected as white colonies from a blue and white colony screen. The purified clones were then analyzed by restriction digest and undigested recombinant BMSV-NCP, BMSV-NCP201 and BMSV-NCP182 were examined on an agarose gel (Figure 4-4A). Clone 1 of each BMSV-NCP wt and mt were used for restriction digest analysis. The first digest was Nco1 and it linearized all the baculovirus recombinant clones, as illustrated in Figure 4-4B. The restriction enzyme, Nde1 was then used to digest, BMSV-NCP201 and BMSV-NCP and Fsp1 was used to digest BMSV-NCP182. The data in lane 2 and 3 demonstrate the results of these digestions and show that each clone was linearized (Figure 4-4B). The results in lane 4 illustrate the double digestion of BMSV-NCP201 and BMSV-NCP with Nde1 and Nco1; and BMSV-NCP182 with Nco1 and Fsp1. The data confirms that the recombinant clones contain the MSV-NCP wt and mt genes.

Wild Type and Mutant BMSV-N CP Expression

To determine the time for maximum protein expression before CP degradation as well as the best MOI to use for virus amplification and titration several time course experiments were performed. The time course experiment recorded in Figure 4-5A and B. All the mutants appear to produce proteins that are positive to the MSV-N antibody but only MSV-NCP and the MSV-NCP201N appear to show overexpression of the CP. The time course experiment was also able to show that maximum expression for the MSV-NCP201 is at 48 hr after which the CP appears to be degraded. The MSV-NCP appear to be overexpressed by 72 hr but the study would need more time points in order to determine if this was the maximum expression that could be achieved before CP degradation.

BMSV-NCP Purification (Wt and Mutant)

Ammonium sulphate precipitation was used to purify the baculovirus expressed MSV-NCP wt and mt. The samples were precipitated by sequentially increasing the ammonium sulphate concentration 10% at a time upto 70%. The resuspended pellets were analyzed by coomassie stained SDS-PAGE and western blot analysis. BMSV-NCP182 was observed in the cell lysate (CL) and clarified supernatant (S), no MSV-NCP was observed in the pellet (P). Based on western blot analysis, the BMSV-NCP182 pelleted at 30% ammonium sulphate. BMSV-NCP was observed in cell lysate at 30-40% and 70% ammonium sulphate precipitation according to the western blot (Figure 4-6A). When compared to the corresponding coomassie stained gel, these fractions contained other protein bands apart from MSV-NCP. BMSV-NCP201 at 20% and 30% ammonium sulphate also contained MSV-NCP (Figure 4-6B). Consistent with the results obtained for the BMSV-NCP and 182, the coomassie stained gel for these fractions also appeared to have other protein bands (Figure 4-6C). Consequently, ammonium sulphate precipitation may be used as a method to concentrate the recombinant BMSV-NCP, but cannot be used to purify it and so other CP purification methods were explored.

The calculated PI of MSV-NCP has been predicted to be approximately 10. There are few proteins with this high pI, for example lysozyme, which is a rare occurrence. This concept forms the basis of using ion exchange chromatography a method of purification for MSV-NCP as illustrated in Figure 4-7. The cell lysate (CL) contains over-expressed recombinant MSV-NCP, most of which is in clarified supernatant. The flow through (FT) and the eluant (E) were positive for MSV-NCP. It should be noted that the FT fraction contained CP species with differing molecular masses, some higher or lower than 30kDa, while the eluant contained CP species that were lower than 30kDa. Though this method of purification does offer some success, the purity of the samples eluted as well as the reduction in degradation will have to be addressed.

Discussion

This chapter describes the successful cloning, expression and partial purification of the BMSV-N CP, BMSV-NCP201 and BMSV-NCP182. The mutants of MSV-NCP were generated based on the role of the different regions of the CP on capsid-assembly. It has been shown that the N-terminus of the MSV-CP is important for binding ss- and dsDNA as well as for virus assembly. Similarly CP mutants of 182 has been shown to bind the viral genome, replicate and translate, causing local infection, without generating any observable capsids. The location of 182 is illustrated in Figure 4-1A and B, its position is an intra-pentamer location and previous data implies that this residue is important for capsid assembly.

The time course experiment (Figure 4-5) shows that the majority of the expressed CP is retained in the cell lysate when compared to the secreted sample. The same experiment was repeated for different multiplicity of infection and time course repeated to determine the all the appropriate conditions for maximum expression of the BMSV-NCP.

The purification and characterization of the baculovirus expressed MSV-NCP wt and mt will provide information about the structure of the CP and their relevance to the assembly of the viral capsid. The ammonium sulphate purification method is insufficient on its own but may be combined with another method that requires pre-concentration. The success of ion exchange chromatography will be explored by first determining the purity of both the flow through and eluant. Depending on the purity of these fractions, this method may be further combined with other methods like gel filtration chromatography. The purification, characterization and crystallization of the MSV-N CP or any components formed, will provide valuable information about the assembly of the unique geminate virus capsid.

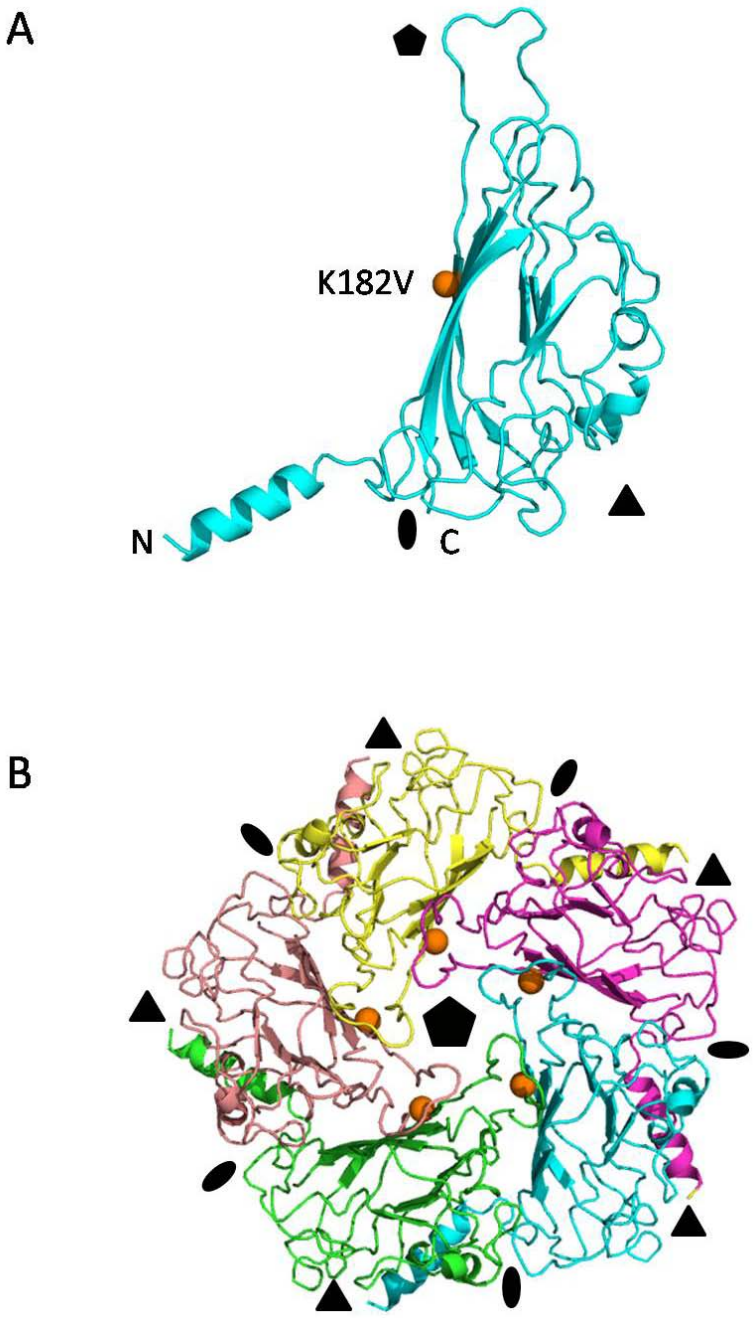

Figure 4-1. Ribbon diagram of MSV-N CP. A) Monomer in cyan, orange ball indicate the location of K182V mutant, N is the N-terminal residue and C is the C-terminal residue. B) 5-fold related monomers, orange ball represents K182V mutant position, The pentagon represents the 5-fold axis, the ellipsoid represent the 2-fold axis and the triangles represent the 3-fold axis.

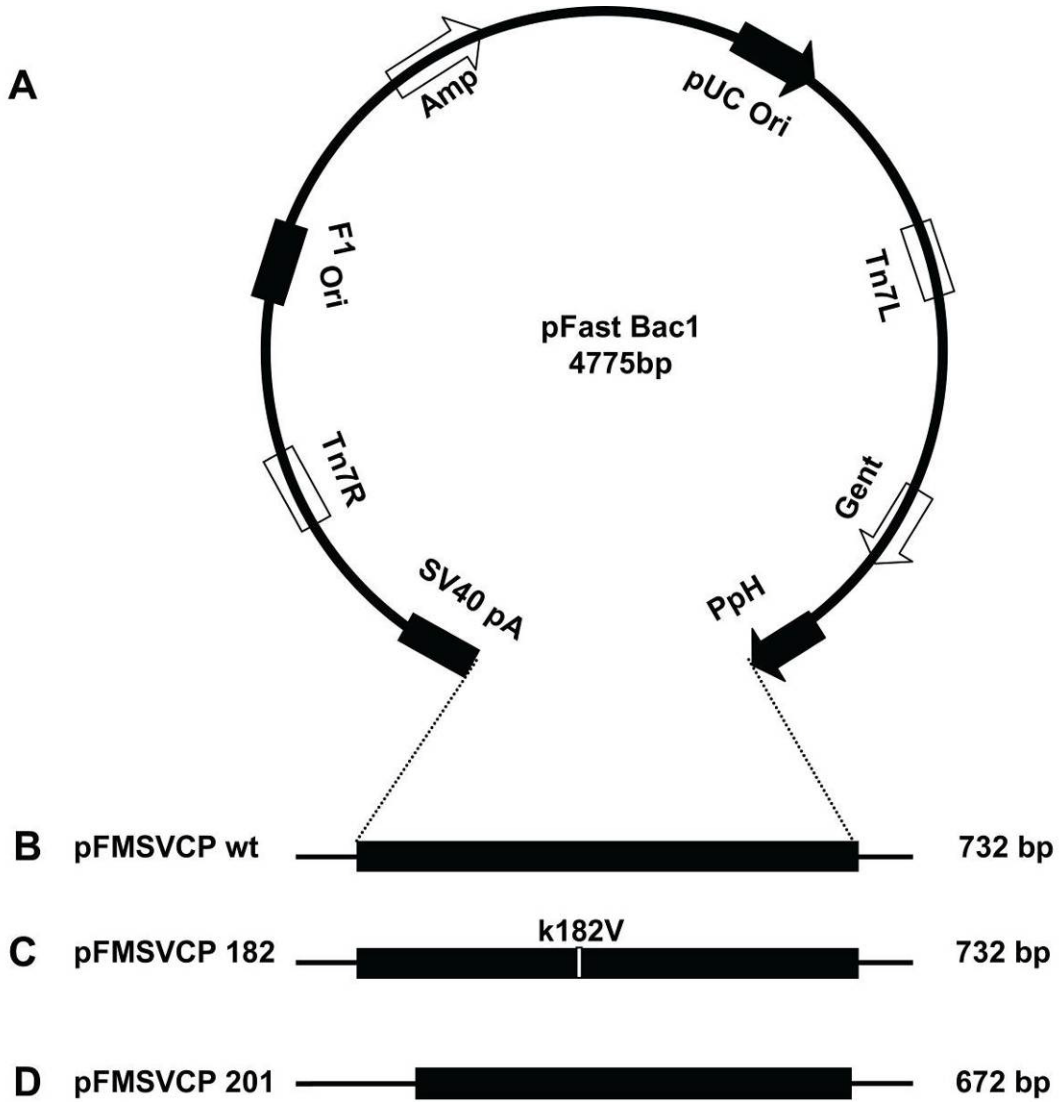

Figure 4-2. pFast Bacmid map and the MSV-NCP wt and mt gene inserted A) pFMSV-NCP wt B) pFMSV-NCP182 and C) pFMSV-NCP201.

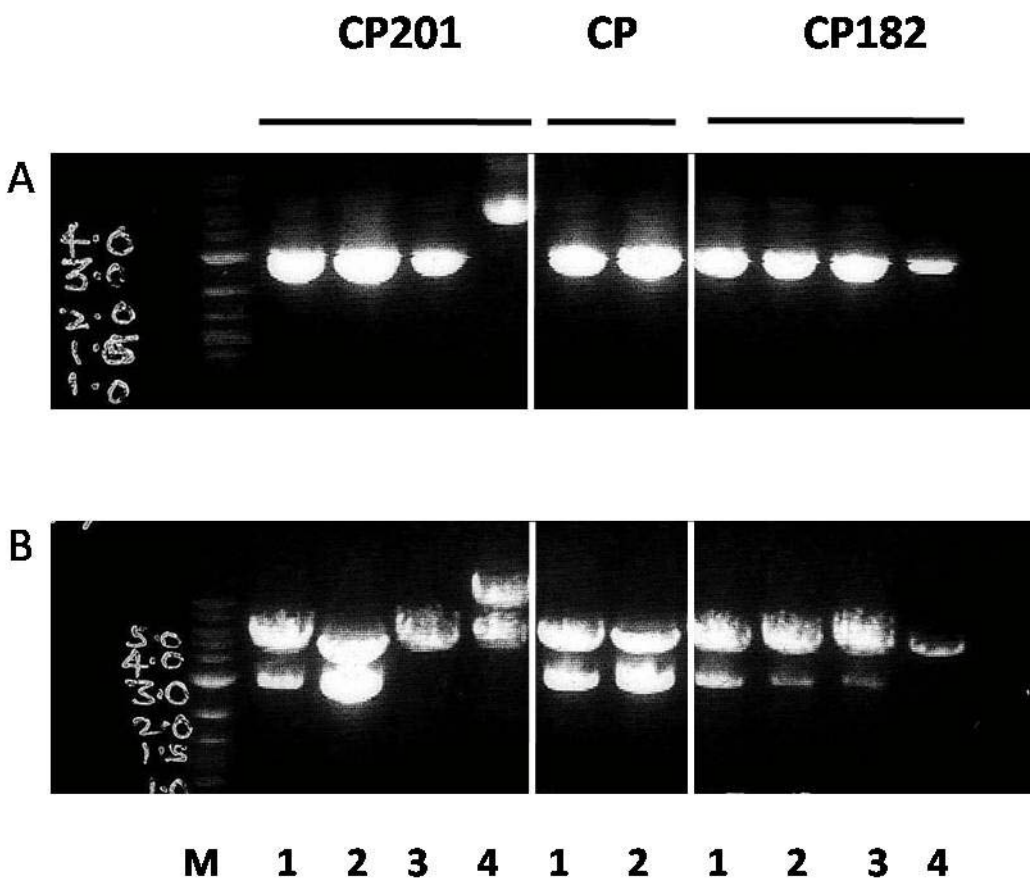

Figure 4-3. pFast Bac MSV-N clones restriction digest analysis. A) The circularized recombinant pFast Bac clones before restriction digest B) DNA fragments on a agaroge gel after restriction digest with appropriate enzymes.

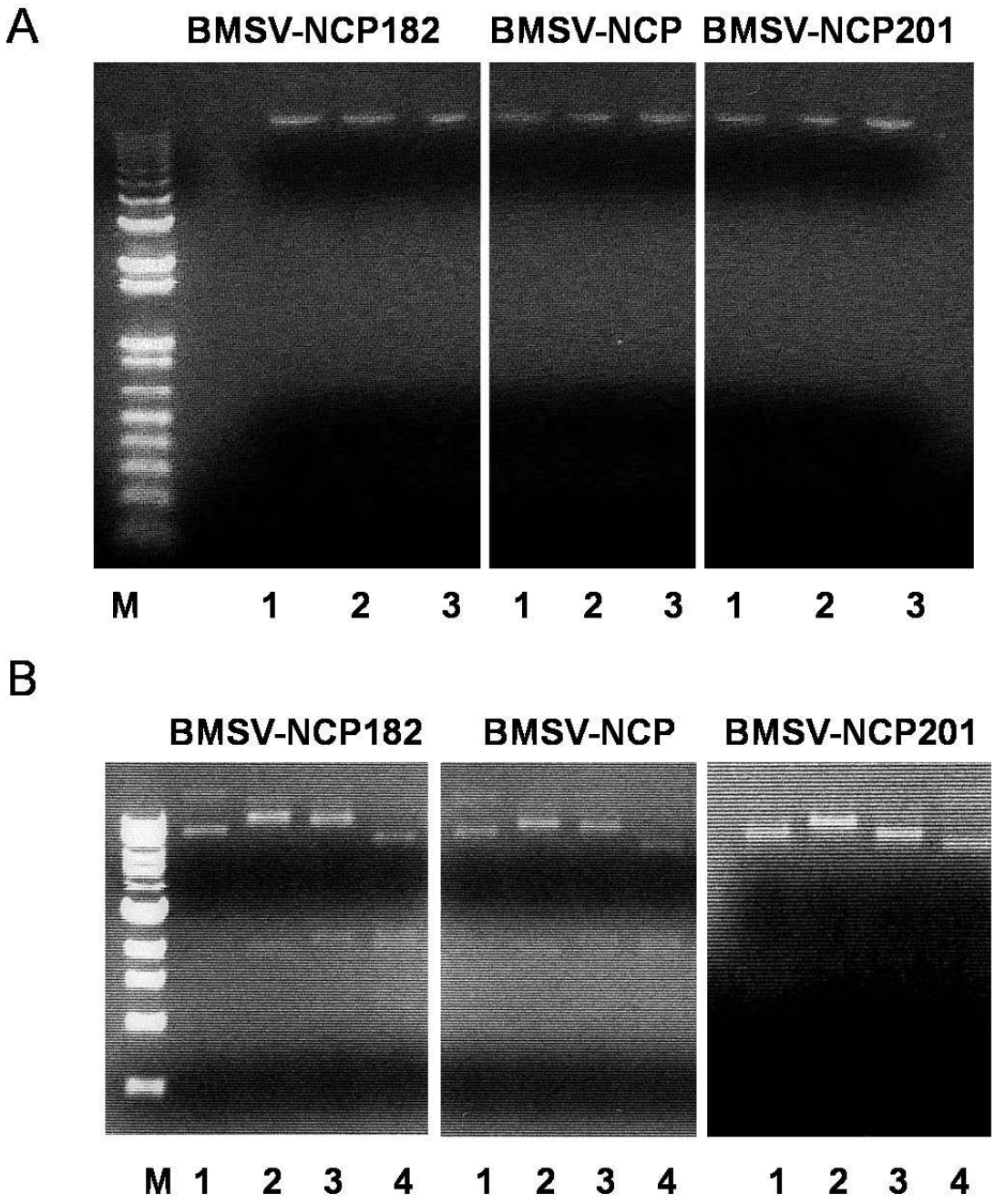

Figure 4-4. BMSV-NCP wt and mt clones restriction digest analysis. A) The circularized recombinant clones before restriction digest. B) DNA fragments of clone 1, after restriction digest, selected from panel of 3 mutants in top figure. Lane 1 for all three BMSV-NCP wt and mt are uncut.Lanes 2and 3 represents single restriction digest and lane 4 represents double digests. Nco1 was the enzyme used in all lane 2, Fsp1 was used for BMSV-NCP182, Nde1 for BMSV-NCP201, and Nde1 for BMSV-NCP

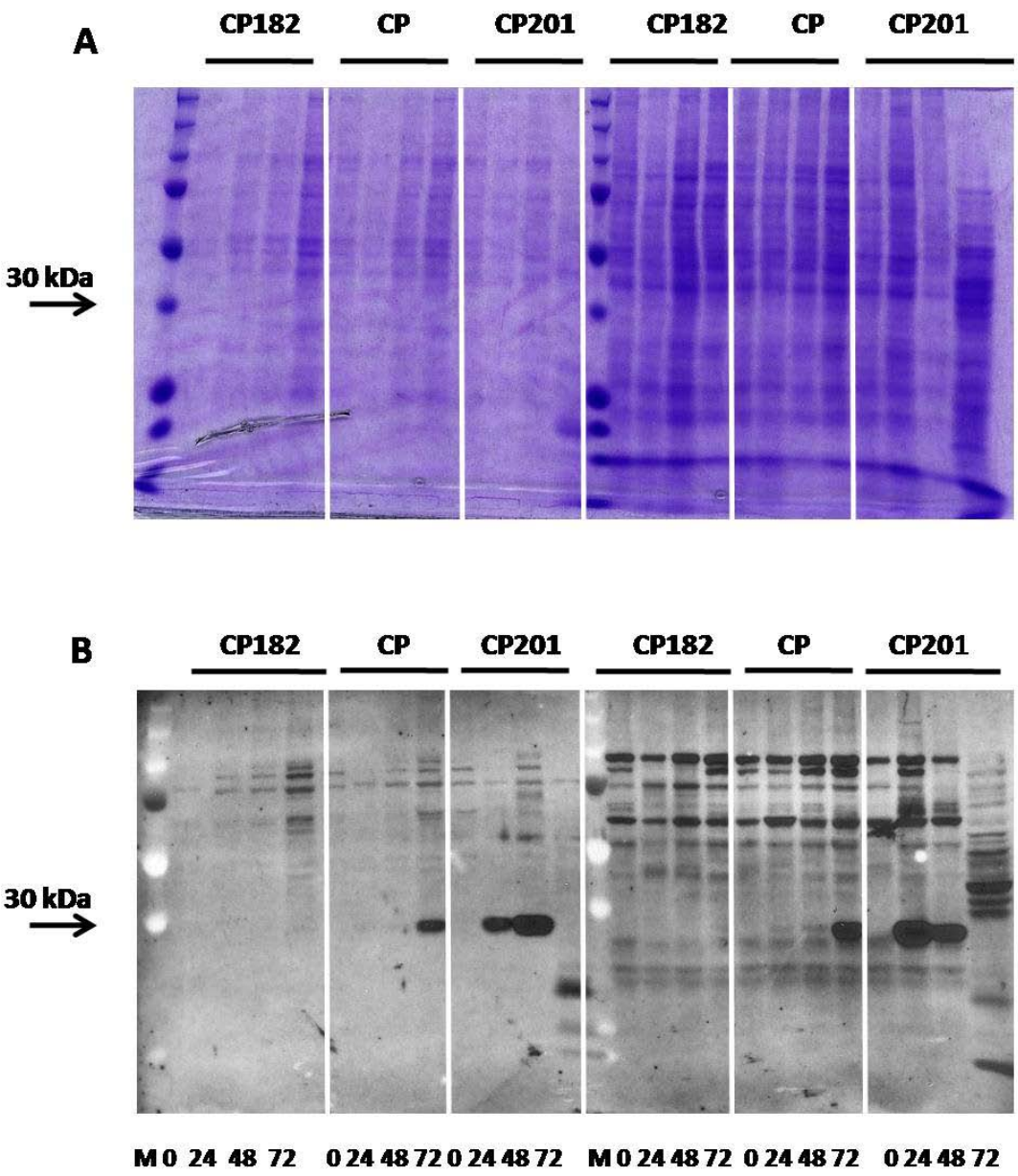

Figure 4-5. Western Blot of the time course experiment of the baculovirus expressed MSV-NCP wt and mutant. A) Coomassie stained gel of the supernatant (on the left) and cell lysate (on the right) harvested at 0, 24, 48 and 72 hr.post infection. B) Western blot analysis of the same fractions in A.

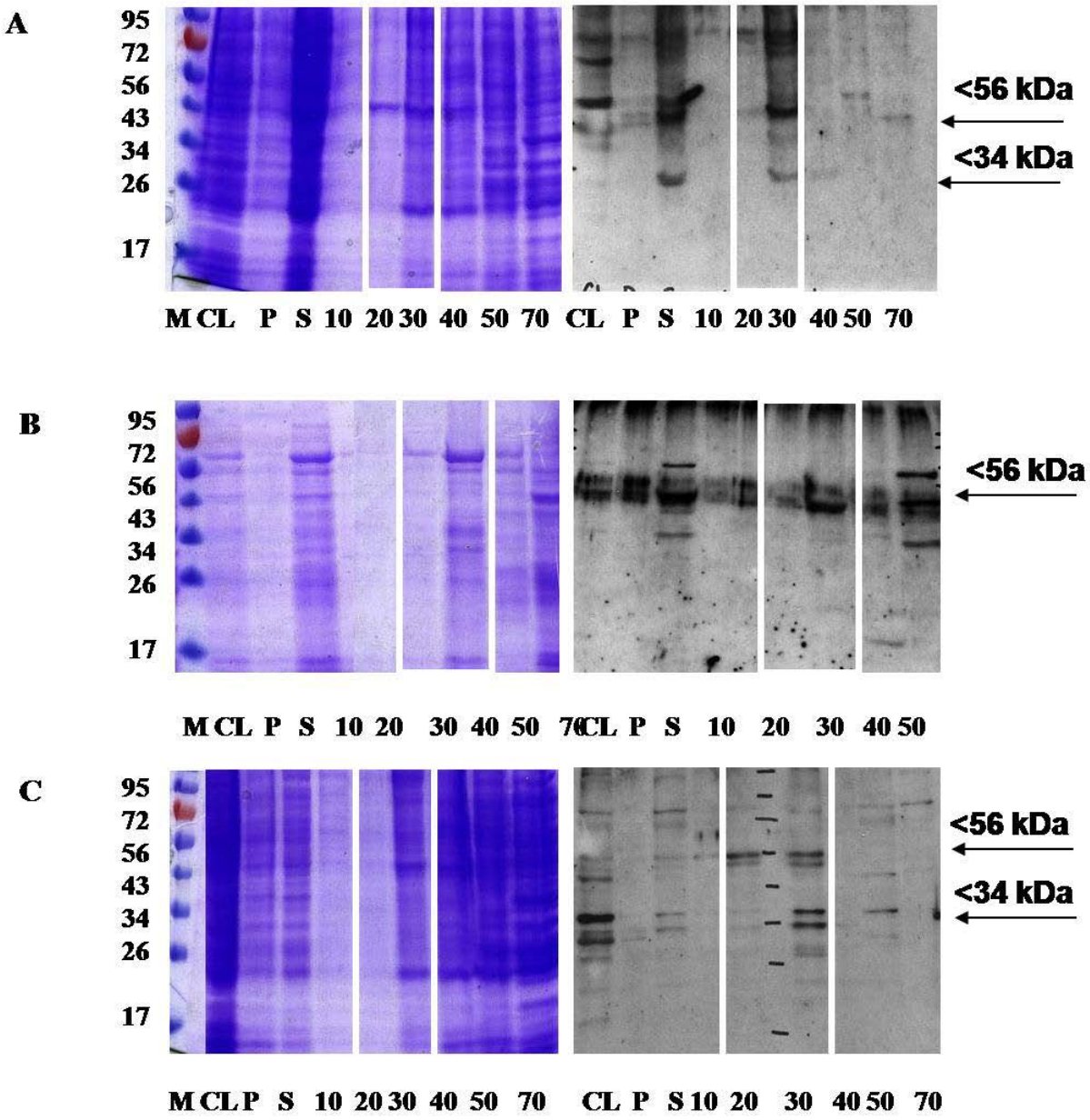

Figure 4-6. Ammonium sulphate precipitation fractions of baculovirus expressed MSV-NCP wt and mt A) BMSV-NCP182, B) pFMSV-NCP and C) pFMSV-NCP201. CL is the crude cell lysate, P is the pellet, S is the clarified supernatant, and the numbers represent the percentage ammonium sulphate used. The figures on the left are the coomassie stained samples and the figures on the right are western blots.

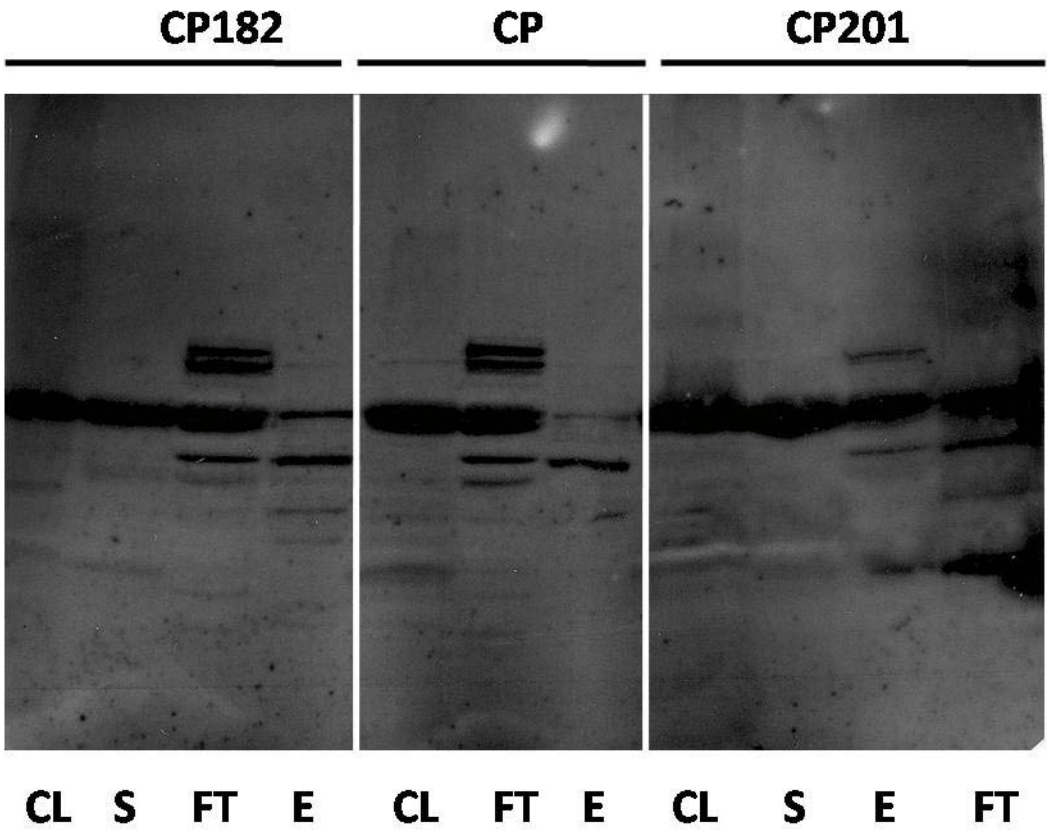

Figure 4-7. Western blot analysis of ion exchange column chromatography of MSV-NCP wt and mt A) BMSV-NCP182, B) pFMSV-NCP and C) pFMSV-NCP201. CL is the crude cell lysate, P is the pellet, and S is the clarified supernatant after centrifugation, FT is the flow through after the clarified supernatant was loaded on unto the ion exchange column and E refers to the eluant

CHAPTER 5
BIOPHYSICAL CHARACTERIZATION OF THE ASSEMBLY/DISASSEMBLY OF AAV2

Introduction

AAV2 is a non-pathogenic, non-enveloped parvovirus. It is a prototypic *Dependovirus* (64) as it requires the help of either Adenovirus or Herpes Simplex virus for a productive infection. The architecture of the AAV2 capsid is a T=1 icosahedral which is formed by 60 copies of VP1, VP2 and VP3 in a ratio of 1:1:8 respectively (130). The VPs share the same ORF, but different splice and translational start sites. The amino acid sequence of VP2 is encoded in VP1 and the sequence of VP3 is common to VP1 and VP2. The three dimensional structure of the AAV2 as described by X-ray crystallography (168) and cryo-em reconstruction (90) illustrates that each VPs forms an eight-stranded β sheet that forms the core contiguous structure, and each strand is connected by the interconnecting loops that are responsible for the capsid surface features. The AAV2 capsid is characterized by a shallow depression at the 2-fold symmetry axis, fingerlike projections surrounding the 3-fold symmetry axis and a pentameric pore surrounding the 5-fold symmetry axis. To date, AAV2 is one of the most extensively studied AAV serotypes because of its use in the treatment of several human genetic diseases (16, 51, 69, 142). AAV2 has several advantages as a gene therapy vector as compared to other viruses. It has a broad host range, infects both dividing and non-dividing cells, has low pathogenicity and the recombinant form of the virus can be produced and purified in large quantities (40, 86).

There is a considerable amount of data available about almost all aspects of the AAV2 replicative life cycle which is illustrated in Figure 1-1. It has been shown that AAV2 infection is initiated by binding to its primary receptor heparin sulphate proteoglycan (96, 119, 129, 148). This facilitates the binding of the AAV2 capsid to either integrin $\alpha_v\beta_5$ (95, 141) and or fibroblast growth factor1 (127), which are both secondary receptors. The AAV2 capsid is then internalized

by endocytosis in clathrin coated pits (15). The AAV2 capsid is acidified in the endosome, which is believed to facilitate the externalization of VP1. The externalized VP1 has two functions: phospholipase activity of the unique region of VP1 which allows the virus to escape the endosome (55), and nuclear localization sequences located within both VP1 and VP2 (145), which target the virus to the nucleus. The virus is transported to the nucleus by microfilaments and microtubules (141). The nucleus is the site of DNA replication and transcription. The viral transcripts are transported to the cytoplasm where they are translated, then the translated proteins are transported to the nucleus where the newly synthesized VP is believed to be assembled and the viral genome packaged (68, 117, 160). In the case of a lytic infection the viral capsid is released or in the absence of helper virus the viral genome becomes integrated into the host genome(17, 34, 35, 87, 88, 92). There is limited information available on the mechanism involved in the assembly of the mature particle.

There is substantial information available about the roles of the VPs. It has been shown that mutagenesis of both the N-terminus and C-terminus of VP3 abolishes the formation of the viral capsid (135), has shown that VP1 is important for capsid infectivity (66), VP1 and VP2 are required for the nuclear transport of VP3 (66, 135). It has also been shown that VP2 alone can transport VP3 to the nucleus, as well as both VP2 and VP3 are required for the assembly of the viral capsid (135) and for the sequestering and accumulation of the virus progeny ssDNA, this is still not completely settled as both Samulski and Worrington has made VP3 only capsids. Furthermore, time course immunofluorescence experiments illustrate the formation and accumulation of capsid intermediates (pentamers) which are transported to the nucleus, specifically, the nucleolus which is believed to be the site of AAV2 capsid assembly (160, 161). This information now leads us to ask other questions, namely: what is the signal used by the

three capsid protein to transport them to the nucleus and is this signal based on the three dimensional structure of the VPs and their interaction with each other, it also raises the question as to the possible order of capsid assembly. Is a trimer formed as in the case of MVM (133) and CPV (163) or is it a dimer or a pentamer? To address these questions a series of mutations were made in the AAV2 capsid, and all VP structures (capsid and intermediates) expressed in a baculovirus system was characterized with the overall goal of deciphering the steps involved in the assembly of the AAV2 capsids.

To date, at least 130 AAV2 capsid mutants have been made, Wu, et al (165), made 67 AAV2 capsid mutants, 48 of which were charge cluster mutants and found 11 mutants that did not assemble. Lochrie, et al(106), made only surface mutants; none of which turned out to be assembly mutants. Blekker et al. (18) and Sonntag et al. (145), made 5-fold pore mutants hoping to find packaging mutants; 3 of them were also assembly mutants. AAV2 shows regions of high sequence conservation with other AAV serotypes as well as high structural conservation with other parvoviruses which might suggest residues that are required for capsid integrity and stability (56, 121). Our first specific goal was to identify the residues that are essential for holding the capsid together. We hypothesized that conserved residues at icosahedral symmetry related interfaces are likely to participate in assembly enabling interactions, and that mutation will disrupt assembly. Second, as stated above, we also hoped that the mutational analysis might reveal the steps involved in capsid assembly. This would be accomplished by the isolation and purification of capsid intermediates that may be formed. Third, the biophysical characterization of baculovirus expressed intermediate would provide information about the steps in viral assembly.

We constructed a total of 22 mutants. Experimental data presented in this chapter indicates that the mutation of amino acid residues at the 2-fold and 5-fold symmetry related interfaces either adversely affects or prevents the assembly of AAV2 capsids. Furthermore, in addition to 5-fold interface mutations not assembling capsids, they also don't make any detectable capsid intermediates suggesting that the 5-fold intermediate is formed first during capsid assembly. This data is consistent with the purification of pentameric intermediates obtained from our baculovirus expressed AAV2. The mutations at the 3 fold interface had minimal or no effect on capsid assembly, suggesting redundant non-mutant residues can compensate.

Results

Selection of Residues for Mutagenesis

The AAV2 residues selected for mutagenesis were based primarily on the available high resolution X-ray crystal structure of AAV2 (90, 168). Residues were identified based on their interaction at the 2–fold, 3-fold and 5-fold symmetry related monomer interfaces. Residues that are within a 3.4Å (hydrogen bond distance) from each other were generated by the program Contact. The contact list obtained for the 3-fold monomer related interactions was almost 2.5 times the number of that obtained for the 5-fold and the 2-fold monomer related interactions. The list was then trimmed by comparison with similar lists obtained for other parvovirus whose structures had been determined, and residues/interactions that were conserved were selected. Finally some residues that had previously been implicated in assembly by alanine scanning mutagenesis (165) were included. Table 5-1 contains a list of the mutants as well as their location in the viral capsid monomer, and their symmetry related interactions. Figure 5-2 and Figure 5-3 illustrate the positions of the mutated amino acids within the VP monomer structure. The mutants have been generated in the AAV2 plasmid pIM45 which expresses all three capsid proteins and all 4 replication proteins. All the mutations are located in VP3 since this protein is

sufficient for capsid assembly and is the only structure observed in all the 3-D structures of AAV2 so far determined (90, 168, 169). A total of 22 residues were selected for site directed mutagenesis and their phenotypes were characterized.

Symmetry Related Location of VP3 Mutants

There are 7 mutants that are located within the 2 fold symmetry related monomer interface. Four are located within the wall of the 2- fold depression (R294A, Q297A, R298A and R294/8A) on the conserved α-A helix and 3 of them (K692A, W694A and P696A) are located on the C terminal loop which forms the floor of the 2-fold depression. K692 and W694 are exceptions within the group as these positions also have 3-fold related interactions (Figure 5-4A and Figure 5-4B). The buried surface area of the 2-fold interface is 3060 $Å^2$ and represents the weakest of all the symmetry related interface interactions.

Seven of the 22 mutants are involved in 3-fold related interactions. The 3-fold interface is the strongest of all the symmetry related interactions. The buried surface area of this interface is 10352 $Å^2$. The large area is related to the fact that the interactions at this interface are extensive and are generated predominantly by the βEF and βGH loops that interlock to form the 3-fold axis. The positions of these mutants are illustrated in Figure 5-5A and Figure 5-5B.

There are 8 mutant positions that are potentially involved in 5-fold related interactions. Two of these are double mutants V221/S224A and H255/K258A. The 5-fold pore is generated by the monomer related interaction of the conserved ribbon between βD and βE (324-338) forming a turret like structure interacting with N-terminus of the adjacent monomer (219-229). The depression surrounding the 5-fold pore contains loops and conserved β strands and is the location of all the other 5-fold related mutants. The buried surface area of the 5-fold interface is 4949 $Å^2$ which is intermediate in size compared to that of the 2-fold and 3-fold monomer related interactions. The other distinguishing feature of the 5-fold axis is the loop extending over each

interface monomer from the highly conserved parvovirus HI loop. F661 is a non-interface mutant that sits on the corner of the HI loop (Figure 5-6A and Figure 5-6B). Finally, two mutants, Y413 and F415 were chosen because they are highly conserved residues; they also do not sit on an interface.

Immunoblots of Mutant Cell Lysate

The non-infectious AAV2 plasmid, pIM 45 (wt and mutants), GFP plasmid pTRUF11 and and pXX6, which provides Adenovirus helper function, were triple transfected in HEK 293 cells to make GFP packaged virus.

Immunoblots were used to determine the effects of the mutations on VP1-3 expression and capsid assembly. A panel of 4 monoclonal antibodies (B1, 1F, A20 and C37B) were used to perform preliminary characterization of the mutants. B1 antibody recognizes a linear epitope in the carboxy terminal of all 3 capsid proteins; this antibody was used to determine whether the mutants were capable of producing the capsid proteins. 1F recognizes a linear epitope present in all 4 Rep proteins. Because Rep proteins form complexes with capsid intermediates it was important to demonstrate that Rep expression was not impaired (161). The A20 and C37 antibodies (162) are neutralizing antibodies that recognize non-linear structural epitopes on the AAV2 capsid surface. A20 is unique in that it recognizes only intact, fully assembled capsids, while C37 can recognize some assembly intermediates. When the lysates from the mutants were probed with A20 and C37 it was apparent that all but one of the 2-fold mutants and three of the 5-fold mutants were defective for capsid assembly. In contrast all of the 3-fold mutants appeared to be capable of assembly of at least some capsids (Figure 5-7A). Western blot of all the mutants showed the expression of VP1 and VP3. Most of the mutants that were A20 positive, except Y441A, P622A, and H255A/K258A also showed the expression of VP2. All the other mutants

either did not show VP2 expression, or they appeared to have multiple bands at a molecular mass similar to that of VP2, and is illustrated in Figure 5-7B.

AAV2 Total Particle Titration

To determine more precisely the severity of the capsid assembly defect we used A20 ELISA to determine the total amount of AAV2 capsid produced for each mutant. The total capsids produced for each mutant was compared to wt and the log of the ratio was plotted in Fig. 5-8. When this was done it became apparent all of the 2-fold mutants were defective for assembly including K692A which assembled approximately 100 fold fewer than wt capsids. Similarly, all but one of the 5-fold mutants (F661) was found to be significantly defective for capsid assembly. Finally, although none of the 3-fold mutants were found to have defects that were statistically significant, all of them displayed a trend toward lower assembly (2-7 fold) compared to wt.

Packaging Efficiency

Twelve of the 22 mutants produced sufficient yields of intact capsids to determine the relative ability to package DNA and to transduce cells. Real-time PCR, with forward and reverse primers to GFP was used to determine the amount of genome packaged by each mutant. Packaging efficiency was determined by comparing the total number of capsids assembled (as determined by A20 ELISA) with the total genomes packaged (as determined by RT-PCR). As shown in Figure 5-9 only one mutant R389A (in the 3 fold group) was significantly defective for packaging compared to wt. R432 which assembles capsids, was not included in this analysis as we and others have shown previously that this mutant packages little or no detectable DNA (19).

Infectious Particle Titer

To determine the effect of the mutations on particle infectivity, serial dilutions of mutant cell lysate was used to infect HEK 293 cells in the presence of Ad5. The number of green cells

counted for each dilution, at 24 hr post infection, was used to determine the infectious units/ml for each mutant. The number of viral genomes per infectious unit is referred to as the particle-to-infectivity ratio. This ratio is equivalent to the number of genomes required to transduce one cell and provides a measure of the relative infectivity of the mutant compared to wt. Of the twelve mutants that were capable of assembling intact mature capsids, four were severely defective for infectivity (>7 logs): K692A, Y441, L510A and R404A (Figure 5-10). An additional 2 mutants P602A and H255/K258A, were also partially defective (2 logs) for infectivity.

Virus Purification and Visualization

The mutant AAV2 VP capsid and sub-assembled capsid components were purified on a step iodixanol gradient followed by ion exchange column chromatography. The iodixanol fractions were screened using the monoclonal antibody B1, to determine which fractions are positive for the VPs. The capsid containing mutants were B1 positive from the 40/60%, 40/25% and 25% iodixanol fractions (Figure 5-11A, B, and C). The non-capsid mutants on the other hand were B1 posistive only from the 40/25% and 25% iodixanol fractions; this is shown in Figure 5-11A and Figure 5-11C. The B1 iodixanol fractions were further purified by ion exchange chromatography, using a Q Sepharose column. The peak Q Sepharose column fractions were used to prepare EM grids and viral capsids, subassembly intermediates, or monomers were visualized by TEM. The electron micrographs clearly show AAV2 capsids for the mutants that were A20 positive; they are located predominantly in the 3-fold symmetry related interface. There appears to be subassemblies for the 2-fold non-capsid mutants, and is illustrated in Figure 5-12.

Baculovirus AAV2 VP Purification and Characterization

To determine all assembly components in a baculovirus expressed AAV2, the iodixanol fractions were further purified on a Q Sepharose column and the peak fractions were visualized

by EM illustrated in Figure 5-13A. Three main components were identified, a sub-assembled intermediate labeled P, empty capsids with sub-assembled component attached labeled I, and a closed capsid labeled C. The sub-assembled intermediates were and intermediate capsids were purified from the 40/25% and 25% iodixanol fractions and the closed capsids were purified from the 40/60% iodixanol fraction.

To determine the molecular mass of the different bAAV2 components isolated, the samples were sent to BNL for STEM analysis. The shape of each component was visualized on STEM and EM micrographs as illustrated in Figure 5-13A and B. The sample labeled P had a mean, median and modal mass measurement of approximately 600 kDa (Table 5-2 and Figure 5-14) and the micrographs illustrated what appears to be a mixture of single specie or two specie attached to each Figure 5-13B. The molecular mass of the sample labeled P is consistent with the mass of ten VP3s. This data would imply that our subassembled intermediate is either two pentamers beside each other forming a dimer of pentamers (DOP) or five dimers interacting to form a pentamer of dimer (POD). Also of interest were the empty capsids with what appeared to be subassembled intermediates or pentameric intermediates attached. Both the molecular mass of the empty capsids calculated and the histogram showing the distribution of molecular mass in the sample is consistent with the pentameric intermediate attached to empty capsid (Table 5-2 and Figure 5-15). The molecular mass of the closed capsid according to STEM analysis is approximately 3,200 kDa, which is presented in Table 5-3, illustrated as one peak in Figure 5-16, and is consistent with the molecular mass of an empty capsid.

To evaluate the assembly state of the different components, immunoblot analysis was conducted using antibodies against denatured and native baculovirus expressed AAV2 samples. The results are illustrated in Figure 5-17A, which shows that the sample labeled P is B1 positive

when denatured and the native sample is B1 negative. The data prove that the pentameric intermediate contains the VP3, and the C-terminus is not accessible in the native state. The data also show the pentameric intermediates in the native state either does not contain VP1 or VP2, or they are not accessible to the A69 or A1 antibody. The pentameric sample is also A20 negative which would verify the subassemblies observed in the electron micrographs. The intermediate and the closed sample are both A20 positive and they are not positive for A1 and A69 which would indicate that VP1 or VP2 is not externalized. Figure 5-17B illustrates that the pentamer is composed predominantly of VP3 while the capsid containing fraction is composed of VP1, VP2 and VP3.

Discussion

In this study we generated a panel of 22 mutants, 19 of which are icosahedral symmetry related interface mutants and 3 were selected based on the fact that their phenotype had previously been investigated and they appeared to have an assembly defect. Our experimental data clearly shows that the mutants generated were predominantly assembly mutants and, they are located in the 2-fold and 5-fold axis and symmetry related interface. It should be noted that the selection of these mutants were based largely on the available crystal structure of AAV2, MVM, as well as other AAV serotypes, with the goal of identifying residues that were essential for assembling viral capsids and maintaining their integrity. Concurrently we isolated and characterized three different assembly components form a baculovirus expressed AAV2. These components include a pentameric intermediate, an intermediate capsid conformation and a closed capsid. The goal of this experiment was to increase our knowledge of the steps involved in the assembly and disassembly of the virus.

Assembly Mutants

The predominant symmetry related interactions that are considered assembly mutants are the 2-fold and 5-fold. All the mutants located at the 2-fold axis are assembly mutants. Based on the crystal structure, the αA helix forms the wall of the 2-fold depression and the C-terminal loop interlocks with the adjacent monomer to form the floor. It has been shown that the 2-fold axis is the thinnest region of the capsid (169) and we have shown that the mutations of several residues within this interface will either prevent the AAV2 capsid from assembling or it will destabilize the assembled capsid. This data is consistent with information obtained by Pei Wu's mutants' mut 24 and mut 19 (165), which are both double mutants with a non-capsid, non-infectious phenotypes. Mut 24 is R294A/D295A, and both residues are located on αA, helix and mut 19 is H229A/D231A, where D231 interacts with K692A in a 2-fold related interaction (165). The other assembly mutants are located either in the 5-fold axis or at the 5-fold symmetry related interface. The double mutants V221A/S224A are located in the wall of the 5-fold pore as well as within the 5-fold interface, M402A is located on the conserved sheet of a 5-fold interface interaction and they are also assembly mutants. All other 5-fold related mutants, which include, H255/K258A (mut 21), Y397A, and R404A, form capsid in significantly less quantity than wt (Figure 5-8). Other 5-fold symmetry related assembly mutants include V221W, V221C, V221Y (18, 19), H229/D231A (mut 19) which is also a 2-fold related interaction, K321A/E322A (mut26) and N334W (165). The compilation of all AAV2 assembly mutants generated in this work (Table 5-3) as well as previously characterized assembly mutants clearly shows that both the 2-fold and 5-fold symmetry related interactions are critical for capsid assembly and stability (Table 5-4, and Figure 5-15).

Internal Polar Mutants

There are another set of mutants that are not located on any symmetry related interface, but have been characterized as defective as well as partially defective for assembly. These mutants are located primarily in the β sheets of the eight stranded β barrel facing the internal of the capsid (Figure 5-16). These residues are polar and a few are ringed which may be important for their interaction with the viral genome or for the maintenance of the structural integrity of the β barrel and the overall icosahedral shape of the viral capsid.

Packaging and Infectivity Mutants

The mutants that make capsids belong to two 2 main groups, one is based on whether or not it packages genome. R432 and R389 are classified as packaging mutant, because they encapsulate less viral genome, than wt. R432 has been extensively characterized as a packaging mutant. R389 is both a 3-fold as well as a 5-fold monomer related interface. The packaging and release of the viral genome through the AAV pentameric pore has been illustrated for AAV2 based alanine mutants or the substitution of pore residues with larger residues, and has been postulated to occur through its pentameric pore. This phenomenon has also been shown for other viruses; these include the autonomous parvoviruses as well as several picornaviruses (61).

There are 4 mutants that are significantly defective for infectivity. It should be noted that the particle to infectivity ratio of R404A, L510A, Y441A and K692A is reduced by approximately 8 logs compared to wild type which is recorded as 2 logs vector genomes per infectious unit. These mutants are located within three separate symmetry related interfaces, that is, R404A is a 5-fold symmetry related mutant, L510 and Y441 are 3-fold symmetry related mutants, and K692A is both 2-fold and 3-fold symmetry related mutant. They appear to make capsid and package capsid just as well as wt but are defective in terms of their particle infectivity. In this case infectivity may be related to viral trafficking, or genome release

(uncoating). L510 is connected to the N511 which is also important for secondary receptor (α_v β_1) binding site, as well as, genome packaging (8). Residue G512P was also shown to be 5-fold defective in terms of particle infectivity (106). NGR (511-513) has been predicted to be the site of interaction with the secondary integrin receptor (α_v $\beta_{1)}$.

Structure to Function Correlation for AAV2 Capsid Based on Assembly Studies

We have shown that the assembly of AAV2 to form it's T=1 icosahedral is an ordered process in which the first intermediate formed is a pentamer followed by a interaction at the 2-fold interface, we are not sure if the 3-fold interface requires a scaffold or chaperone or if the interactions at the 3-fold interface are so redundant that the effect of the disruption of one interaction does not affect how the capsid assembly. The symmetry related interactions of the T=1 icosahedral AAV2 are critical to the survival of the virus, for example, the 3-fold axis has been shown to be important for host cell recognition, and receptor binding; the 5-fold has been shown to be important for VP1 externalization and endosomal release, and viral genome packaging and based on our study both the 5-fold and 2-fold symmetry related interface appears to be critical to its assembly and stability. These findings are important because the use of AAV2 in treating genetic diseases. The new trend in gene therapy is the generation of chimeric AAVs which will target specific tissues. Knowing the residues as well as the symmetry related interface that are important for assembly and the stability of the virus will guide us in our decisions as to the regions of the capsid that cannot be changed.

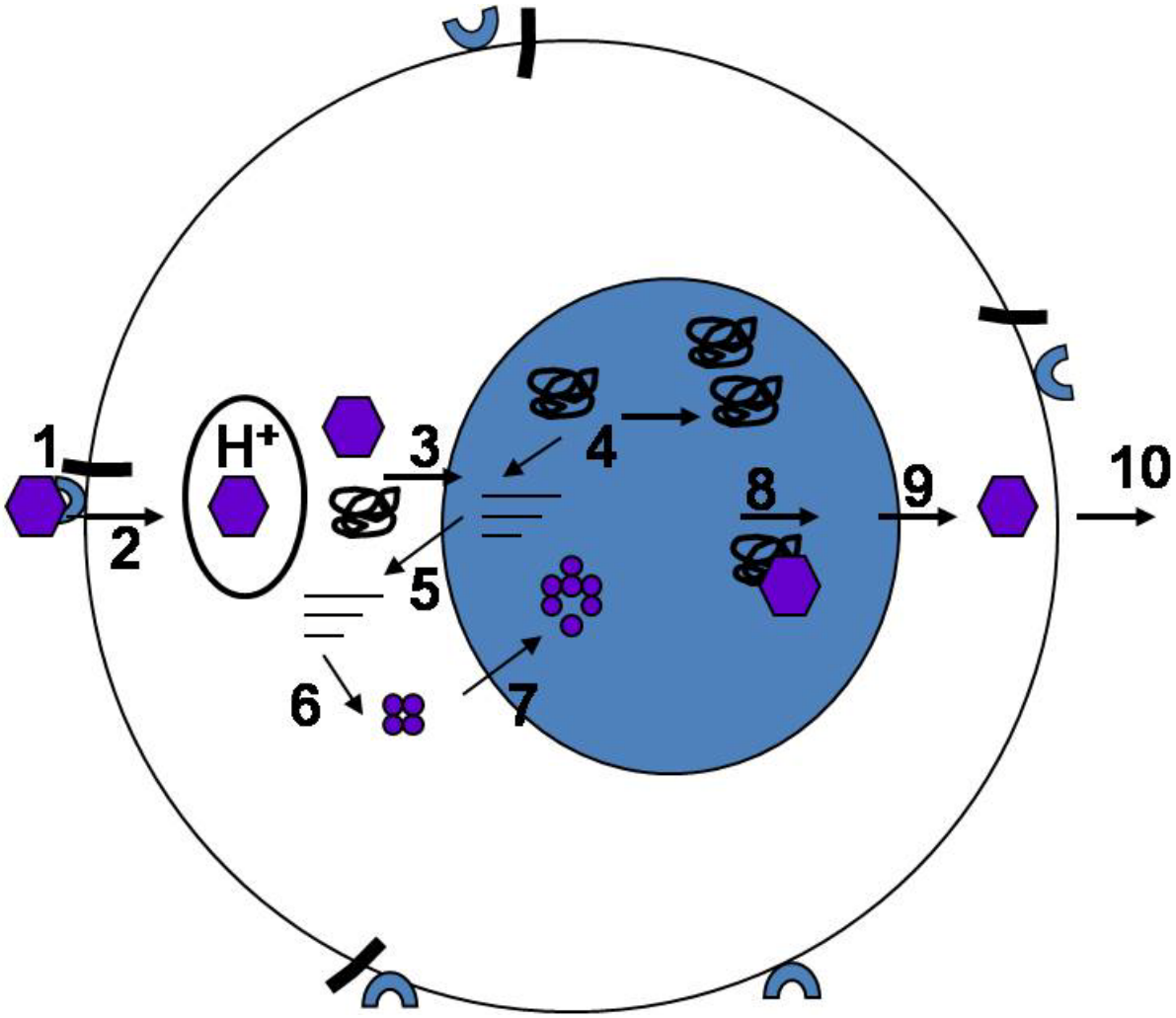

Figure 5-1. Schematic of the life cycle of AAV2. 1) AAV2 infection is initiated by binding to its primary and secondary receptor. 2) Clathrin mediated endocytosis followed by endosomal acidification. 3) Viral capsid disassembly, release of genome and transport to the nucleus. 4) Viral replication and transcription. 5) Export of viral mRNA from the nucleus. 6) Translation of VPs and Reps. 7) Assembly and transport of VPs or empty capsids to the nucleus. 8) Resolution and packaging of viral genome. 9) Egress from the nucleus. 10) Release from host cell during a lytic infection. The purple hexagon represents the AAV2 capsid, blue half circles represent the primary receptor, black quadrilateral represents the secondary receptor, and the purple circles represent the VPs and reps.

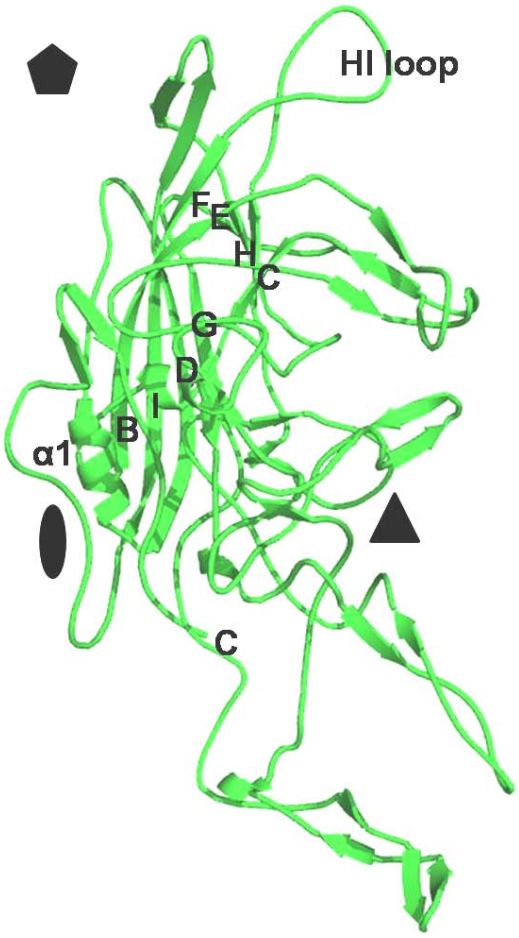

Figure 5-2. Ribbon diagram of AAV2 VP3 based on its crystal structure. The oblong, which marks the icosahedral 2-fold axis, the triangle marks the icosahedral 3-fold axis, and the pentagon represents the icosahedral 5-fold axis.

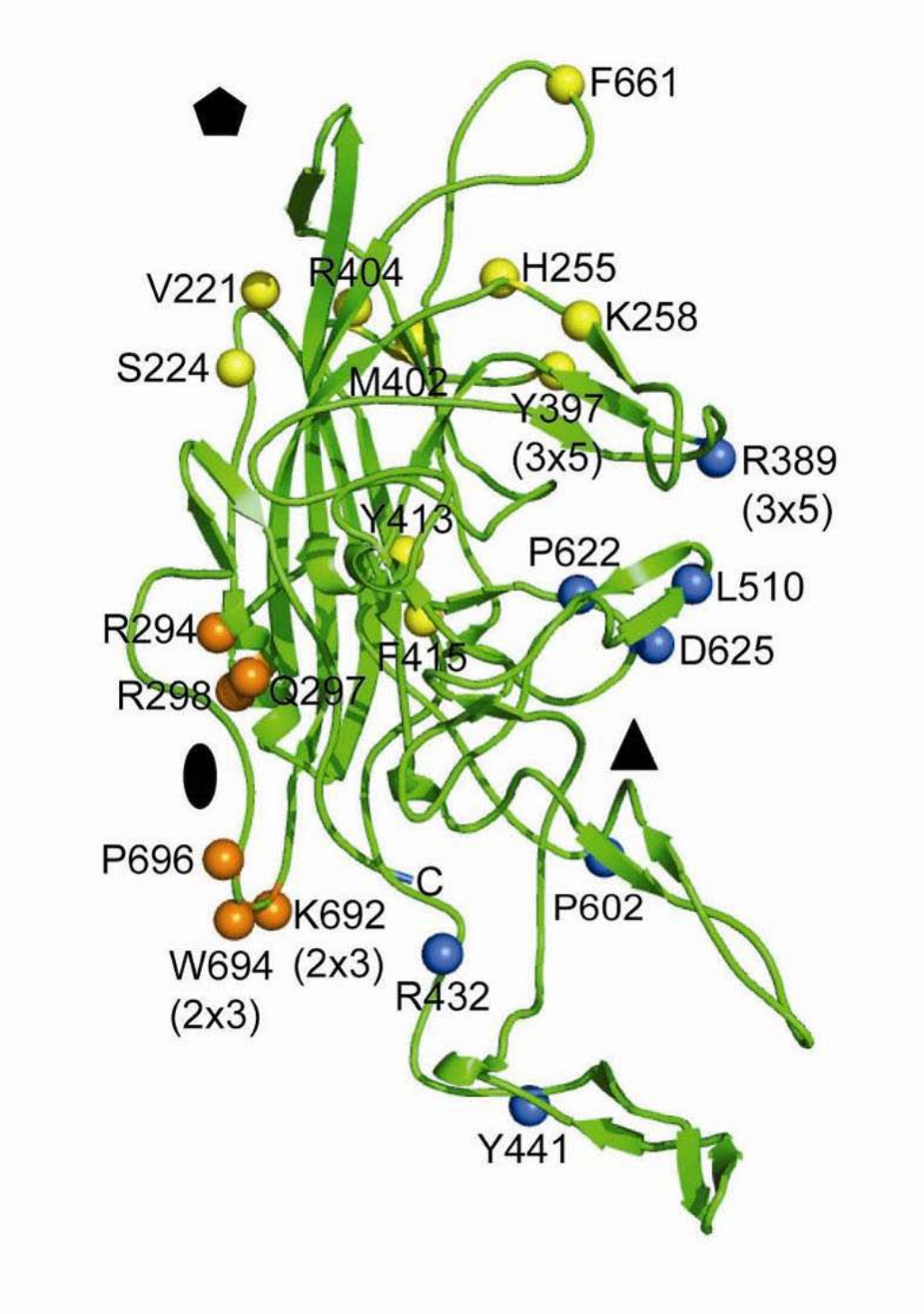

Figure 5-3. Ribbon diagram of AAV2 VP3 based on its crytal structure, and the spheres show the position of each mutant. The orange spheres are the two fold symmetry related mutants and they are located in the immediate vicinity of the oblong, which marks the icsahedral 2-fold axis. The blue spheres are the icosahedral 3-fold mutants and the triangle marks the icosahedral 3-fold axis. The yellow spheres represents the5- fold symmetry related mutants and the pentagon represent the icosahedral 5-fold axis.

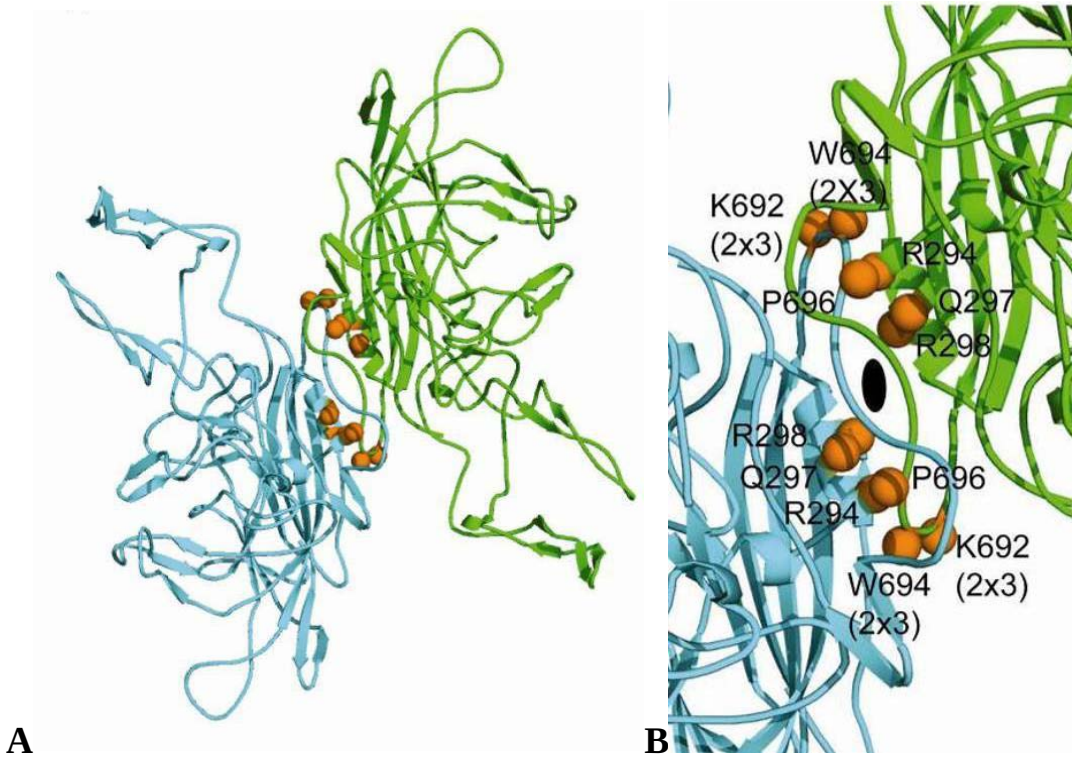

Figure 5-4. Ribbon diagram of the AAV2 icosahedral 2-fold axis with the orange spheres representing 2-fold symmetry related interface mutants. A) 2-VP3 monomers viewed down the 2-fold axis. B) Close-up of 2-fold axis showing location of mutated residues.

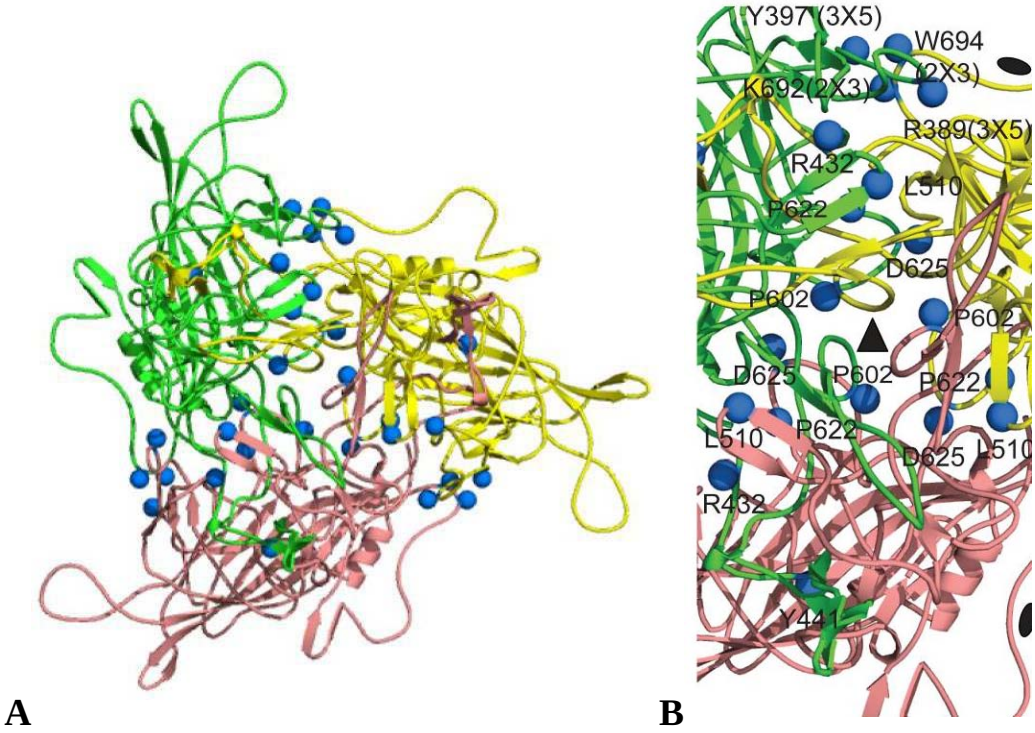

Figure 5-5. Ribbon diagram of the AAV2 icosahedral 3-fold axis with the blue spheres representing 3-fold symmetry related interface mutants. A) 3-VP3 monomers viewed down the 3-fold axis. B) Close-up of 3-fold axis showing location of mutated residues.

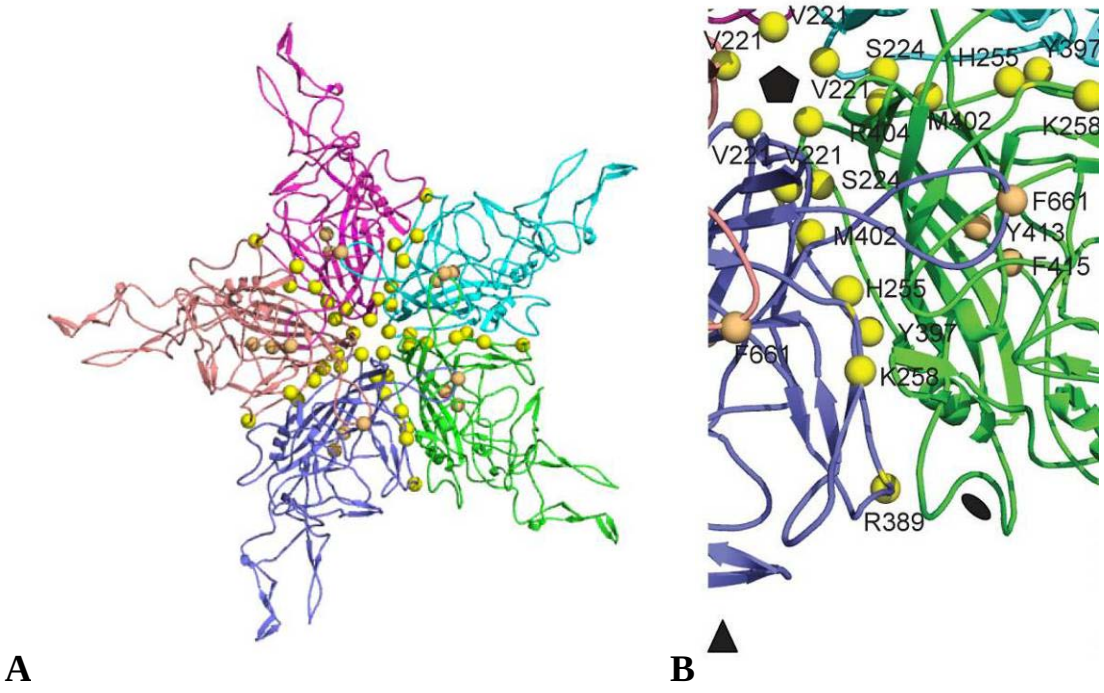

Figure 5-6. Ribbon diagram of the AAV2 icosahedral 5-fold axis with the yellow spheres representing 5-fold symmetry related interface mutants. A) 5-VP3 monomers viewed down the 5-fold axis. B) Close-up of 5-fold axis showing location of mutated residues.

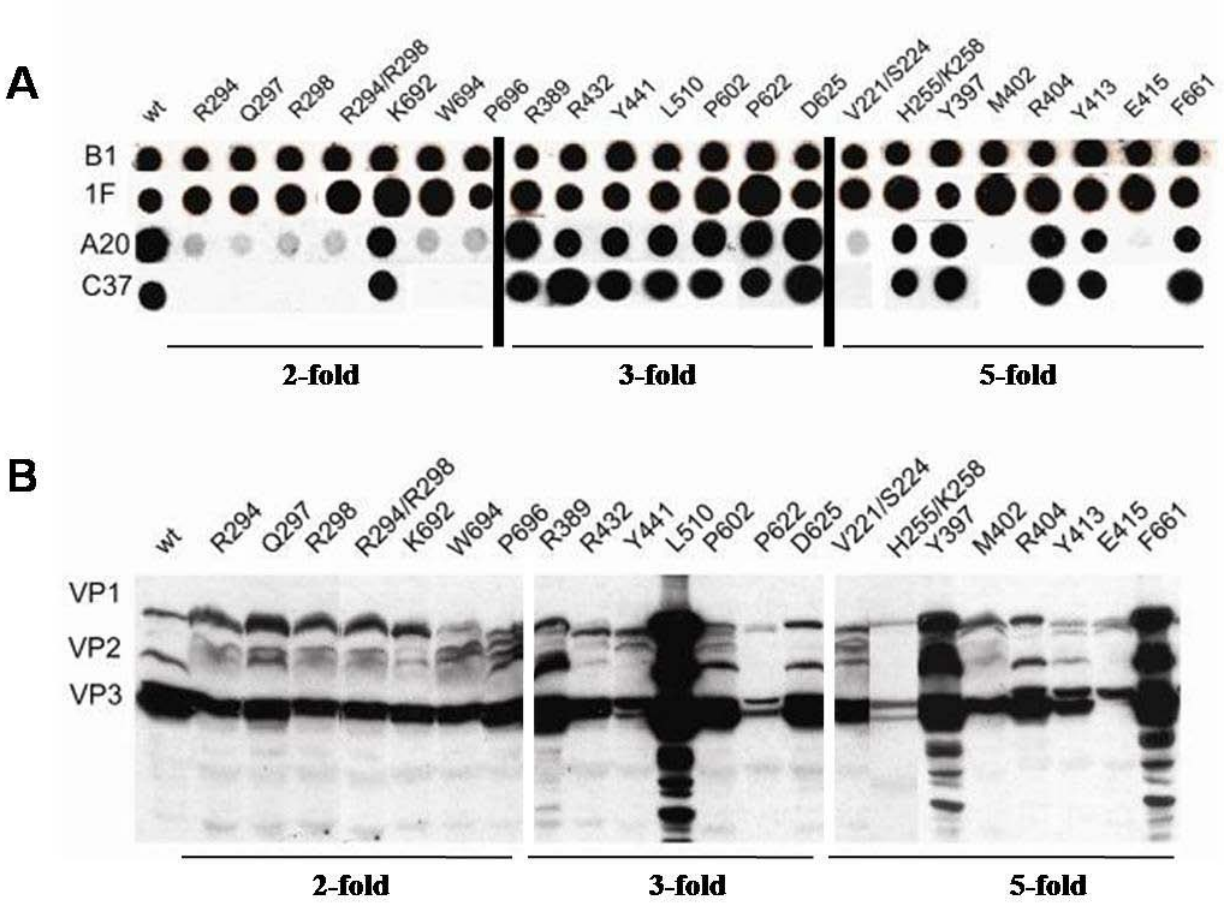

Figure 5-7. Immunoblots of AAV2 mutant cell lysate. A) Denatured Dot Blot utilizing B1 (row 1) for all viral capsid proteins (VP1-3) and 1F (row 2) for all the replication protein (Rep 42, Rep 52, Rep 68 and Rep 78). The A20 and C37 lanes are native dot blots and are used to identify intact AAV2 capsids. B) Western blot utilizing B1 as the primary antibody used to detect all three viral capsid proteins (VP1-3).

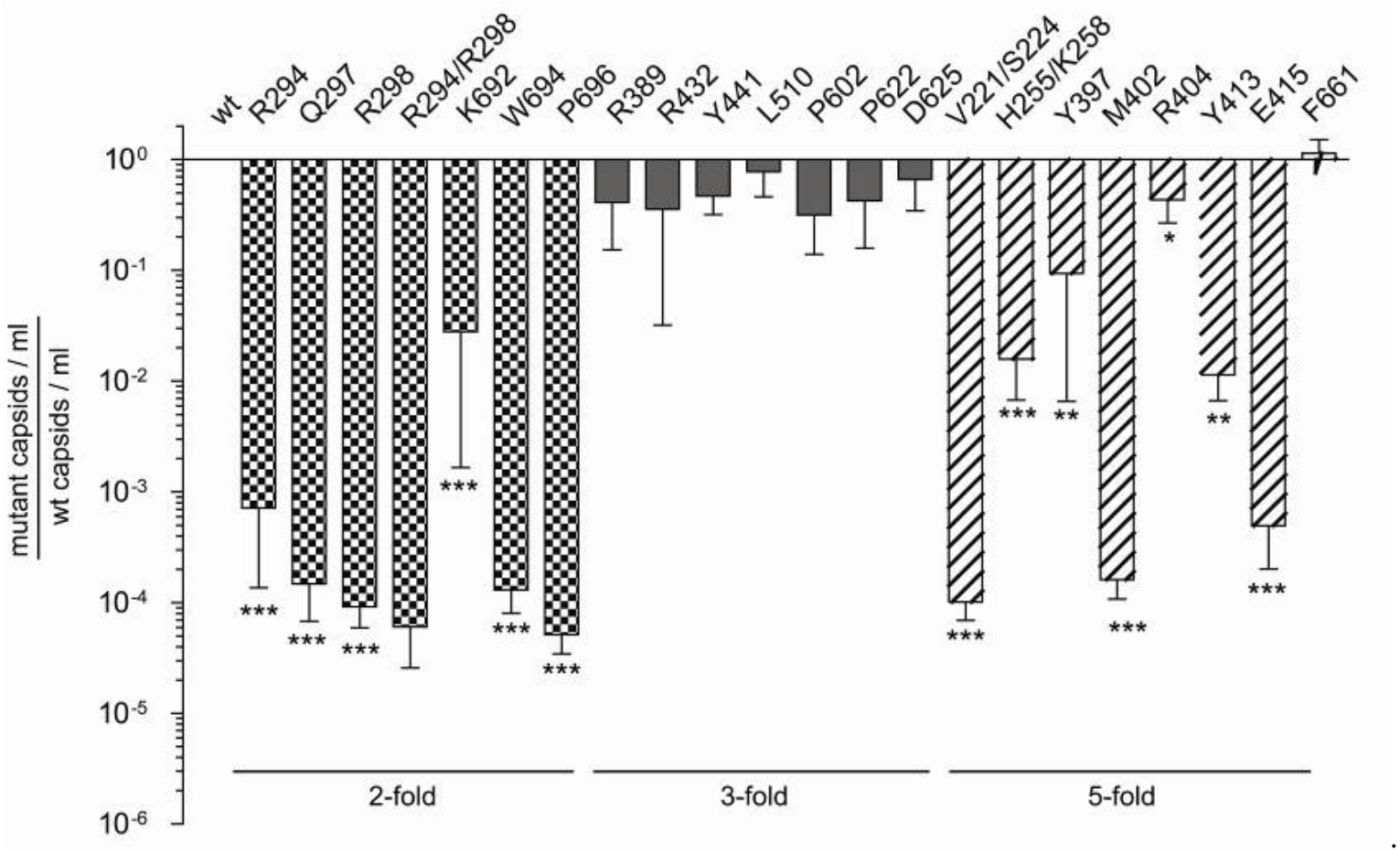

Figure 5-8. Histogram of A20 value for each mutant versus A20 value of the recombinant wt AAV2. The mutants were grouped into three categories; the 2-fold, 3-fold and 5-fold symmetry related interactions. Group ANOVA statistics were determined for :2-fold vs wt. F [6,19]=1294, P=0.0001, for 3-fold vs wt: F [7,21]=1.363, P=0.2674 , and for 5-fold vs wt F[9,29]=11.16, p=0.0001. Tukey's post hoc results are indicated as *, **, *** = P < 0.05, 0.001, and 0.0001 vs wt.

.

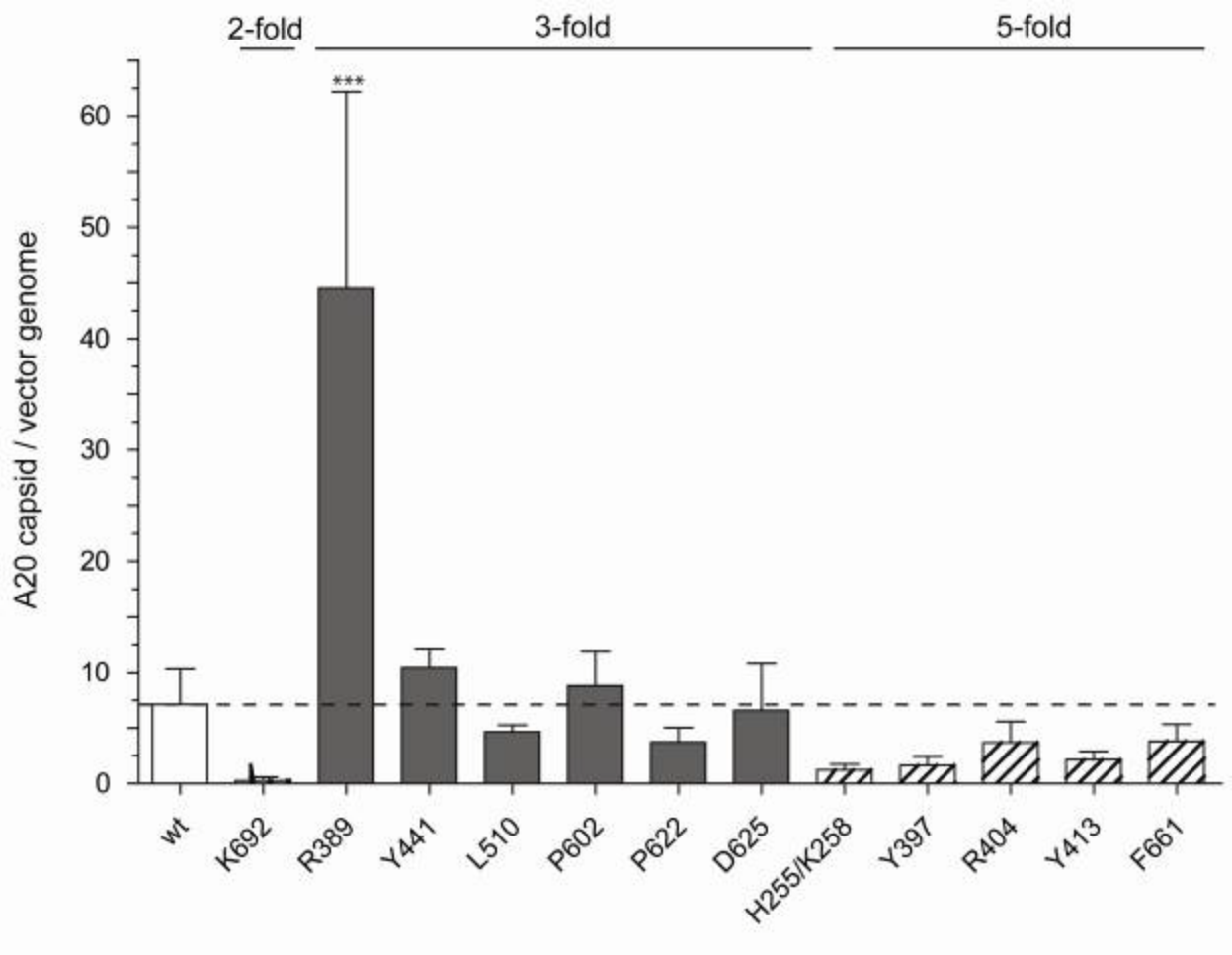

Figure 5-9. Histogram of the packaging ratio obtained for each A20 positive mutant. The packaging ratio is determined by dividing the A20 value obtained by the RT-PCR value for each mutant. Group ANOVA Statistics: F [12, 23] = 6.920, P=0.0001 with Tukey's post hoc results indicated as ***, P< 0.0001

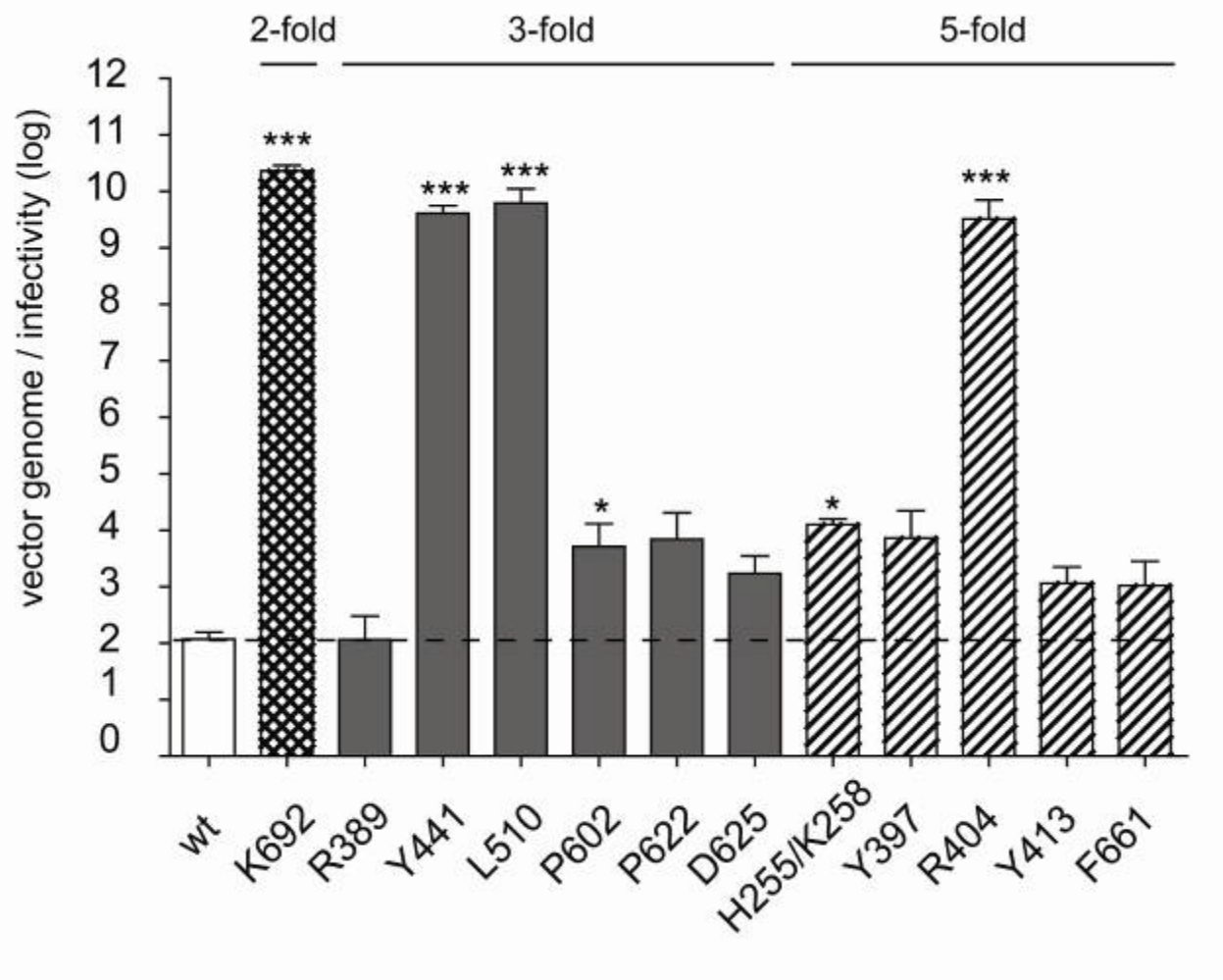

Figure 5-10. Histogram of the log of the particle infectivty ratio obtained for each A20 positive mutant. One Way Anova statistics: F[12, 22] = 98.40, P=0.0001. Tukey's post hoc results are indicated as *, *** = P < 0.05, and 0.0001

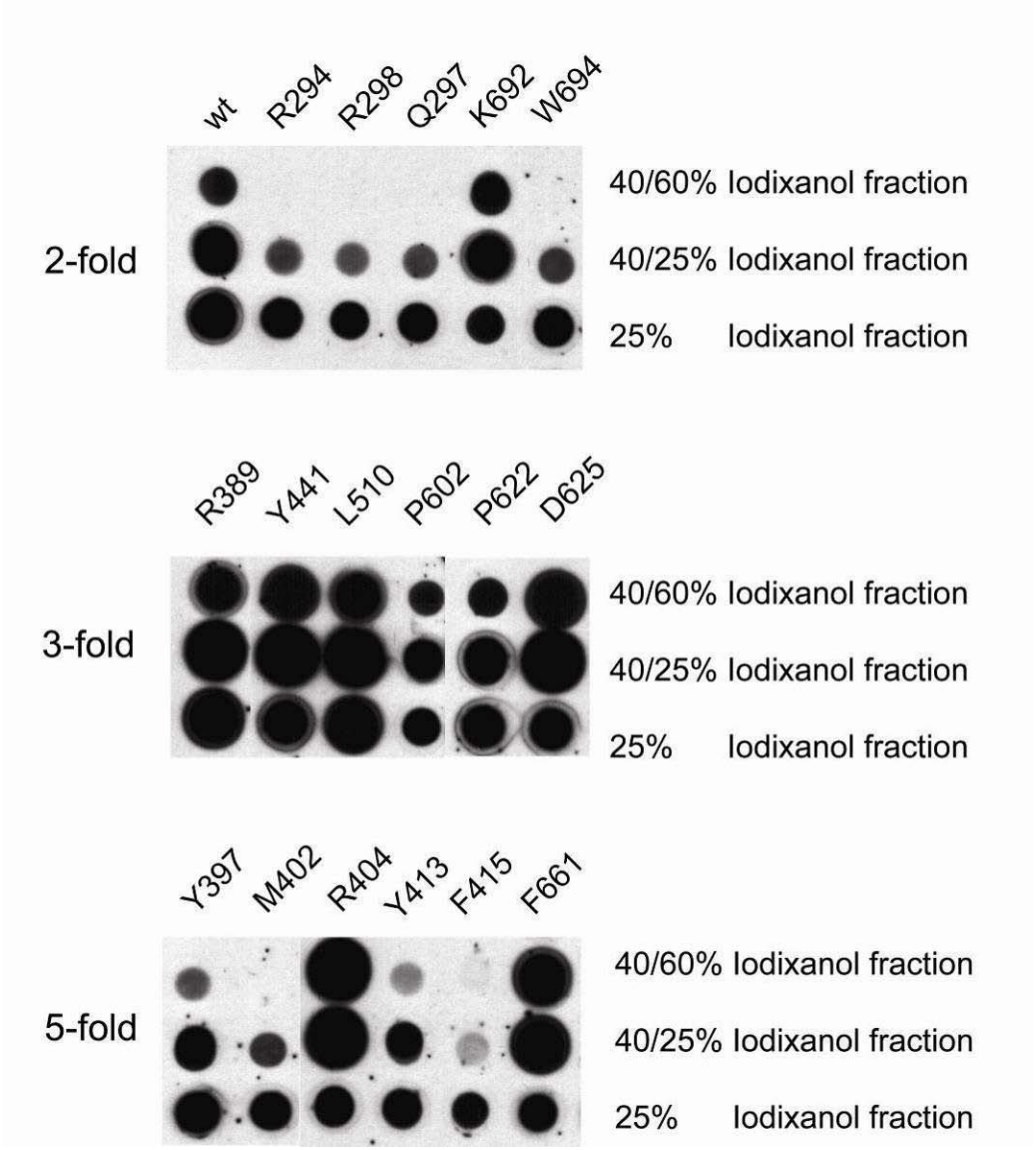

Figure 5-11. B1 dot blot of AAV2 mutants purified on a step iodixanol gradient.

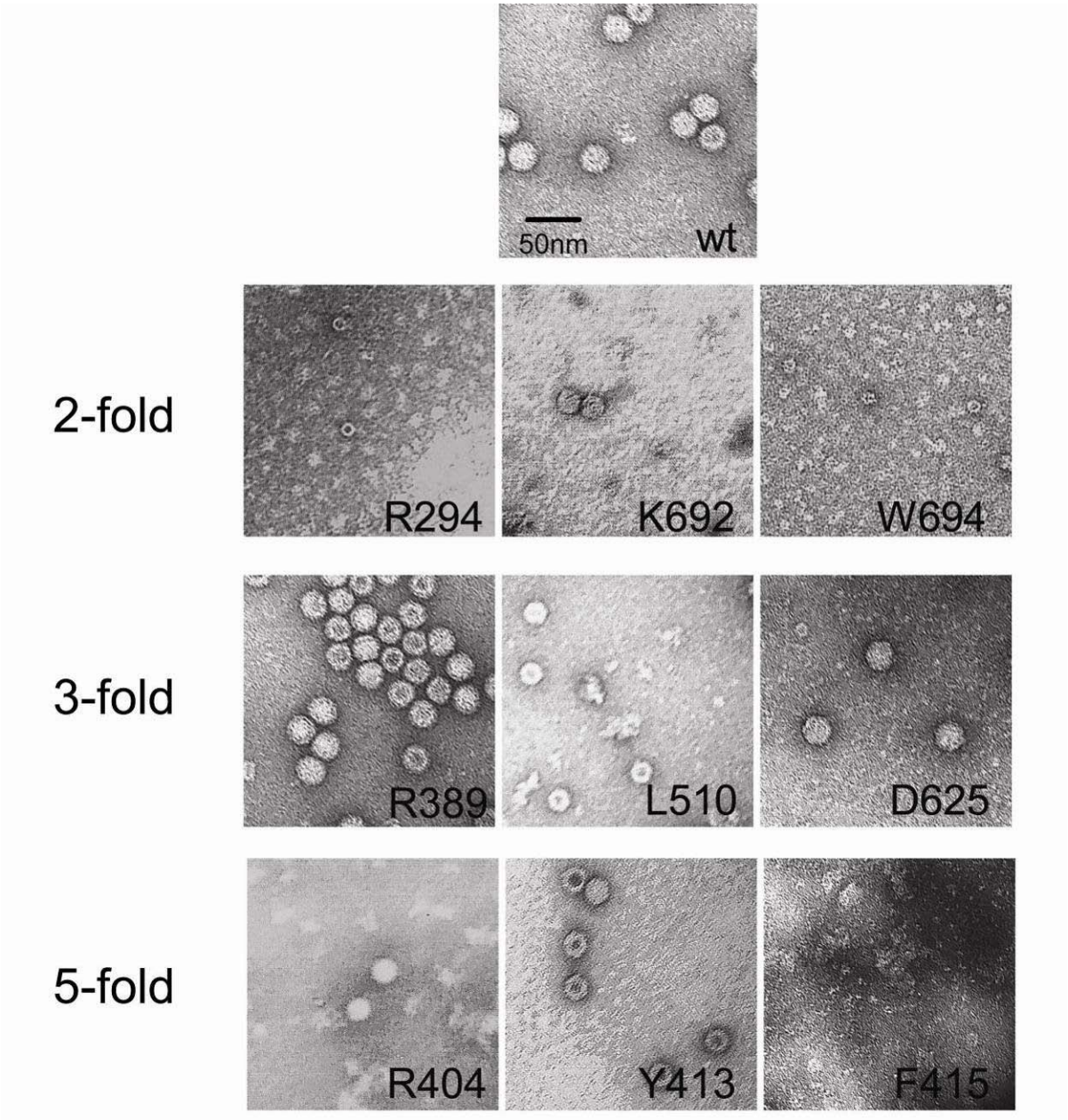

Figure 5-12. Transmission Electron Micrographs of ion exchange column purified AAV2 mutants after iodixanol step gradients.

A

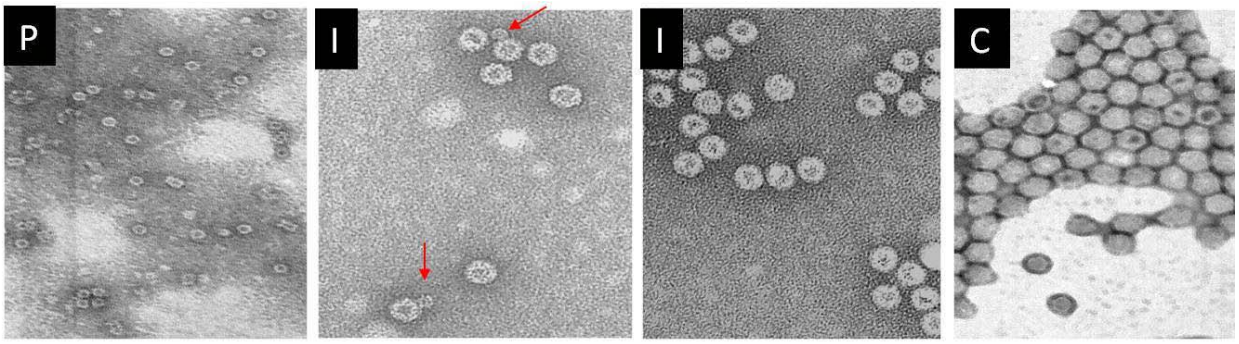

B

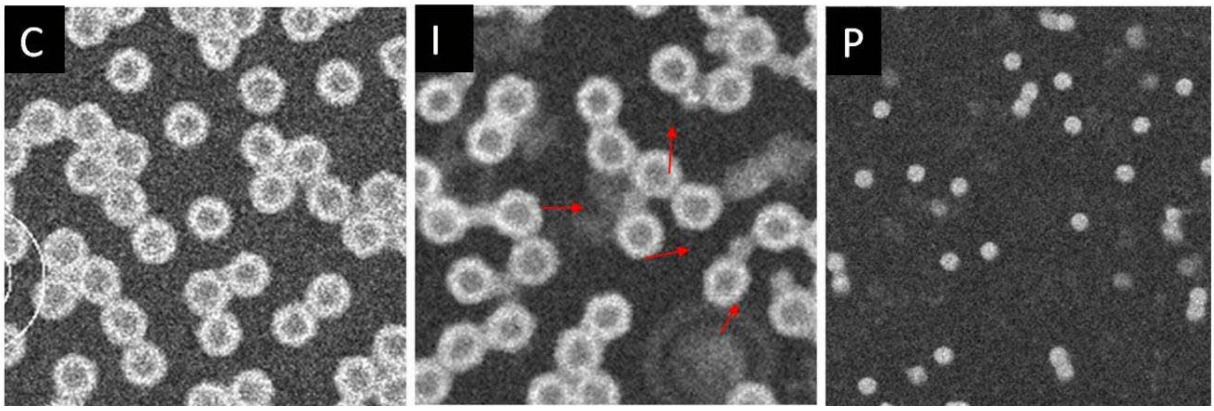

Figure 5-13. Visualization of AAV2 capsids and intermediates. A) Electron micrographs of subassemblies refered to as (P), open conformation with pentamer beside capsid (I) to the left, and the red arrow pointing to a flap, another view of the capsid with a region of the capsid appear to be partially opened (I) to the right, and I and P are isolated from 40/25 % iodixonal gradient, and the closed conformation (C) which was isolated from a 40/60 % iodixonal gradient. B) STEM micrographs of AAV2 components, the red arrows indicating the presence of the pentamer apparently attached to the capsid**.**

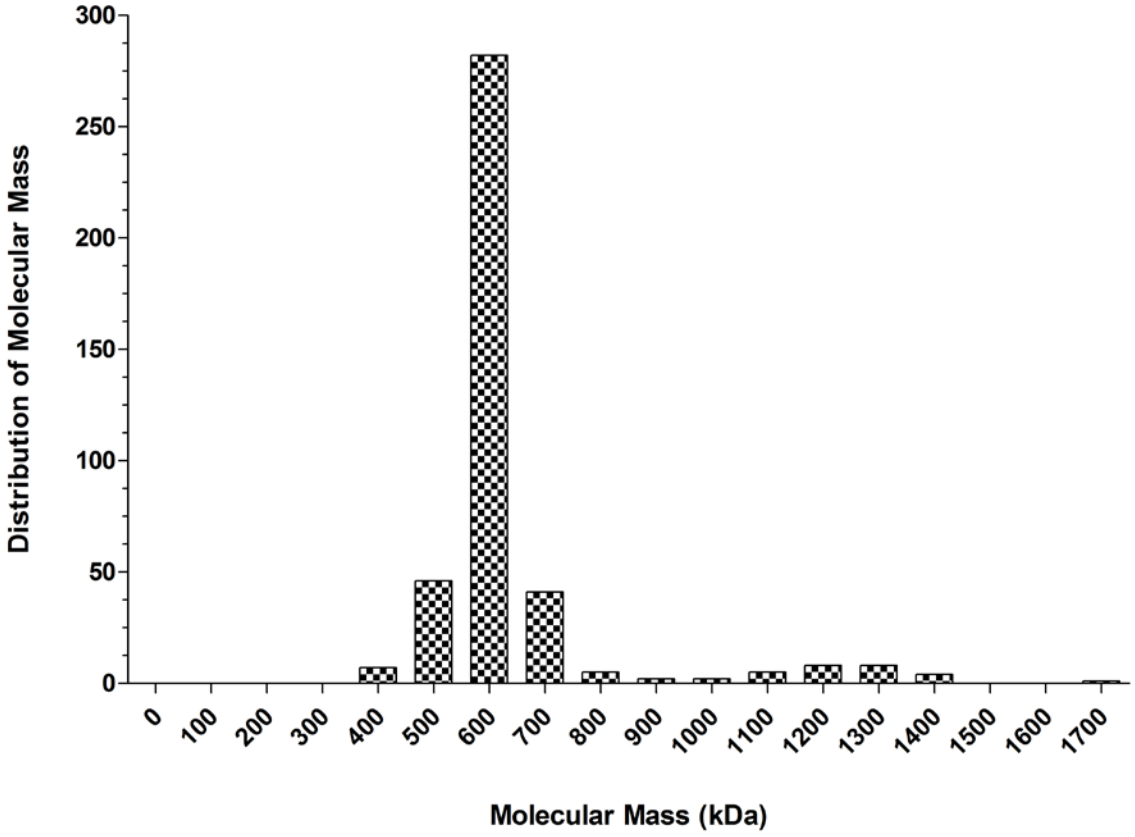

Figure 5-14. STEM histogram of baculovirus expressed AAV2 intermediates.

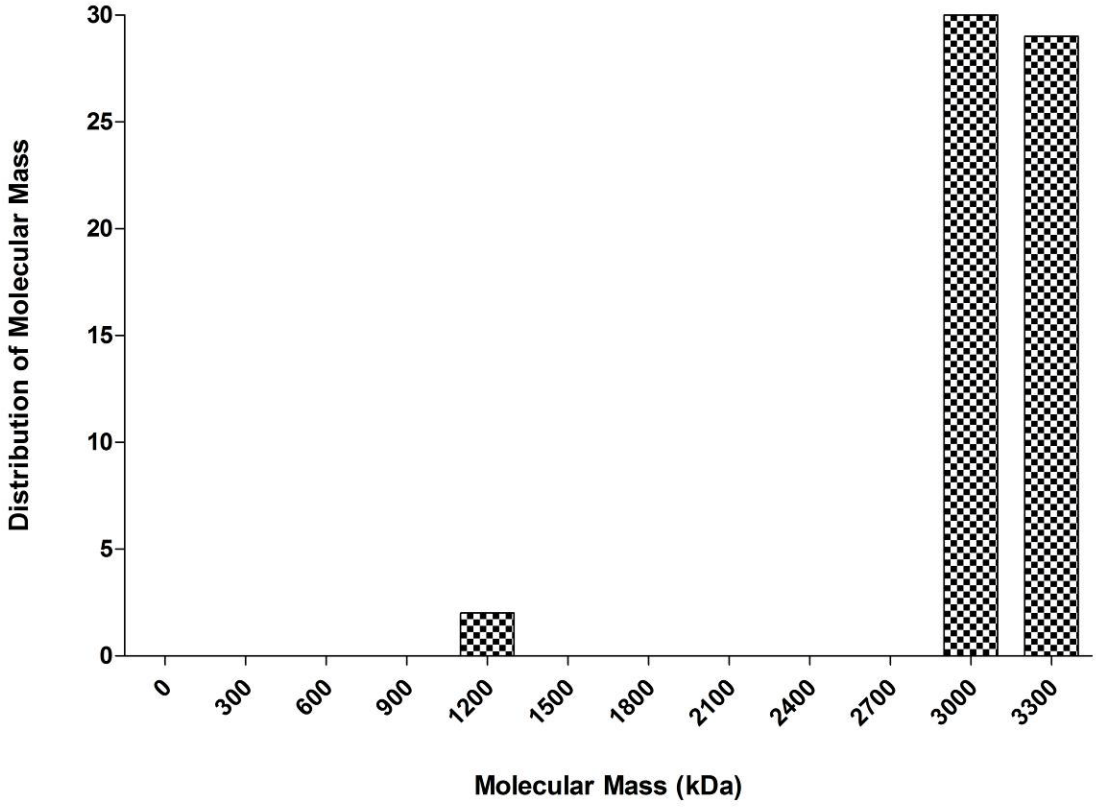

Figure 5-15. STEM histogram of baculovirus expressed AAV2 capsid intermediates with intermediates attached.

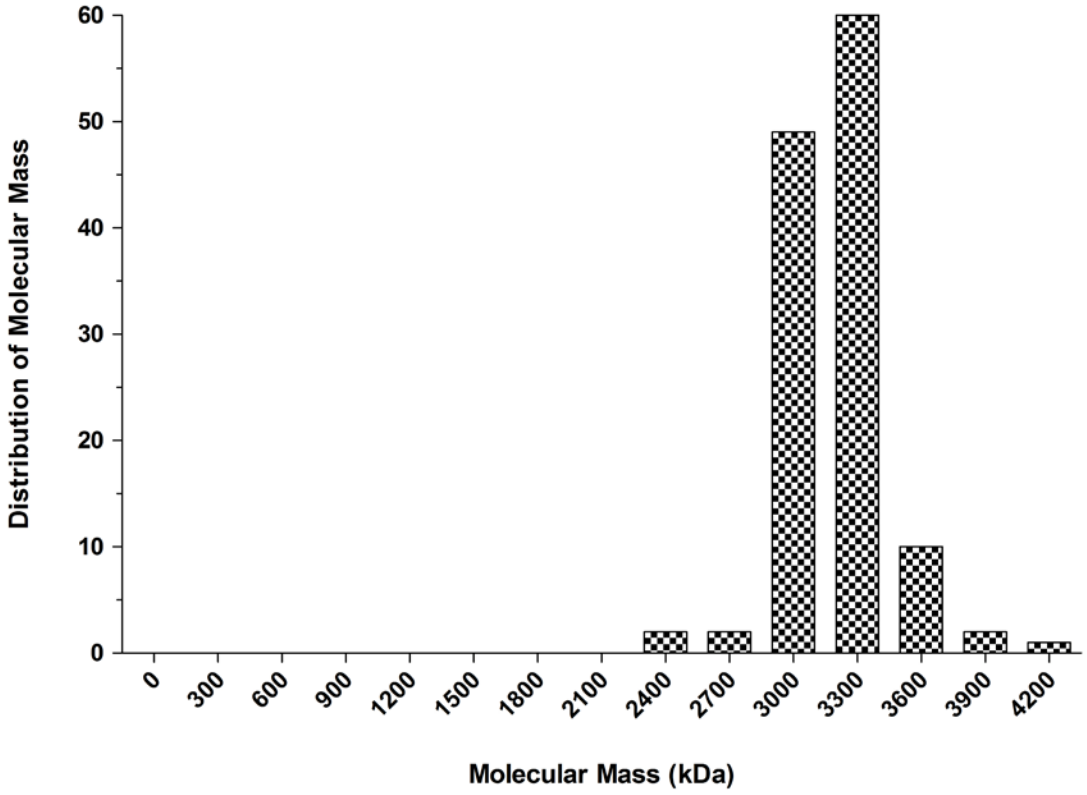

Figure 5-16. STEM histogram of baculovirus expressed AAV2 capsids.

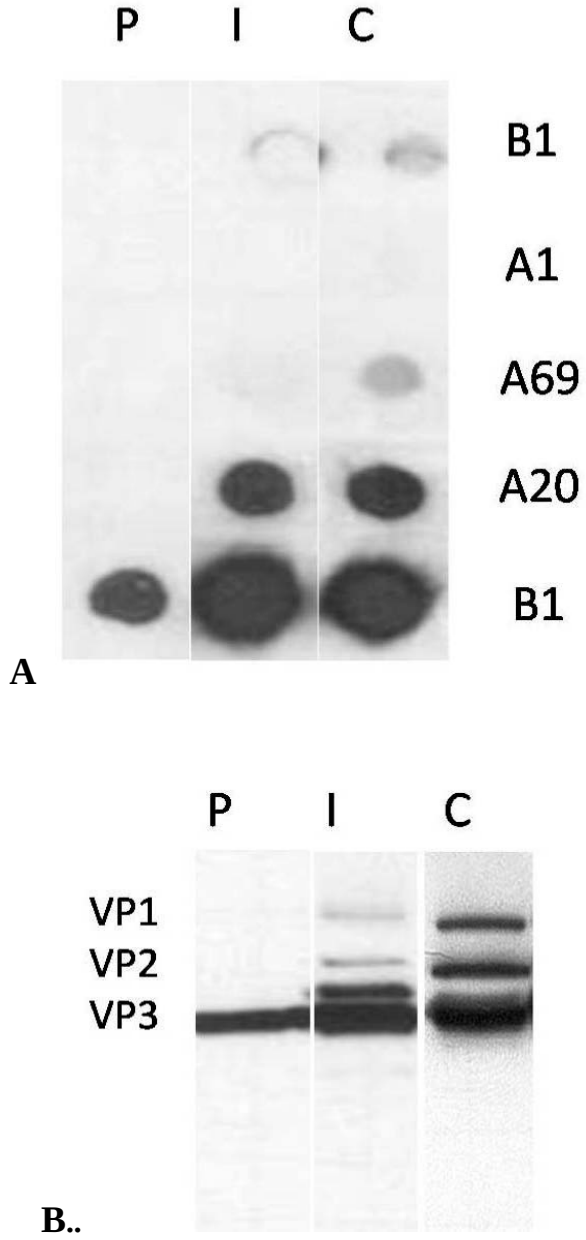

Figure 5-17. Immunoblot and SDS gel characterization of AAV2 capsids and intermediates. A) Dot Blot of AAV2 samples with different antibodies on the left. B) Coomassie stained SDS gel, lane 1 contains intermediate components, lane 2 contains open conformation with the pentamer beside the capsid, and lane 3 contains capsids with a closed conformation.

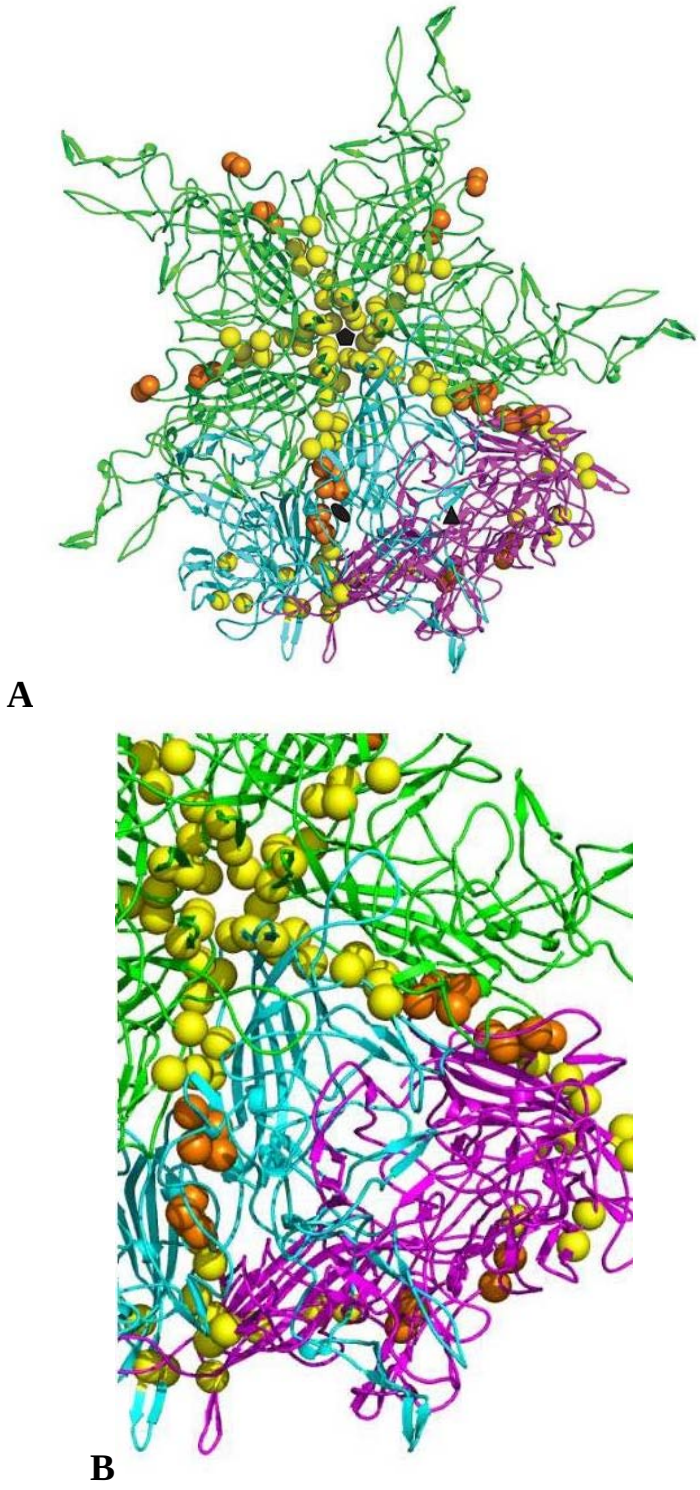

Figure 5-18. Ribbon diagrams of AAV2 assembly mutants. A) The yellow spheres representing 5-fold symmetry related interface mutants and orange spheres representing 2-fold symmetry related interface interactions. B) Close-up of 5-2-3-fold axis showing location of mutated residues.

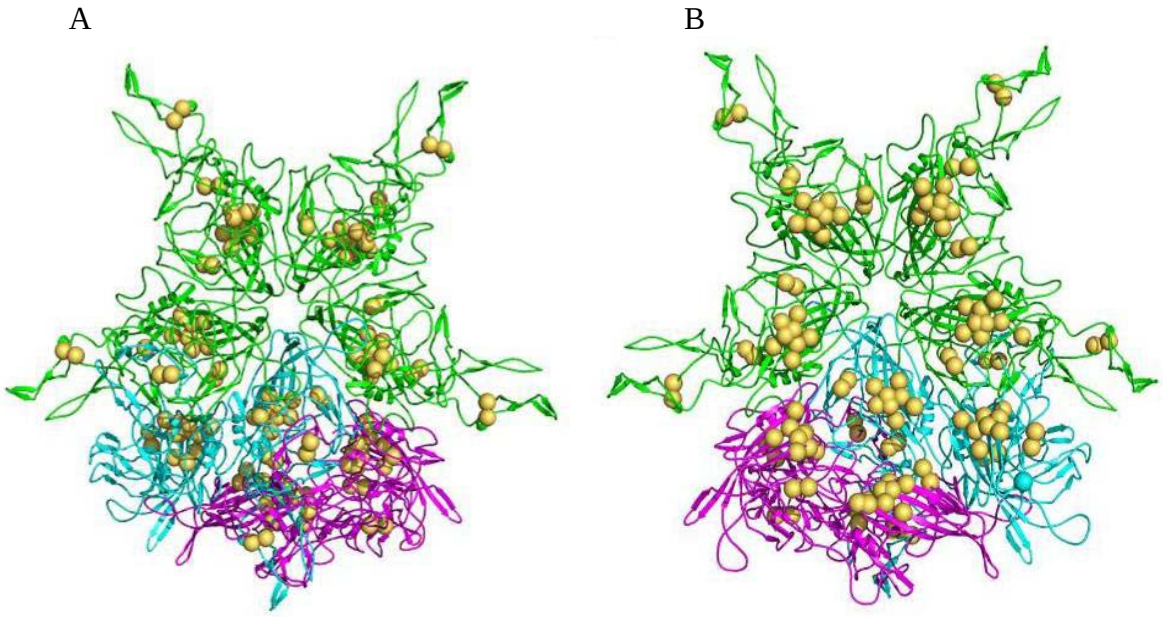

Figure 5-19. Ribbon diagrams of different views of AAV2 internal polar cluster mutants (salmon colored) spheres (A) outside looking in and (B) inside looking out.

Table 5-1. List and location of AAV2 mutants

Mutant	Symmetry related interaction	Position on secondary element	Previously available, associated mutant
R 294A	2-fold axis	αA helix	mut 24 (164)
Q 297A	2-fold axis	αA helix	
R 298A	2-fold axis	αA helix	
R 294A/R298A	2-fold axis	αA helix	
K 692A	2x3-fold axis	C terminal	
W694A	2x3-fold axis	C terminal	
P696A	2-fold axis	C terminal	
R389A	3x5-fold interface	variable region III	mut 29 (164)
R432A	3-fold interface	GH loop	mut 31 (164)
Y441A	3-fold interface	variable region IV	
L510A	3-fold interface	variable region V	
P602A	3-fold axis	variable region VIII	
P622A	3-fold interface	GH loop	
D625A	3-fold interface	GH loop	
V221A/S224A	5-fold axis	A loop	(20, 145)
H255A/K258A	5-fold interface	β strand in variable region I	
Y397A	5x3-fold interface	EF loop	
M402A	5-fold interface	Bf	
R404A	5-fold interface	FG loop	
Y413A	5-fold non-interface	βG	
F415A	5-fold non-interface	GH loop	mut 30 (165)
F661A	5-fold non-interface	HI loop	

Table 5-2. STEM statistical analysis of AAV2 assembly/disassembly components from baculovirus expression.

	Pentamer	Intermediate Capsid	Closed Capsid
Total number of values	411	61	35
Minimum Molecular Mass (kDa)	353	1080	2481
25% Percentile (kDa)	576	3074	3093
Median Molecular Mass (kDa)	600	3145	3184
75% Percentile	629	3207	3294
Maximum Molecular Mass (kDa)	1664	3422	4105
Mean (kDa)	643	3079	3215
Standard Deviation (kDa)	180	382	219
Standard Error (kDa)	8	49	19
Lower 95% CI of mean	625	2981	3177
Upper 95% CI of mean	660	3177	3254

Table 5-3. Summary of AAV2 mutant phenotype.

Mutant	Capsid/ml	Particle titer (Genome/ml)	IU/ml	mutant capsid/ml wt capsid/ml	Packaging efficiency	Log (particle/ml infectivity/ml)
wt	8.60E+11	2.38E+11	1.91E9	1	7.119	2.1
R 294A	4.65E+8	BD	BD	7.13E-4	BD	BD
Q 297A	1.11E+8	BD	BD	1.48E-4	BD	BD
R 298A	7.34E+7	BD	BD	9.17E-5	BD	BD
R294/R298A	5.15E+7	BD	BD	6.12E-5	BD	BD
K 692A	2.72E10	2.37E10	10E+1	2.79E-2	0.1944	10.2
W694A	1.12E+8	BD	BD	1.29E-4	BD	BD
P696A	3.91E+7	BD	BD	5.13E-4	BD	BD
R389A	3.61E+11	1.19E+11	4.31E8	4.10E-1	29.7	2.5
R432A	3.47E+11	BD	BD	3.56E-1	BD	BD
Y441A	3.64E+11	4.49E+10	10E+1	4.68E-1	10.47	9.7
L510A	6.86E+11	8.49E+10	10E+1	7.76E-1	4.636	9.9
P602A	2.51E+11	4.19E+10	1.02E7	3.16E-1	8.794	3.9
P622A	3.52E+11	2.10E+11	4.90E+7	4.24E-1	3.73	4.0
D625A	5.67E+11	1.49E+11	1.09E+8	6.62E-1	6.571	3.4
V221/S224A	8.35E+7	BD	BD	1.01E-4	BD	BD
H255/K258A	1.38E+10	1.79E+10	1.96E+6	1.58E-2	1.228	4.1
Y397A	9.10E+10	2.10E+10	4.58E+6	9.35E-2	1.627	4.0
M402A	1.51E+8	BD	BD	1.61E-4	BD	BD
R404A	3.82E+11	6.02E+10	10E+1	4.32E-1	27.04	9.7
Y413A	9.96E+9	4.33E+9	2.46E+6	1.14E-2	2.156	3.2
F415A	3.34E8	BD	BD	4.94E-4	BD	BD
F661A	1.09E12	3.25E11	1.74E8	1.14	3.812	3.3

Table 5-4. Summary of all AAV2 Assembly Mutants.

Mutant	Other Name	Pheno type	Asse m bly	Packag ing	Part/ inf (log)	Comment/ (Reference)
V221W		pd	X	<3 fold	2	5 fold pore (19)
V221C		Pd	X	3 fold	2	5 fold pore defective for extruding pla after heating (20)
V221Y		pd	X	3 fold	3	5 fold pore (20)
V221A,S224A			X	?	?	4-5 log assembly defect, (AB)
WHCDS 228-232 WACAS	*mut*19	ni	X		>5	No capsid, 5 fold axis, inside surface (165)
M235L		wt	X			(159)
MGDRV 235-239 MGAAV	*mut*20	ni	X		>5	No capsid(165)
NHLYK 254-258 NALYA	*mut*21	pd	X			Unstable capsid, N, L, K are on the surface (165)
H255A/K258A		pd	X			2 log assembly defect, 5 fold axis (AB)
NRFHC 285-289 NAFAC	*mut*23	ni	X		>5	No capsid, not on an axis of symmetry(165)
FSPRD 291-295 FSPAA	*mut*24	ni	X		>5	No capsid, 2 fold axis (165)
R294A		ni	X	?	?	~3 log assembly defect, 2 fold axis (AB)
Q297A		ni	X			~ 4 log assembly defect, 5 fold axis (AB)
R298A		ni	X	?	?	~ 4 log assembly defect, 2 fold axis (AB)
R294A/R298A		ni	X	?	?	~ 4 log assembly defect, 2 fold (AB)
RPKRL 307-311 APAAL	*mut*25	ni	X		>5	No capsid, all residues on the inside surface (165)
K309N/R310N		ni	X			No capsid (58)
VKEVT 320-324 VAAVT	*mut*26	hs	X		>5	5 fold pore, this ts mutant does not make capsids at 37C and capsid protein is degraded(165) (Hartledge thesis, unpublished)

Table 5-4. Continued

Mutant	Other Name	Pheno type	Asse m bly	Packag ing	Part/ inf (log)	Comment/ (Reference)
E322A		ni	X		>5	5 fold pore (20)
E322A/V323D/T324 N		ni	X		>5	5 fold pore (20)
T324Y		pd		<1	<2	5 fold pore (20)
N334A		pd		4 fold		(20)
N334W		ni	X			5 fold pore (19)
N335A		pd			2	5 fold pore (20)
L336A		pd			2	5 fold pore, does not extrude VP1 even when heated (20)
L336W		pd	X	5 fold	2	5 fold pore (19)
S338A		pd		9 fold	1	5 fold pore (19)
L336W/D219A		pd		3 fold	2	5 fold pore (19)
S338A/V221W		ni	X			5 fold pore (19)
TDSEY 344-348 TASAY	*mut27*	hs	X		>5	(165)
Y397A		pd	X		1-2	~ 1 log assembly defect, and 1-2 log infectivity defect, 5 fold axis (AB)
M402A		ni	X		?	4 log reduced capsid, 5 fold axis (AB)
R404A		ni	X	14 fold	>8	Slight (~5x) reduced capsid (not statistically significant), reduced packaging, non-infectious, 5 fold axis (AB)
Y413A		pd	X		<1	2 log assembly defect, 5 fold axis , close to conserved F415 (AB)
FEDVP 415-419 FAAVP	*mut30*	pd			2	(165)
F415A		ni	X		>3	No capsid (AB)

Table 5-4. Continued

Mutant	Other Name	Pheno type	Asse m bly	Packag ing	Part/ inf (log)	Comment/ (Reference)
DIRD 469-472 AIAA	*mut*33	hs	X		>5	This virus is apparently ts for assembly but once assembled at 32, it's normal for infection at all temperatures (165) (Van Fliet, unpublished)
QDRDV 607-611 QAAAV	*mut*42	ni	X		>6	Not likely to be the C37 binding site (165) (162)
EIE 681-683 AAA	*mut*46	ni	X			No capsid (165)
K692A		ni	X		8	1-2 log deficit for assembly may reflect lower affinity for A20, severe defect for infectivity probably due to trafficking or uncoating, 2, 3, and 5 fold axes (AB)
W694A		ni	X			4 log assembly defect, 2 fold axis (AB)
P696A		ni	X			4 log assembly defect, 2 fold axis (AB)

CHAPTER 6
CONCLUSIONS AND FUTURE DIRECTIONS

The focus of this study was to understand the mechanism by which two families of ssDNA viruses, *Geminiviridae* and *Parvoviridae*, assemble and disassemble. MSV-N was selected as a model for the *Geminiviridae* and AAV2 was selected as a model for the *Parvoviridae*. These viruses provided two different examples of capsid assembly, in that, AAV2 infects animal cells, and it assembles to form a T = 1 capsid which is formed from a total 60 copies of the VPs (VP1-3). MSV-N on the other hand is a plant virus which assembles to form a twinned pseudo T = 1 capsid: the MSV-N capsid is generated by the assembly of two incomplete T=1 capsid shells and 110 copies of the same CP to accommodate its genome. The conclusion obtained from the assembly disassembly of each virus, as well as, the future directions will be summarized in this chapter.

MSV-N Assembly/Disassembly Model

The assembly/disassembly studies of MSV-N were divided into two parts. The first part was the characterization of MSV-N CP capsids and subassemblies present in infected maize leaves. The second part is focused on the reversible disassemble and assemble of the gemininate capsid. A model of MSV-N assembly/ disassembly has been generated based on our experimental data (Figure 6-1).

Three stable components have been isolated from a wild type infection; they include the geminate, singles and capsomers. The geminate and single capsids have been previously identified and characterized, and our data confirms what was already known about the genomic content, molecular mass and particle dimensions. The capsomeric components appear to be assembled from pentameric components and three species have been identified by STEM analysis, they are 5CPs, 10CPs and 20CPs; this interpretation was supported by native gel

electrophoresis and gel filtration. The dimension of this pentameric building block was confirmed by DLS. These pentamers, unlike the singles and geminates, are not associated with any detectable genomic material. There is an interesting feature of our capsomer, namely the presence of 2CP species, one at 27kDa and the other at 29kDA. The larger CP species has been observed to be the predominant species in the singles and geminate capsids suggesting that there is a requirement for a CP modification for assembly. This is summarized in the model of MSV assembly (Figure 6-1) and it is believed that both CP species exist in solution at the initiation of assembly.

Stability studies of another geminivirus, African cassava mosaic virus (ACMV), have shown that it is stable between pH4.0 – 8-5, while aggretating at pH6.0 or lower. ACMV was reported to dis-assemble by releasing the viral genome preferably from the apical and peritoneal region at pH8.0 and more. The virus also appears to extrude its DNA by the removal of a pentamer, similar to the parvovirus which appears to extrude their DNA through a pentameric pore. The dis-assembly/assembly of MSV was examined in this study by varying the pH as well as ions of the sample buffer. In this study, we reported the dis-assembly of MSV-N geminates with the increase of environmental pH, and re-assembly with the pH is decreased. Similar to the wt infection, MSV geminates have been shown to dis-assemble via a pentameric intermediate 5CPs and 10CPs units. More importantly, the disassembly/assembly assay may recapitulate the environmental conditions experienced by the virus while being trafficked through its insect vector and plant host. There is no report of viral replication in the insect vector; this information is consistent with our experimental observation which shows that the geminate capsid is intact between pH4.8 and 6.0. This observation that the internal passage of the vector utilized by the virus is between pH4.5-5.8 implies that the capsid is likely to remain intact during transmission.

The exposure of the MSV-N geminate capsid to pH6.4 and greater results in its disassembly to form a pentameric intermediate (POD or DOP) that is still associated with the viral genome. The pentameric intermediate continues to disassemble with increasing pH (7.2), which is similar to the internal environment of the maize plant cell cytoplasm. The disassembled capsomer at pH7.2 is still associated with the viral genome and this data is confirmed by DNA electrophoresis. Disassembly and the release of the viral genome is an important step in the viral life cycle as it allows the genome to be replicated. The replicated genome is transcribed and translated in the host cytoplasm; the pH of this environment (pH7.4) ensures that the CP is not assembled. The data shows that the CP likely assembles into geminate capsids provided they are exposed to pH4.8 and they interact with ssDNA. The assembly of the geminate capsid in the presence of protease inhibitor is still missing several CPs, this would imply that either host factors may be required or the effective CP concentration in the assay is less than optimal to recapitulate "*in vivo*" assembly conditions.

AAV2 Assembly/Disassembly Model

The assembly/disassembly studies of AAV2 were divided into two parts. The first part of this section was site directed mutagenesis of the VP, to disrupt symmetry related interface interactions of the virus, to test to see if the interface is important for assembly. The second part of the AAV2 section was focused on the characterization of all VP intermediates and capsids from AAV2 baculovirus expression. The conclusions for the assembly studies of AAV2 are illustrated in figure 6-2.

The model illustrates that the first step in the assembly process is the formation of the VP pentamer. Based on the mutational analysis of the VP, the mutants that were made in the 2-fold interface formed what appeared to be pentameric structures compared to the mutants made in the 5-fold interface, which appears to form an aggregated mass once expressed. Our experimental

data clearly shows that the mutants generated were predominantly assembly mutants and, they are located in the 2-fold and 5-fold axis and symmetry related interface. Based on the crystal structure of AAV2, the αA helix forms the wall of the 2-fold depression and the C-terminal loop interlocks with the adjacent monomer to form the floor. It has been shown that the 2-fold axis is the thinnest region of the capsid and we have shown that the mutations of several residues within this interface will either prevent the AAV2 capsid from assembling or it will destabilize the assembled capsid. The other assembly mutants are located either in the 5-fold axis or at the 5-fold symmetry related interface. The loop extensions from the narrow end of the β-barrel wedge form the icosahedral 5-fold VP3 symmetry related interactions with elements of the BIDG sheet and the N-terminal residues in the adjacent monomer. In addition, the βHI loop (structurally conserved in all parvoviruses) is positioned above the β-strands of adjacent VP3 monomers forming the floor of the conserved depression that surrounds the icosahedral 5-fold axis. AAV2 also forms a channel that connects the inside and outside of the capsid at the 5-fold axis formed by the βDE ribbon which assembles a surface turret at this axis. The compilation of all AAV2 assembly mutants generated in this work (Table 5-3) as well as previously characterized assembly mutants clearly shows that both the 2-fold and 5-fold symmetry related interactions are critical for capsid assembly and stability. It is the data obtained from the wt AAV2 purification that points to the presence of either POD or a DOP. To date the other steps involved in the formation of the empty capsid is still not known.

Structure to function correlation for the ssDNA viruses

The bacteriophage *Microviridae* is the only family among the ssDNA viruses for which a model has been proposed to describe the mechanism of assembly and disassembly. The *Microviridae* phi X has been shown to utilize two different pentameric intermediates, one made from the F protein and the other from the G protein. 12 F protein pentamers interact to form the

body of the T=1 capsid and 12 of the G proteins pentamers form the spikes which are important for binding the bacterial host glyco-protein, and for the formation of the 5-fold pore, which is important for the ejection of the viral genome. Assembly intermediates has been identified for the autonomous parvovirus CPV and MVM have been shown to utilize a trimeric intermediate to form their T=1 capsid. Both MSV-N (member of the Geminiviridae family of virus), and AAV2 (member of the Parvoviridae family of virus) appear to use a pentameric intermediate to form either a pseudo T=1 geminate capsid or a T=1 single.

Future Directions

The assembly/disassembly studies of both AAV2 and MSV-N has provided new information about the steps involved in the assembly and disassembly of these two prototypic ssDNA viruses. Despite the availability of this new data there are still several unanswered questions that need to be addressed. The future plans for the MSV-N and AAV2 disassembly assembly studies will be covered in this section.

The first part of our aim was to determine the mechanism by which MSV-N assembles based on the purification of the MSV-N components. The second aim was to decipher the environmental conditions critical to the function of the virus capsid. The pH assay developed has added further details to our model. The ultimate goal of our model is to use the information to assist in the development or the testing of small molecule inhibitors of viral assembly or disassembly. The main future aim is to test our assembly model by purifying the baculovirus expressed MSV-NCP, MSV-NCP201, and MSV-NK182Vand to crystallize the purified protein as well as any isolated assembly components.

The AAV2 assembly study also has limitations due to our inability to isolate and fully characterize pure intermediates generated by the mutation of the VP. Our future plans for AAV2 will be focused on generating VP intermediates which are tagged with a series of histidines. It

has been shown that VP2 N-terminus that can tolerate insertions without affecting virus assembly. The characterization of a purified 2-fold or 5-fold mutant will confirm without a doubt the size of the intermediate in the assembly of the AAV2 capsid.

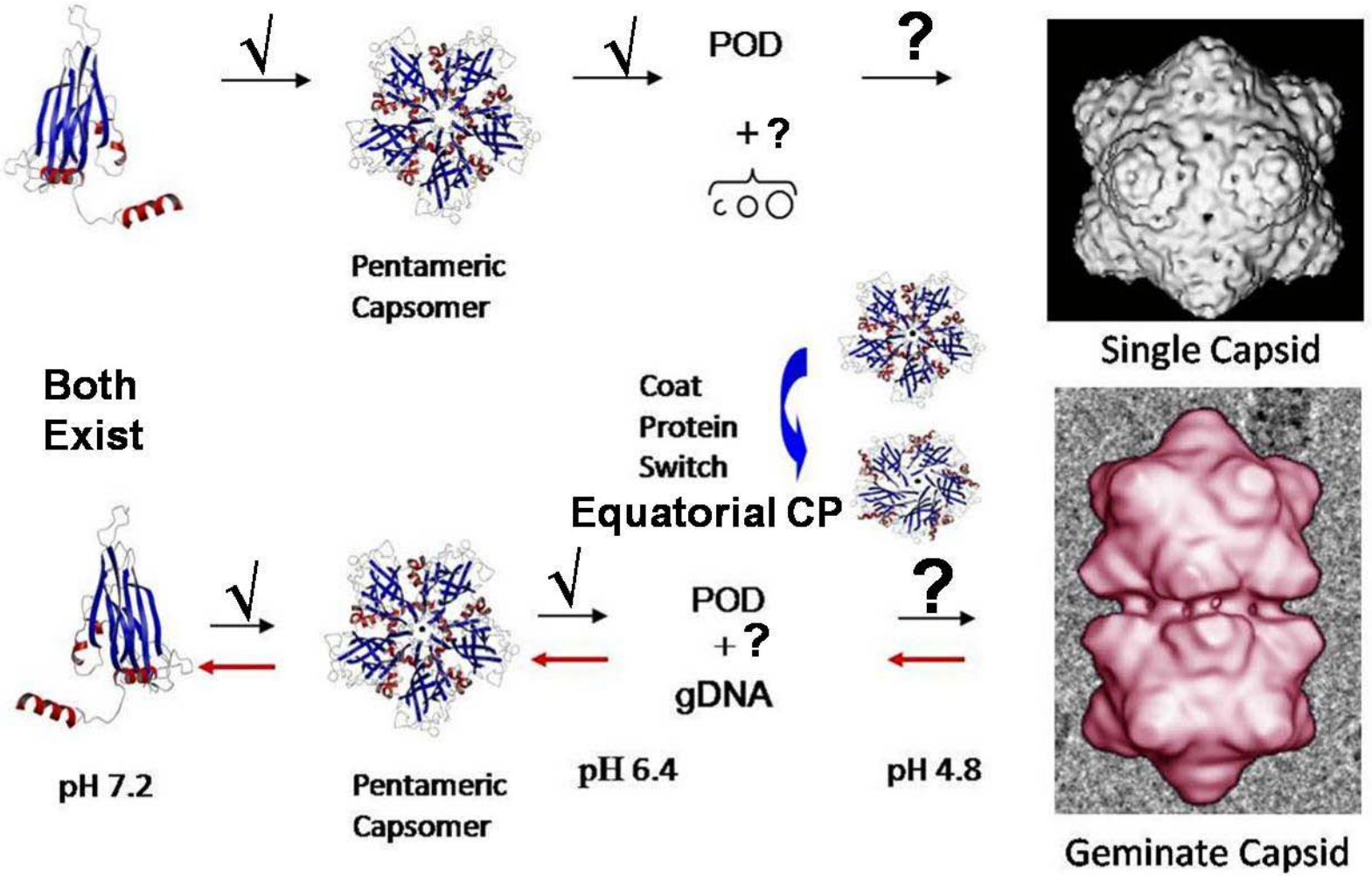

Figure 6-1. Proposed model for the assembly and disassembly of MSV-N

.

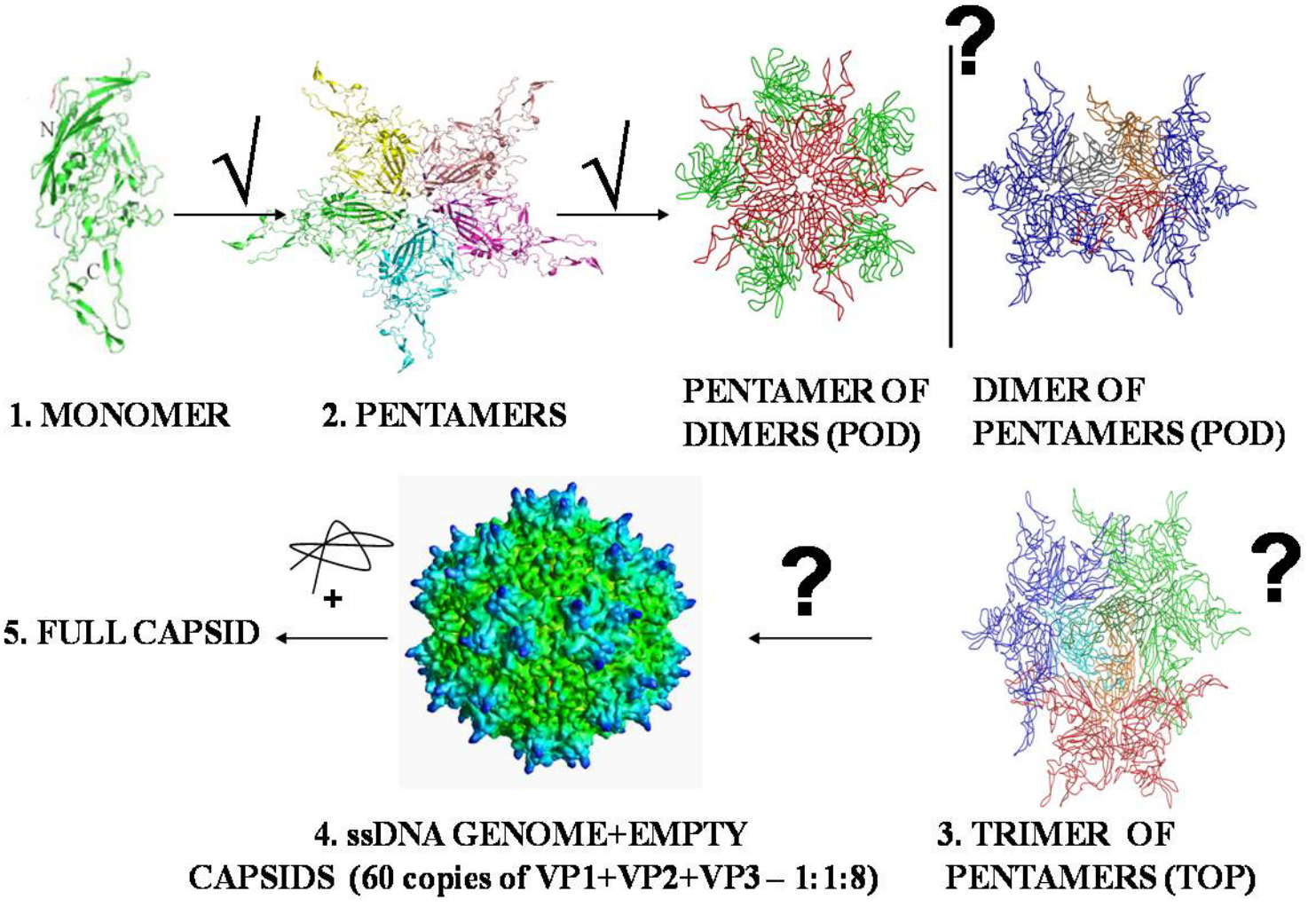

Figure 6-2. Proposed model for the assembly of AAV2.

LIST OF REFERENCES

1. **Acland, G. M., G. D. Aguirre, J. Bennett, T. S. Aleman, A. V. Cideciyan, J. Bennicelli, N. S. Dejneka, S. E. Pearce-Kelling, A. M. Maguire, K. Palczewski, W. W. Hauswirth, and S. G. Jacobson. 2005**. Long-term restoration of rod and cone vision by single dose rAAV-mediated gene transfer to the retina in a canine model of childhood blindness. Mol Ther 12:1072-82.

2. **Acland, G. M., G. D. Aguirre, J. Ray, Q. Zhang, T. S. Aleman, A. V. Cideciyan, S. E. Pearce-Kelling, V. Anand, Y. Zeng, A. M. Maguire, S. G. Jacobson, W. W. Hauswirth, and J. Bennett**. 2001. Gene therapy restores vision in a canine model of childhood blindness. Nat Genet 28:92-5.

3. **Agbandje-McKenna, M. S. C. a. M**. 2006. Atomic structure of viral particles, in Parvoviruses. . Edward Arnold, Ltd, New York.

4. **Al-Mawsawi, L. Q., and N. Neamati**. 2007. Blocking interactions between HIV-1 integrase and cellular cofactors: an emerging anti-retroviral strategy. Trends Pharmacol Sci 28:526-35.

5. **Ambati, J., B. K. Ambati, S. H. Yoo, S. Ianchulev, and A. P. Adamis. 2003**. Age-related macular degeneration: etiology, pathogenesis, and therapeutic strategies. Surv Ophthalmol 48:257-93.

6. **Ammar el, D., D. Gargani, J. M. Lett, and M. Peterschmitt. 2009**. Large accumulations of maize streak virus in the filter chamber and midgut cells of the leafhopper vector Cicadulina mbila. Arch Virol 154:255-62.

7. **Andries, K., B. Dewindt, J. Snoeks, L. Wouters, H. Moereels, P. J. Lewi, and P. A. Janssen**. 1990. Two groups of rhinoviruses revealed by a panel of antiviral compounds present sequence divergence and differential pathogenicity. J Virol 64:1117-23.

8. **Asokan, A., J. B. Hamra, L. Govindasamy, M. Agbandje-McKenna, and R. J. Samulski.** 2006. Adeno-associated virus type 2 contains an integrin alpha5beta1 binding domain essential for viral cell entry. J Virol 80:8961-9.

9. Azzam, O., J. Frazer, D. de la Rosa, J. S. Beaver, P. Ahlquist, and D. P. Maxwell. 1994. Whitefly transmission and efficient ssDNA accumulation of bean golden mosaic geminivirus require functional coat protein. Virology 204:289-96.

10. **Badger, J., I. Minor, M. A. Oliveira, T. J. Smith, and M. G. Rossmann. 1989**. Structural analysis of antiviral agents that interact with the capsid of human rhinoviruses. Proteins 6:1-19.

11. **Bailey, T. R., G. D. Diana, P. J. Kowalczyk, V. Akullian, M. A. Eissenstat, D. Cutcliffe, J. P. Mallamo, P. M. Carabateas, and D. C. Pevear**. 1992. Antirhinoviral activity of heterocyclic analogs of Win 54954. J Med Chem 35:4628-33.

12. Baker, T., and J. Johnson. 1997. Principles of virus structure determination, p. 39-79. *In* W. Chui (ed.), Structural Biology of Vruses. Oxford University press, New York.

13. Bancroft, J. B., C. E. Bracker, and G. W. Wagner. 1969. Structures derived from cowpea chlorotic mottle and brome mosaic virus protein. Virology 38:324-35.

14. Bancroft, J. B., E. Hiebert, and C. E. Bracker. 1969. The effects of various polyanions on shell formation of some spherical viruses. Virology 39:924-30.

15. Bartlett, J. S., R. Wilcher, and R. J. Samulski. 2000. Infectious entry pathway of adeno-associated virus and adeno-associated virus vectors. J Virol 74:2777-85.

16. Bennett, J. 2004. Gene therapy for Leber congenital amaurosis. Novartis Found Symp 255:195-202; discussion 202-7.

17. Berns, K. I., and R. M. Linden. 1995. The cryptic life style of adeno-associated virus. Bioessays 17:237-45.

18. Bleker, J. 2005. [Preliminary remarks from the editor]. Medizinhist J 40:107-8.

19. Bleker, S., M. Pawlita, and J. A. Kleinschmidt. 2006. Impact of capsid conformation and Rep-capsid interactions on adeno-associated virus type 2 genome packaging. J Virol 80:810-20.

20. Bleker, S., F. Sonntag, and J. A. Kleinschmidt. 2005. Mutational analysis of narrow pores at the fivefold symmetry axes of adeno-associated virus type 2 capsids reveals a dual role in genome packaging and activation of phospholipase A2 activity. J Virol 79:2528-40.

21. Bosque-Perez, N. A. 2000. Eight decades of maize streak virus research. Virus Res 71:107-21.

22. Boulton, M. I., D. I. King, J. Donson, and J. W. Davies. 1991. Point substitution in a promoter-like region and the V1 gene affect the host range and symptoms of maize streak virus. Virology 183:114-21.

23. Boulton, M. I., D. I. King, P. G. Markham, M. S. Pinner, and J. W. Davies. 1991. Host range and symptoms are determined by specific domains of the maize streak virus genome. Virology 181:312-8.

24. Boulton, M. I., C. K. Pallaghy, M. Chatani, S. MacFarlane, and J. W. Davies. 1993. Replication of maize streak virus mutants in maize protoplasts: evidence for a movement protein. Virology 192:85-93.

25. Boulton, M. I., H. Steinkellner, J. Donson, P. G. Markham, D. I. King, and J. W. Davies. 1989. Mutational analysis of the virion-sense genes of maize streak virus. J Gen Virol 70 (Pt 9):2309-23.

26. **Briddon, R. W., M. S. Pinner, J. Stanley, and P. G. Markham. 1990**. Geminivirus coat protein gene replacement alters insect specificity. Virology 177:85-94.

27. **Brown, C. S., J. W. Van Lent, J. M. Vlak, and W. J. Spaan**. 1991. Assembly of empty capsids by using baculovirus recombinants expressing human parvovirus B19 structural proteins. J Virol 65:2702-6.

28. **Carrington, J. C., K. D. Kasschau, S. K. Mahajan, and M. C. Schaad**. 1996. Cell-to-Cell and Long-Distance Transport of Viruses in Plants. Plant Cell 8:1669-1681.

29. **Casado, C. G., G. Javier Ortiz, E. Padron, S. J. Bean, R. McKenna, M. Agbandje-McKenna, and M. I. Boulton**. 2004. Isolation and characterization of subgenomic DNAs encapsidated in "single" T = 1 isometric particles of Maize streak virus. Virology 323:164-71.

30. **Casini, G. L., D. Graham, D. Heine, R. L. Garcea, and D. T. Wu**. 2004. In vitro papillomavirus capsid assembly analyzed by light scattering. Virology 325:320-7.

31. **Caspar, D. L., and A. Klug**. 1962. Physical principles in the construction of regular viruses. Cold Spring Harb Symp Quant Biol 27:1-24.

32. **Chen, J., J. Chen, and M. J. Adams**. 2001. A universal PCR primer to detect members of the Potyviridae and its use to examine the taxonomic status of several members of the family. Arch Virol 146:757-66.

33. **Chen, X. S., G. Casini, S. C. Harrison, and R. L. Garcea**. 2001. Papillomavirus capsid protein expression in Escherichia coli: purification and assembly of HPV11 and HPV16 L1. J Mol Biol 307:173-82.

34. **Cheung, A. K., M. D. Hoggan, W. W. Hauswirth, and K. I. Berns**. 1980. Integration of the adeno-associated virus genome into cellular DNA in latently infected human Detroit 6 cells. J Virol 33:739-48.

35. **Chiorini, J. A., S. M. Wiener, L. Yang, R. H. Smith, B. Safer, N. P. Kilcoin, Y. Liu, E. Urcelay, and R. M. Kotin**. 1996. The roles of AAV Rep proteins in gene expression and targeted integration. Curr Top Microbiol Immunol 218:25-33.

36. **Choi, V. W., D. M. McCarty, and R. J. Samulski**. 2005. AAV hybrid serotypes: improved vectors for gene delivery. Curr Gene Ther 5:299-310.

37. **Chowda-Reddy, R. V., F. Achenjang, C. Felton, M. T. Etarock, M. T. Anangfac, P. Nugent, and V. N. Fondong.** 2008. Role of a geminivirus AV2 protein putative protein kinase C motif on subcellular localization and pathogenicity. Virus Res 135:115-24.

38. **Christensen, J., T. Storgaard, B. Bloch, S. Alexandersen, and B. Aasted**. 1993. Expression of Aleutian mink disease parvovirus proteins in a baculovirus vector system. J Virol 67:229-38.

39. Chromy, L. R., J. M. Pipas, and R. L. Garcea. 2003. Chaperone-mediated in vitro assembly of Polyomavirus capsids. Proc Natl Acad Sci U S A 100:10477-82.

40. Conway, J. E., C. M. Rhys, I. Zolotukhin, S. Zolotukhin, N. Muzyczka, G. S. Hayward, and B. J. Byrne. 1999. High-titer recombinant adeno-associated virus production utilizing a recombinant herpes simplex virus type I vector expressing AAV-2 Rep and Cap. Gene Ther 6:986-93.

41. Cotmore, S. F., J. Christensen, J. P. Nuesch, and P. Tattersall. 1995. The NS1 polypeptide of the murine parvovirus minute virus of mice binds to DNA sequences containing the motif [ACCA]2-3. J Virol 69:1652-60.

42. Cotmore, S. F., and P. Tattersall. 1989. A genome-linked copy of the NS-1 polypeptide is located on the outside of infectious parvovirus particles. J Virol 63:3902-11.

43. Cotmore, S. F., and P. Tattersall. 2005. Genome packaging sense is controlled by the efficiency of the nick site in the right-end replication origin of parvoviruses minute virus of mice and LuIII. J Virol 79:2287-300.

44. Crick, F. H., and J. D. Watson. 1956. Structure of small viruses. Nature 177:473-5.

45. Daly, T. M., and M. S. Sands. 1998. Gene therapy for lysosomal storage diseases. Expert Opin Investig Drugs 7:1673-82.

46. Denti, M. A., A. Rosa, G. D'Antona, O. Sthandier, F. G. De Angelis, C. Nicoletti, M. Allocca, O. Pansarasa, V. Parente, A. Musaro, A. Auricchio, R. Bottinelli, and I. Bozzoni. 2006. Chimeric adeno-associated virus/antisense U1 small nuclear RNA effectively rescues dystrophin synthesis and muscle function by local treatment of mdx mice. Hum Gene Ther 17:565-74.

47. Dubielzig, R., J. A. King, S. Weger, A. Kern, and J. A. Kleinschmidt. 1999. Adeno-associated virus type 2 protein interactions: formation of pre-encapsidation complexes. J Virol 73:8989-98.

48. Flotte, T. R. 2005. Adeno-associated virus-based gene therapy for inherited disorders. Pediatr Res 58:1143-7.

49. Flotte, T. R. 2008. In utero efficacy of cystic fibrosis gene therapy: difficult studies, positive or negative. Mol Ther 16:806-7.

50. Flotte, T. R., S. A. Afione, and P. L. Zeitlin. 1994. Adeno-associated virus vector gene expression occurs in nondividing cells in the absence of vector DNA integration. Am J Respir Cell Mol Biol 11:517-21.

51. Flotte, T. R., and B. J. Carter. 1997. In vivo gene therapy with adeno-associated virus vectors for cystic fibrosis. Adv Pharmacol 40:85-101.

52. Flotte, T. R., and B. L. Laube. 2001. Gene therapy in cystic fibrosis. Chest 120:124S-131S.

53. **Flotte, T. R., P. Ng, D. E. Dylla, P. B. McCray, Jr., G. Wang, J. K. Kolls, and J. Hu**. 2007. Viral vector-mediated and cell-based therapies for treatment of cystic fibrosis. Mol Ther 15:229-41.

54. **Flotte, T. R., I. Virella-Lowell, and K. A. Chesnut**. 2002. Adeno-associated viral vectors for CF gene therapy. Methods Mol Med 70:599-608.

55. **Girod, A., C. E. Wobus, Z. Zadori, M. Ried, K. Leike, P. Tijssen, J. A. Kleinschmidt, and M. Hallek**. 2002. The VP1 capsid protein of adeno-associated virus type 2 is carrying a phospholipase A2 domain required for virus infectivity. J Gen Virol 83:973-8.

56. **Govindasamy, L., E. Padron, R. McKenna, N. Muzyczka, N. Kaludov, J. A. Chiorini, and M. Agbandje-McKenna**. 2006. Structurally mapping the diverse phenotype of adeno-associated virus serotype 4. J Virol 80:11556-70.

57. **Grieger, J. C., J. S. Johnson, B. Gurda-Whitaker, M. Agbandje-McKenna, and R. J. Samulski.** 2007. Surface-exposed adeno-associated virus Vp1-NLS capsid fusion protein rescues infectivity of noninfectious wild-type Vp2/Vp3 and Vp3-only capsids but not that of fivefold pore mutant virions. J Virol 81:7833-43.

58. **Grieger, J. C., S. Snowdy, and R. J. Samulski**. 2006. Separate basic region motifs within the adeno-associated virus capsid proteins are essential for infectivity and assembly. J Virol 80:5199-210.

59. **Grimm, D., J. S. Lee, L. Wang, T. Desai, B. Akache, T. A. Storm, and M. A. Kay**. 2008. In vitro and in vivo gene therapy vector evolution via multispecies interbreeding and retargeting of adeno-associated viruses. J Virol 82:5887-911.

60. **Grunewald, K., P. Desai, D. C. Winkler, J. B. Heymann, D. M. Belnap, W. Baumeister, and A. C. Steven**. 2003. Three-dimensional structure of herpes simplex virus from cryo-electron tomography. Science 302:1396-8.

61. **Hauck, B., L. Chen, and W. Xiao**. 2003. Generation and characterization of chimeric recombinant AAV vectors. Mol Ther 7:419-25.

62. **Hauswirth, W. W., and A. M. Timmers**. 2000. The eyes have it. Mol Med Today 6:51.

63. **Hennig, A. K., J. M. Ogilvie, K. K. Ohlemiller, A. M. Timmers, W. W. Hauswirth, and M. S. Sands**. 2004. AAV-mediated intravitreal gene therapy reduces lysosomal storage in the retinal pigmented epithelium and improves retinal function in adult MPS VII mice. Mol Ther 10:106-16.

64. **Hermonat, P. L., M. A. Labow, R. Wright, K. I. Berns, and N. Muzyczka.** 1984. Genetics of adeno-associated virus: isolation and preliminary characterization of adeno-associated virus type 2 mutants. J Virol 51:329-39.

65. **Hiebert, E., and J. B. Bancroft**. 1969. Factors affecting the assembly of some spherical viruses. Virology 39:296-311.

66. **Hoque, M., K. Ishizu, A. Matsumoto, S. I. Han, F. Arisaka, M. Takayama, K. Suzuki, K. Kato, T. Kanda, H. Watanabe, and H. Handa**. 1999. Nuclear transport of the major capsid protein is essential for adeno-associated virus capsid formation. J Virol 73:7912-5.

67. **Howell, S. H**. 1984. Physical structure and genetic organisation of the genome of maize streak virus (Kenyan isolate). Nucleic Acids Res 12:7359-75.

68. **Hunter, L. A., and R. J. Samulski**. 1992. Colocalization of adeno-associated virus Rep and capsid proteins in the nuclei of infected cells. J Virol 66:317-24.

69. **Im, D. S., and N. Muzyczka**. 1992. Partial purification of adeno-associated virus Rep78, Rep52, and Rep40 and their biochemical characterization. J Virol 66:1119-28.

70. **Jeske, K. K. a**. J. 2008. Africa Cassava Mosaic Virus. Journal of General Virology 89:2029-2036.

71. **Johnson, J. E**. 1996. Functional implications of protein-protein interactions in icosahedral viruses. Proc Natl Acad Sci U S A 93:27-33.

72. **Johnson, J. E., and J. A. Speir**. 1997. Quasi-equivalent viruses: a paradigm for protein assemblies. J Mol Biol 269:665-75.

73. **Johnson, J. S., and R. J. Samulski**. 2009. Enhancement of adeno-associated virus infection by mobilizing capsids into and out of the nucleolus. J Virol 83:2632-44.

74. **Jones, D. T**. 1999. Protein secondary structure prediction based on position-specific scoring matrices. J Mol Biol 292:195-202.

75. **Kajigaya, S., T. Shimada, S. Fujita, and N. S. Young**. 1989. A genetically engineered cell line that produces empty capsids of B19 (human) parvovirus. Proc Natl Acad Sci U S A 86:7601-5.

76. **Kay, M. A., and K. High**. 1999. Gene therapy for the hemophilias. Proc Natl Acad Sci U S A 96:9973-5.

77. **Kay, M. A., C. S. Manno, M. V. Ragni, P. J. Larson, L. B. Couto, A. McClelland, B. Glader, A. J. Chew, S. J. Tai, R. W. Herzog, V. Arruda, F. Johnson, C. Scallan, E. Skarsgard, A. W. Flake, and K. A. High**. 2000. Evidence for gene transfer and expression of factor IX in haemophilia B patients treated with an AAV vector. Nat Genet 24:257-61.

78. **Kay, M. A., and H. Nakai**. 2003. Looking into the safety of AAV vectors. Nature 424:251.

79. **Klein, C., and K. Lohmann-Hedrich**. 2007. Impact of recent genetic findings in Parkinson's disease. Curr Opin Neurol 20:453-64.

80. **Klein, C., and M. G. Schlossmacher**. 2006. The genetics of Parkinson disease: Implications for neurological care. Nat Clin Pract Neurol 2:136-46.

81. **Klein, C., and M. G. Schlossmacher**. 2007. Parkinson disease, 10 years after its genetic revolution: multiple clues to a complex disorder. Neurology 69:2093-104.

82. **Klein, R. L., R. D. Dayton, J. B. Tatom, C. G. Diaczynsky, and M. F. Salvatore**. 2008. Tau expression levels from various adeno-associated virus vector serotypes produce graded neurodegenerative disease states. Eur J Neurosci 27:1615-25.

83. **Klein, R. L., M. A. King, M. E. Hamby, and E. M. Meyer**. 2002. Dopaminergic cell loss induced by human A30P alpha-synuclein gene transfer to the rat substantia nigra. Hum Gene Ther 13:605-12.

84. **Klein, R. L., R. J. Mandel, and N. Muzyczka**. 2000. Adeno-associated virus vector-mediated gene transfer to somatic cells in the central nervous system. Adv Virus Res 55:507-28.

85. **Klein, R. L., E. M. Meyer, A. L. Peel, S. Zolotukhin, C. Meyers, N. Muzyczka, and M. A. King**. 1998. Neuron-specific transduction in the rat septohippocampal or nigrostriatal pathway by recombinant adeno-associated virus vectors. Exp Neurol 150:183-94.

86. **Kohlbrenner, E., G. Aslanidi, K. Nash, S. Shklyaev, M. Campbell-Thompson, B. J. Byrne, R. O. Snyder, N. Muzyczka, K. H. Warrington, Jr., and S. Zolotukhin**. 2005. Successful production of pseudotyped rAAV vectors using a modified baculovirus expression system. Mol Ther 12:1217-25.

87. **Kotin, R. M., R. M. Linden, and K. I. Berns**. 1992. Characterization of a preferred site on human chromosome 19q for integration of adeno-associated virus DNA by non-homologous recombination. Embo J 11:5071-8.

88. **Kotin, R. M., J. C. Menninger, D. C. Ward, and K. I. Berns**. 1991. Mapping and direct visualization of a region-specific viral DNA integration site on chromosome 19q13-qter. Genomics 10:831-4.

89. **Kotlizky, G., M. I. Boulton, C. Pitaksutheepong, J. W. Davies, and B. L. Epel**. 2000. Intracellular and intercellular movement of maize streak geminivirus V1 and V2 proteins transiently expressed as green fluorescent protein fusions. Virology 274:32-8.

90. **Kronenberg, S., J. A. Kleinschmidt, and B. Bottcher**. 2001. Electron cryo-microscopy and image reconstruction of adeno-associated virus type 2 empty capsids. EMBO Rep 2:997-1002.

91. **Kube, D. M., S. Ponnazhagan, and A. Srivastava. 1997**. Encapsidation of adeno-associated virus type 2 Rep proteins in wild-type and recombinant progeny virions: Rep-mediated growth inhibition of primary human cells. J Virol 71:7361-71.

92. **Laughlin, C. A., C. B. Cardellichio, and H. C. Coon**. 1986. Latent infection of KB cells with adeno-associated virus type 2. J Virol 60:515-24.

93. **Lazarowitz, S. G**. 1988. Infectivity and complete nucleotide sequence of the genome of a South African isolate of maize streak virus. Nucleic Acids Res 16:229-49.

94. **Lazarowitz, S. G., A. J. Pinder, V. D. Damsteegt, and S. G. Rogers**. 1989. Maize streak virus genes essential for systemic spread and symptom development. Embo J 8:1023-1032.

95. **Leppard, K. N**. 1997. E4 gene function in adenovirus, adenovirus vector and adeno-associated virus infections. J Gen Virol 78 (Pt 9):2131-8.

96. **Levy, H. C., V. D. Bowman, L. Govindasamy, R. McKenna, K. Nash, K. Warrington, W. Chen, N. Muzyczka, X. Yan, T. S. Baker, and M. Agbandje-McKenna**. 2009. Heparin binding induces conformational changes in Adeno-associated virus serotype 2. J Struct Biol 165:146-56.

97. **Li, W., A. Asokan, Z. Wu, T. Van Dyke, N. DiPrimio, J. S. Johnson, L. Govindaswamy, M. Agbandje-McKenna, S. Leichtle, D. E. Redmond, Jr., T. J. McCown, K. B. Petermann, N. E. Sharpless, and R. J. Samulski. 2008. Engineering and selection of shuffled AAV genomes: a new strategy for producing targeted biological nanoparticles**. Mol Ther 16:1252-60.

98. **Li, W., L. Zhang, J. S. Johnson, W. Zhijian, J. C. Grieger, X. Ping-Jie, L. M. Drouin, M. Agbandje-McKenna, R. J. Pickles, and R. J. Samulski**. 2009. Generation of Novel AAV Variants by Directed Evolution for Improved CFTR Delivery to Human Ciliated Airway Epithelium. Mol Ther.

99. **Li, Y., Z. Zhou, and C. B. Post. 2005. Dissociation of an antiviral compound from the internal pocket of human rhinovirus 14 capsid**. Proc Natl Acad Sci U S A 102:7529-34.

100. **Lingappa, J. R., and B. K. Thielen. 2009. Assembly of immature HIV-1 capsids using a cell-free system**. Methods Mol Biol 485:185-95.

101. **Liu, H., M. I. Boulton, and J. W. Davies. 1997. Maize streak virus coat protein binds single- and double-stranded DNA** in vitro. J Gen Virol 78 (Pt 6):1265-70.

102. **Liu, H., M. I. Boulton, K. J. Oparka, and J. W. Davies. 2001. Interaction of the movement and coat proteins of Maize streak virus: implications for the transport of viral DNA**. J Gen Virol 82:35-44.

103. **Liu, H., M. I. Boulton, C. L. Thomas, D. A. Prior, K. J. Oparka, and J. W. Davies**. 1999. Maize streak virus coat protein is karyophyllic and facilitates nuclear transport of viral DNA. Mol Plant Microbe Interact 12:894-900.

104. **Liu, H., A. P. Lucy, J. W. Davies, and M. Boulton**. 2001. A single amino acid change in the coat protein of Maize streak virus abolishes systemic infection, but not interaction with viral DNA or movement protein. Molecular Plant Pathology 2:223-228.

105. Liu, L., M. S. Pinner, J. W. Davies, and J. Stanley. 1999. Adaptation of the geminivirus bean yellow dwarf virus to dicotyledonous hosts involves both virion-sense and complementary-sense genes. J Gen Virol 80 (Pt 2):501-6.

106. Lochrie, M. A., G. P. Tatsuno, B. Christie, J. W. McDonnell, S. Zhou, R. Surosky, G. F. Pierce, and P. Colosi. 2006. Mutations on the external surfaces of adeno-associated virus type 2 capsids that affect transduction and neutralization. J Virol 80:821-34.

107. Lombardo, E., J. C. Ramirez, M. Agbandje-McKenna, and J. M. Almendral. 2000. A beta-stranded motif drives capsid protein oligomers of the parvovirus minute virus of mice into the nucleus for viral assembly. J Virol 74:3804-14.

108. **M.I Boulton 2002. Functions and interactions of Mastrevirus gene products**,. Physiology. Mol. Plant. Pathol. 60:243-255.

109. **Makhov, A. M., A. Sen, X. Yu, M. N. Simon, J. D. Griffith, and E. H. Egelman.** 2009. The bipolar filaments formed by herpes simplex virus type 1 SSB/recombination protein (ICP8) suggest a mechanism for DNA annealing. J Mol Biol 386:273-9.

110. **Maruri-Avidal, L., S. Lopez, and C. F.** Arias. 2008. Endoplasmic reticulum chaperones are involved in the morphogenesis of rotavirus infectious particles. J Virol 82:5368-80.

111. **Mazithulela, G., D. Sudhakar, T. Heckel, L. Mehlo, P. Christou, J. W. Davies, and M. I. Boulton.** 2000. The maize streak virus coat protein transcription unit exhibits tissue-specific expression in transgenic rice. Plant Sci 155:21-29.

112. **McCarty, D. M., M. Christensen, and N. Muzyczka**. 1991. Sequences required for coordinate induction of adeno-associated virus p19 and p40 promoters by Rep protein. J Virol 65:2936-45.

113. **Morris-Krsinich, B. A., P. M. Mullineaux, J. Donson, M. I. Boulton, P. G. Markham, M. N. Short, and J. W. Davies.** 1985. Bidirectional transcription of maize streak virus DNA and identification of the coat protein gene. Nucleic Acids Res 13:7237-56.

114. **Motulsky, H. 2005. Graph Pad Prism *In* H. J. Motulsky** (ed.), Graph Pad Software 4ed. GraphPad Software Inc., San Diego CA, 2003.

115. **Mullineaux, P. M., J. Donson, B. A. Morris-Krsinich, M. I. Boulton, and J. W. Davies. 1984**. The nucleotide sequence of maize streak virus DNA. Embo J 3:3063-8.

116. **Muzyczka, N., R. J. Samulski, P. Hermonat, A. Srivastava, and K. I. Berns**. 1984. The genetics of adeno-associated virus. Adv Exp Med Biol 179:151-61.

117. **Myers, M. W., and B. J. Carter**. 1980. Assembly of adeno-associated virus. Virology 102:**71-82.**

118. Nayak, D. P., E. K. Hui, and S. Barman. 2004. Assembly and budding of influenza virus. Virus Res 106:147-65.

119. **Opie, S. R., K. H. Warrington, Jr., M. Agbandje-McKenna, S. Zolotukhin, and N. Muzyczka**. 2003. Identification of amino acid residues in the capsid proteins of adeno-associated virus type 2 that contribute to heparan sulfate proteoglycan binding. J Virol 77:6995-7006.

120. **Osbourn, J. K., S. Sarkar, and T. M. Wilson.** 1990. Complementation of coat protein-defective TMV mutants in transgenic tobacco plants expressing TMV coat protein. Virology 179:921-5.

121. **Padron, E., V. Bowman, N. Kaludov, L. Govindasamy, H. Levy, P. Nick, R. McKenna, N. Muzyczka, J. A. Chiorini,** T. S. Baker, and M. Agbandje-McKenna. 2005. Structure of adeno-associated virus type 4. J Virol 79:5047-58.

122. **Pechan, P., H. Rubin, M. Lukason, J. Ardinger, E. DuFresne, W. W. Hauswirth, S. C. Wadsworth, and A. Scaria**. 2009. Novel anti-VEGF chimeric molecules delivered by AAV vectors for inhibition of retinal neovascularization. Gene Ther 16:10-6.

123. **Pintel, D., M. J. Merchlinsky, and D. C. Ward**. 1984. Expression of minute virus of mice structural proteins in murine cell lines transformed by bovine papillomavirus-minute virus of mice plasmid chimera. J Virol 52:320-7.

124. **Pogany, J., J. Stork, Z. Li, and P. D. Nagy**. 2008. In vitro assembly of the Tomato bushy stunt virus replicase requires the host Heat shock protein 70. Proc Natl Acad Sci U S A 105:19956-61.

125. **Prasad, K. M., C. Zhou, and J. P. Trempe.** 1997. Characterization of the Rep78/adeno-associated virus complex. Virology 229:183-92.

126. **Pringle, C. R. 1999.** Virus Taxanomy at the XI th International Congress of Virology, vol. 144, Sydney, Australia.

127. **Qing, K., C. Mah, J. Hansen, S. Zhou, V. Dwarki, and A. Srivastava**. 1999. Human fibroblast growth factor receptor 1 is a co-receptor for infection by adeno-associated virus 2. Nat Med 5:71-7.

128. **Qiu, J., and K. E. Brown**. 1999. A 110-kDa nuclear shuttle protein, nucleolin, specifically binds to adeno-associated virus type 2 (AAV-2) capsid. Virology 257:373-82.

129. **Qiu, J., A. Handa, M. Kirby, and K. E. Brown**. 2000. The interaction of heparin sulfate and adeno-associated virus 2. Virology 269:137-47.

130. **Rabinowitz, J. E., F. Rolling, C. Li, H. Conrath, W. Xiao, X. Xiao, and R. J. Samulski.** 2002. Cross-packaging of a single adeno-associated virus (AAV) type 2 vector genome into multiple AAV serotypes enables transduction with broad specificity. J Virol 76:791-801.

131. **Redinbaugh, M. G**. 2003. Transmission of Maize streak virus by vascular puncture inoculation with unit-length genomic DNA. J Virol Methods 109:95-8.

132. **Regenmortel, M. H. V.** v. 1999. Vrus Taxonomy . Seventh Repot of the International Committee on Taxanomy of Viruses. Academic Press , London, San Diego,.

133. **Riolobos, L., J. Reguera, M. G. Mateu, and J. M. Almendral**. 2006. Nuclear transport of trimeric assembly intermediates exerts a morphogenetic control on the icosahedral parvovirus capsid. J Mol Biol 357:1026-38.

134. **Ross, C. J., L. Bastedo, S. A. Maier, M. S. Sands, and P. L. Chang.** 2000. Treatment of a lysosomal storage disease, mucopolysaccharidosis VII, with microencapsulated recombinant cells. Hum Gene Ther 11:2117-27.

135. **Ruffing, M., H. Zentgraf, and J. A. Kleinschmidt**. 1992. Assembly of viruslike particles by recombinant structural proteins of adeno-associated virus type 2 in insect cells. J Virol 66:6922-30.

136. **Saliki, J. T., B. Mizak, H. P. Flore, R. R. Gettig, J. P. Burand, L. E. Carmichael, H. A. Wood, and C. R. Parrish**. 1992. Canine parvovirus empty capsids produced by expression in a baculovirus vector: use in analysis of viral properties and immunization of dogs. J Gen Virol 73 (Pt 2):369-74.

137. **Salunke, D. M., D. L. Caspar, and R. L. Garcea.** 1989. Polymorphism in the assembly of polyomavirus capsid protein VP1. Biophys J 56:887-900.

138. **Samad, M. A., M. Okuwaki, H. Haruki, and K. Nagata.** 2007. Physical and functional interaction between a nucleolar protein nucleophosmin/B23 and adenovirus basic core proteins. FEBS Lett 581:3283-8.

139. **Sands, M. S., and M. E. Haskins.** 2008. CNS-directed gene therapy for lysosomal storage diseases. Acta Paediatr Suppl 97:22-7.

140. **Sands, M. S., J. H. Wolfe, E. H. Birkenmeier, J. E. Barker, C. Vogler, W. S. Sly, T. Okuyama, B. Freeman, A. Nicholes, N. Muzyczka, P. L. Chang, and H. R. Axelrod**. 1997. Gene therapy for murine mucopolysaccharidosis type VII. Neuromuscul Disord 7:352-60.

141. **Sanlioglu, S., P. K. Benson, J. Yang, E. M. Atkinson, T. Reynolds, and J. F. Engelhardt**. 2000. Endocytosis and nuclear trafficking of adeno-associated virus type 2 are controlled by rac1 and phosphatidylinositol-3 kinase activation. J Virol 74:9184-96.

142. **Scheets, K., and M. G. Redinbaugh**. 2006. Infectious cDNA transcripts of Maize necrotic streak virus: infectivity and translational characteristics. Virology 350:171-83.

143. **Shen, X., T. Storm, and M. A. Kay**. 2007. Characterization of the relationship of AAV capsid domain swapping to liver transduction efficiency. Mol Ther 15:1955-62.

144. **Shepherd, D. N., T. Mangwende, D. P. Martin, M. Bezuidenhout, F. J. Kloppers, C. H. Carolissen, A. L. Monjane, E. P. Rybicki, and J. A**. Thomson. 2007. Maize streak virus-resistant transgenic maize: a first for Africa. Plant Biotechnol J 5:759-67.

145. **Sonntag, F., S. Bleker, B. Leuchs, R. Fischer, and J. A. Kleinschmidt**. 2006. Adeno-associated virus type 2 capsids with externalized VP1/VP2 trafficking domains are generated prior to passage through the cytoplasm and are maintained until uncoating occurs in the nucleus. J Virol 80:11040-54.

146. **Speir, J. A., S. Munshi, G. Wang, T. S. Baker, and J. E. Johnson.** 1995. Structures of the native and swollen forms of cowpea chlorotic mottle virus determined by X-ray crystallography and cryo-electron microscopy. Structure 3:63-78.

147. **Spier, R. E. 1995**. The proceedings of of an international congress on hepatitis B: the story of an unfinished business. Vaccine 13 Suppl 1:S4.

148. **Summerford, C., and R. J. Samulski.** 1998. Membrane-associated heparan sulfate proteoglycan is a receptor for adeno-associated virus type 2 virions. J Virol 72:1438-45.

149. **Sun, B., H. Zhang, D. K. Benjamin, Jr., T. Brown, A. Bird, S. P. Young, A. McVie-Wylie, Y. T. Chen, and D. D. Koeberl**. 2006. Enhanced efficacy of an AAV vector encoding chimeric, highly secreted acid alpha-glucosidase in glycogen storage disease type II. Mol Ther 14:822-30.

150. **Tatersall, P. 2006**. The evolution of parvovirus taxonomy, in Parvoviruses, . Edward Arnold , Ltd.

151. **Tresnan, D. B., L. Southard, W. Weichert, J. Y. Sgro, and C. R. Parrish**. 1995. Analysis of the cell and erythrocyte binding activities of the dimple and canyon regions of the canine parvovirus capsid. Virology 211:123-32.

152. **Tripathi, S., J. Y. Suzuki, S. A. Ferreira, and D. Gonsalves**. 2008. Papaya ringspot virus-P: characteristics, pathogenicity, sequence variability and control. Mol Plant Pathol 9:269-80.

153. **Unseld, S., T. Frischmuth, and H. Jeske**. 2004. Short deletions in nuclear targeting sequences of African cassava mosaic virus coat protein prevent geminivirus twinned particle formation. Virology 318:90-101.

154. **Unseld, S., M. Hohnle, M. Ringel, and T. Frischmuth**. 2001. Subcellular targeting of the coat protein of African cassava mosaic geminivirus. Virology 286:373-83.

155. **van der Graaf, M., C. P. van Mierlo, and M. A. Hemminga**. 1991. Solution conformation of a peptide fragment representing a proposed RNA-binding site of a viral coat protein studied by two-dimensional NMR. Biochemistry 30:5722-7.

156. **Vanderschuren, H., M. Stupak, J. Futterer, W. Gruissem, and P. Zhang**. 2007. Engineering resistance to geminiviruses--review and perspectives. Plant Biotechnol J 5:207-20.

157. **Vogler, C., J. Barker, M. S. Sands, B. Levy, N. Galvin, and W. S. Sly**. 2001. Murine mucopolysaccharidosis VIL: impact of therapies on the phenotype, clinical course, and pathology in a model of a lysosomal storage disease. Pediatr Dev Pathol 4:421-33.

158. **Vriend, G., B. J. Verduin, and M. A. Hemminga**. 1986. Role of the N-terminal part of the coat protein in the assembly of cowpea chlorotic mottle virus. A 500 MHz proton nuclear magnetic resonance study and structural calculations. J Mol Biol 191:453-60.

159. **Warrington, K. H., Jr., O. S. Gorbatyuk, J. K. Harrison, S. R. Opie, S. Zolotukhin, and N. Muzyczka**. 2004. Adeno-associated virus type 2 VP2 capsid protein is nonessential and can tolerate large peptide insertions at its N terminus. J Virol 78:6595-609.

160. **Wistuba, A., A. Kern, S. Weger, D. Grimm, and J. A. Kleinschmidt**. 1997. Subcellular compartmentalization of adeno-associated virus type 2 assembly. J Virol 71:1341-52.

161. **Wistuba, A., S. Weger, A. Kern, and J. A. Kleinschmidt**. 1995. Intermediates of adeno-associated virus type 2 assembly: identification of soluble complexes containing Rep and Cap proteins. J Virol 69:5311-9.

162. **Wobus, C. E., B. Hugle-Dorr, A. Girod, G. Petersen, M. Hallek, and J. A. Kleinschmidt**. 2000. Monoclonal antibodies against the adeno-associated virus type 2 (AAV-2) capsid: epitope mapping and identification of capsid domains involved in AAV-2-cell interaction and neutralization of AAV-2 infection. J Virol 74:9281-93.

163. **Wu, K. Y., J. Ma, Y. L. Ye, and C. G. Yuan**. 2006. [The migration and differentiation of subventricular zone neural stem cells transplanted into the adult striatum]. Fen Zi Xi Bao Sheng Wu Xue Bao 39:357-64.

164. **Wu, P., M. I. Phillips, J. Bui, and E. F. Terwilliger**. 1998. Adeno-associated virus vector-mediated transgene integration into neurons and other nondividing cell targets. J Virol 72:5919-26.

165. **Wu, P., W. Xiao, T. Conlon, J. Hughes, M. Agbandje-McKenna, T. Ferkol, T. Flotte, and N. Muzyczka**. 2000. Mutational analysis of the adeno-associated virus type 2 (AAV2) capsid gene and construction of AAV2 vectors with altered tropism. J Virol 74:8635-47.

166. **Wu, Z., A. Asokan, and R. J. Samulski**. 2006. Adeno-associated virus serotypes: vector toolkit for human gene therapy. Mol Ther 14:316-27.

167. **Xiao, X., J. Li, and R. J. Samulski**. 1998. Production of high-titer recombinant adeno-associated virus vectors in the absence of helper adenovirus. J Virol 72:2224-32.

168. **Xie, Q., W. Bu, S. Bhatia, J. Hare, T. Somasundaram, A. Azzi, and M. S. Chapman**. 2002. The atomic structure of adeno-associated virus (AAV-2), a vector for human gene therapy. Proc Natl Acad Sci U S A 99:10405-10.

169. **Xie, Q., H. M. Ongley, J. Hare, and M. S. Chapman**. 2008. Crystallization and preliminary X-ray structural studies of adeno-associated virus serotype 6. Acta Crystallogr Sect F Struct Biol Cryst Commun 64:1074-8.

170. **Young, P. P., C. Vogler, A. A. Hofling, and M. S. Sands**. 2003. Biodistribution and efficacy of donor T lymphocytes in a murine model of lysosomal storage disease. Mol Ther 7:52-61.

171. **Yuan, J., A. Amend, J. Borkowski, R. DeMarco, W. Bailey, Y. Liu, G. Xie, and R. Blevins**. 1999. MULTICLUSTAL: a systematic method for surveying Clustal W alignment parameters. Bioinformatics 15:862-3.

172. Y**uan, W., and C. R. Parrish**. 2001. Canine parvovirus capsid assembly and differences in mammalian and insect cells. Virology 279:546-57.

173. **Zhang, W., N. H. Olson, T. S. Baker, L. Faulkner, M. Agbandje-McKenna, M. I. Boulton, J. W. Davies, and R. McKenna**. 2001. Structure of the Maize streak virus geminate particle. Virology 279:471-7.

174. **Zhao, X., J. M. Fox, N. H. Olson, T. S. Baker, and M. J. Young**. 1995. In vitro assembly of cowpea chlorotic mottle virus from coat protein expressed in Escherichia coli and in vitro-transcribed viral cDNA. Virology 207:486-94.

175. **Zhong, L., B. Li, G. Jayandharan, C. S. Mah, L. Govindasamy, M. Agbandje-McKenna, R. W. Herzog, K. A. Weigel-Van Aken, J. A. Hobbs, S. Zolotukhin, N. Muzyczka, and A. Srivastava**. 2008. Tyrosine-phosphorylation of AAV2 vectors and its consequences on viral intracellular trafficking and transgene expression. Virology 381:194-202.

176. **Zlotnick, A., R. Aldrich, J. M. Johnson, P. Ceres, and M. J. Young**. 2000. Mechanism of capsid assembly for an icosahedral plant virus. Virology 277:450-6.

177. **Zlotnick, A., and S. J. Stray**. 2003. How does your virus grow? Understanding and interfering with virus assembly. Trends Biotechnol 21:536-42.

178. **Zolotukhin, S., M. Potter, I. Zolotukhin, Y. Sakai, S. Loiler, T. J. Fraites, Jr., V. A. Chiodo, T. Phillipsberg, N. Muzyczka, W. W. Hauswirth, T. R. Flotte, B. J. Byrne, and R. O. Snyder**. 2002. Production and purification of serotype 1, 2, and 5 recombinant adeno-associated viral vectors. Methods 28:158-67.

BIOGRAPHICAL SKETCH

Antonette Bennett was born in Kingston, Jamaica on July1, 1971. In August of 1989, Antonette started her first year of her undergraduate career at the University of the West Indies (Mona Campus Jamaica). Her major was in Chemistry. She graduated with a B.S. in July of 1993. She was then employed by the Ministry of National Security as a forensic officer in August of 1993. She worked as a Forensic for 5 years (1993-1998). She started a second Bachelor of Science degree at Florida Atlantic University in the year 2000 and completed it in 2001. In August of 2003 she joined the IDP program of University of Florida, College of Medicine to pursue her PhD. In May 2004, she joined the laboratory of Professor Mavis-Agbanje McKenna. Antonette spent five years studying the mechanism by which the ssDNA viruses Maize Streak Virus and Adeno Associated Virus serotype 2 assembles and disassembles, under the guidance of Professor McKenna.